UiT The Arctic University of Norway

Faculty of Science and Technology
Department of Geosciences

Grounding-line fan formation during an Early Holocene readvance of Aldegondabreen, Svalbard.

Jóhanna Kristín Jóhannesdóttir
Master's Thesis in Geology, GEO-3900
December 2021

Abstract

In this study, two ridge-shaped cross-valley sedimentary landforms, in the lower forefield of Aldegondabreen, a small valley glacier on the west coast of Spitsbergen, Svalbard, were studied to reconstruct the Holocene glacial history of Aldegondabreen prior to the Little Ice Age. Sedimentological and geomorphological methods were used in conjunction with radiocarbon dating to examine the sediments in the landforms. Three sedimentary lithofacies associations were identified within the studied landforms of the lower forefield. 1) Gravel with small bivalve shell fragments formed in a grounding-line fan, 2) glaciotectonised gravel formed in a subaerial glaciofluvial outwash plain, and 3) glaciogenic sediments, including subglacial till with supra- and englacial components, and glaciotectonised marine sediments. The results suggest that Aldegondabreen readvanced in the Early Holocene into the shallow fjord during a relative high sea level. The maximum age for this event is suggested to be 10.79 cal. ka BP, constructed with radiocarbon dating of bivalve shells and fragments from glacially overridden marine sediments in the forefield. It is proposed that during this Early Holocene readvance, a grounding-line fan formed at the grounding zone of the tidewater glacier. The minimum ice margin position of the glacier during this advance was at least 2 km beyond the modern ice margin (2020) constructed with the location of the grounding-line fan deposit. The data from this study adds to the Late Glacial - Early Holocene glacial record from Svalbard and provides new insights into pre-LIA Holocene glacial history of Aldegondabreen.

Acknowledgements

First, I want to think my previous supervisor Lena Håkansson for giving me the chance to study in Svalbard and for the opportunity to work on this master project.

My current supervisors, Anders Schomacker and Mark Furze, thank you for all the appreciated help and support along the way. Thanks for all the feedback and for always providing me with detailed and thorough explanations.

I am very grateful for Mark who came in later and decided to supervise me on this project. Thanks for all the fieldwork opportunities and all the very lively discussion and explanations in the field. These field excursions were absolutely the highlight of my master project and motivated me when needed.

I want to think Anders Schomacker for the support through the writing process and for valuable constructive feedback. It was very nice to be able to express myself sometimes in Icelandic! Thanks for always being positive with “að redda hlutunum”.

All the students in the UNIS course AG-210 in 2019 and 2021 thanks for all the help and the discussions during fieldwork, especially the digging!

Amélie, Tenna and Anna, thanks for a great assistance during fieldworks.

To Erik, thanks for providing me with aerial images of Aldegondabreen and helping me with data processing.

Thanks to all my friends in Iceland, Tromsø and Svalbard who made this challenging period fun. Björg, Armin, Arthur and Dagny, thanks for coming and visiting us in Tromsø during the final phase of this thesis. To Tim, thank you so much for proof-reading the thesis and for great feedback.

My parents and siblings are thanked for the endless support and to encourage me to follow my dreams.

Last but not least, Palli thanks for proof-reading this thesis and for always supporting my ideas and plans, encouraging me, and believing in me.

Contents

1 Introduction

1.1 Motivation

Most regions on Earth have experienced increased air temperature since around AD 1860 (Oerlemans, 2005; IPCC, 2021). In the last decades it has become more important to study the global climate systems to improve understanding of how climate is changing in space and time (IPCC, 2021). Glaciers are sensitive to changes in climate, especially changes to winter precipitation and summer temperatures. They are therefore important indicators for climate variations, and studying them can provide valuable information to reconstruct past climate fluctuations and modern climate change (Evans and Benn, 2004; Oerlemans, 2005; Yde and Paasche, 2010). Many glaciers on Earth are currently experiencing negative mass balance, retreat, and stagnation as a response to the global change in climate (Oerlemans, 2005; Schomacker, 2008). Glaciers shape and erode the landscape in glaciated areas. As they retreat, sediments and landforms are exposed which can be used for studying the past extent and behaviour of former ice sheets and glaciers (Benn and Evans, 2010).

Climatic shifts are amplified in the Arctic, evidenced by faster air temperature increase than in any other region in the Northern hemisphere over the past decades (IPCC, 2007; Miller et al., 2010; van der Bilt et al., 2015). As the Arctic is particularly sensitive to changes in the climate, it is important to improve understanding of the region and its environmental settings. Many Arctic glaciers have been experiencing overall retreat and negative mass balance in the last decades. This has resulted in heavy focus on their climatic correlation and how they will respond to future climate change (IPCC, 2007; Nuth et al., 2013).

The Svalbard region is an ideal place to study Arctic glaciers and past glacial and climate history (Humlum et al., 2005). Svalbard and the Barents Sea region have undergone repeated glaciations through the Quaternary. During the Last Glacial Maximum (LGM) (25 - 15 ka BP) the region was covered with the Svalbard-Barents Sea Ice Sheet (SBSIS). Now, evidence from the last deglaciation is found in the modern landscape of Svalbard (Mangerud et al., 1998; Ingólfsson and Landvik, 2013). Holocene climate has been the subject of many studies in Svalbard. The Early Holocene in Svalbard (11.7 - 8.2 ka BP) has been described as a period with temperature of 6 - 7°C warmer than at present (Mangerud and Svendsen, 2018; Farnsworth et al., 2020) and the period is therefore considered a potential analogue for future climate.

Holocene glacier studies from Svalbard have mainly examined Late Holocene (4.2 ka BP to present; the Neoglaciation (4.2 ka BP - 1920 AD) and the Little Ice Age, LIA (1250 - 1920 AD)) landforms with fewer focusing on Late Glacial and Early Holocene glacial deposits (Larsen et al., 2018). The few studies analysing glacial landforms and sediments older than Late Holocene have provided a new understanding of that period and many indicate that some glaciers on Svalbard readvanced in the Late Glacial - Early Holocene (Salvigsen et al., 1990; Lønne, 2005; Forwick et al., 2010; Farnsworth et al., 2017; Farnsworth et al., 2018; Larsen et al., 2018; Farnsworth et al., 2022).

To fully understand Early Holocene glacier fluctuations, more studies are needed. Glacial sedimentary and geomorphological records can provide us with an understanding of the palaeoenvironment and insight into past climates.

1.2 Aims and approach

The aim of this study is to reconstruct the pre-LIA Holocene glacial history of Aldegondabreen, a small valley glacier on the west coast of Svalbard, from sedimentary and geomorphological archives in the glacier forefield. Glacial meltwater has eroded the forefield significantly since the LIA, revealing natural exposures of many sedimentary successions. The main focus of this study is on two ridge-shaped cross-valley landforms in the lower forefield of the glacier and sedimentary sections within these landforms exposed by meltwater erosion. A combination of sedimentological and geomorphological analyses, together with radiocarbon dating of these sediments and landforms is used to elucidate Aldegondabreen's glacial history prior to the LIA. To this end, this study will focus on answering the following research questions:

- What information can the sedimentary archives of Aldegondabreen's recently deglaciated forefield reveal about glacier and sea level fluctuations in inner Grønfjorden during the Holocene?

- To what extent are earlier sediments and landforms preserved in the forefield or does the modern landsystem only record LIA events?

- What is the age and origin of two prominent ridge-shaped cross-valley landforms in Aldegondabreen's lower forefield and what information can they reveal about the glacier's former behavior?

- Is the Holocene behavior of Aldegondabreen similar to other glacial systems in Svalbard and what can that tells us about palaeoclimate and glacier dynamics during this interval?

1.3 Glacier dynamics and thermal regimes

Glaciers are important indicators of past climate variations. Glaciers are sensitive to changes in the climate, especially in response to winter precipitation and summer temperatures (Oerlemans, 2005). How a particular glacier will respond to climate change depends on its geometry, physics, and the climatic settings (Oerlemans, 2005; Yde and Paasche, 2010). The glacier mass balance, the balance between accumulation and ablation in a glacier, is a function of atmospheric temperature and precipitation (Benn and Evans, 2010; Hambrey and Glasser, 2012). Glacier temperature is a balance between the input and output of energy at the surface and the bed, and the heat produced within the glacier by ice flow. Therefore, the ice temperature and mass balance of a glacier must both be considered to fully understand how a glacier will respond to climate change (Benn and Evans, 2010).

The whole glacier is influenced by the glacier mass balance and thermal structure. In particular, the thermal regime of a glacier is influential when it comes to patterns of glacial erosion and deposition, glacier movement and amount of geomorphological activity. It is possible to obtain information of the thermal and dynamic regimes of a former glacier by studying the nature of the deposited sedimentary products (Lovell et al., 2015). Sediment entrainment in a glacier is at the bed or on the surface and the characteristics of the glacial sediments will therefore be linked to the thermal and dynamic characteristics of the glacier (Hambrey and Glasser, 2012).

The pressure melting point is the temperature at which ice begins to melt under a given amount of pressure (Cuffey and Paterson, 2010), and glaciers can be classified into three groups based on their thermal regimes, whether the ice is at or below the pressure melting point: temperate, cold and polythermal (Benn and Evans, 2010; Hambrey and Glasser, 2012).

In temperate glaciers, the ice throughout the bed is at the pressure-melting point. These glaciers are commonly referred to as wet-based as most of the meltwater discharges from the base at the glacier terminus. This basal meltwater can increase the glacier basal sliding and the sub-sole deformation (Hambrey and Glasser, 2012). Temperate glaciers are efficient when it comes to glacial erosion and their surfaces are often covered with large amounts of supraglacial debris derived from rockfall from the surrounding valley walls. These glaciers can deposit a variety of sediments and landforms including flutes, drumlins, dump- and push moraines (Benn and Evans, 2010; Hambrey and Glasser, 2012).

Cold-based glaciers consist of ice which is below the pressure melting point throughout and are frozen to their bed. These glaciers move by internal deformation in the ice. Cold-based glaciers are known for little or no erosion at their beds; however, basal erosion is not always absent beneath cold-based ice. Basal debris load below a cold-based glacier can be considerable, especially near their margins (Benn and Evans, 2010; Hambrey and Glasser, 2012).

Polythermal glaciers are composed of cold and temperate ice. Polythermal valley glaciers often contain ice below the pressure melting point at the snout, in the lateral margins and at the surface layer. Warm-based ice is usually situated in the accumulation area where the ice is thickest. This mixture of thermal regimes complicates the dynamics of polythermal valley glaciers. These glaciers typically slide on their bed or exhibit a sub-sole deformation. Where cold ice is found at the snout and in the lateral margins, the glaciers move only by internal deformation. Basal debris load can be high for polythermal glaciers and supraglacial medial moraines are common in the ablation areas. Polythermal glaciers often contain supraglacial and englacial meltwater channels (Benn and Evans, 2010; Hambrey and Glasser, 2012).

The majority of glaciers in Svalbard have been classified as polythermal (Hagen et al., 1993). However, many valley glaciers in Svalbard have exhibited a continuous retreat and thinning since the end of the LIA signalling negative mass balance. Therefore, it is likely that majority of small land-terminating valley glaciers in Svalbard are now becoming entirely cold-based and frozen to their beds. Studies have demonstrated that many glaciers are currently in the process of this thermal switch from polythermal to cold-based (Lovell et al., 2015).

1.4 Glacial sediment

Glacial erosion appears in the form of abrasion, plucking and quarrying, meltwater- and freeze-thaw processes and chemical action (Benn, 2009). Glacial sediments, produced by glacial erosion, are transported and later deposited in the glacial system and can form a range of different landforms. Sediments and landforms exposed after glacial retreat or following a glaciation can provide important information about the past environment and climate. Analyses of glacial sediments and landforms can be used to reconstruct past glacial environments such as past extent and behaviour of former ice masses (Evans and Benn, 2004; Benn and Evans, 2010).

A combination of glacial geomorphic- and sedimentological methodologies is likely the best approach for a detailed reconstruction of former glacial environment, linking sediments to landforms and vice versa. Glacial geomorphology is the study of processes, landscapes and landforms which are made by glaciers and other ice masses. The processes studied include how ice masses move, and how glacial ice erodes, transports and deposits sediments (Menzies, 2009). Geomorphological mapping yields both information on the morphology and the genesis of landforms (Lowe and Walker, 2015). Even though geomorphological evidence can help to reconstruct the glacial history of an area, sedimentary records can provide more detailed reconstructions of the events leading to deposition of the sediments. Both spatial and temporal aspects of a former glacial environment are reflected in sediment sequences as the sediment accumulation occurs over an extended time period (Lowe and Walker, 2015).

Glacial sediments are highly variable and complex. This diversity is due to the variety of ways in which debris can travel through the glacial system from source to deposition. Deformation, reworking and re-sedimentation are all processes that debris in the glacial system can be subjected to and they can also exhibit several cycles of reworking before the final deposition and preservation in the geological record (Benn and Evans, 2010).

1.5 Debris cascade system

As sediments travel through the glacial system, their physical properties develop during erosion, transport and deposition. The sequence of steps, referred as the debris cascade system (Chorley et al., 1984), can be used as a basis to understand the physical properties of glacial sediments (Evans and Benn, 2004; Benn and Evans, 2010). The debris cascade system can be divided into three stages: debris source, transport path, and deposition.

Debris sources in a glacial system can be subglacial (including plucked and abraded bedrock), overridden sediments, or extraglacial (e.g., rocks from valley sides and nunataks, or windblown dust) (Evans and Benn, 2004). The source of the debris can influence grain size distribution of the sediments, clast morphology, and clast lithology (Benn and Ballantyne, 1994).

Debris is carried through the glacial system along one or more transport paths and debris can shift from one path to another before final deposition. Transportation can occur with ice flow in supraglacial, englacial and subglacial positions. Other transport paths in glacial environments can include meltwater rivers and streams, along with wind and suspension in lakes or the sea (Evans and Benn, 2004). The transport of a particle through the glacial system has a strong influence on clast morphology, as it determines the erosional processes which a sediment particle will experience (Boulton, 1978; Benn and Ballantyne, 1994). The glacial transportation can also control the grain size distribution of sediments when clasts are sorted with wind, gravitational processes, and water (Evans and Benn, 2004).

Deposition is the process of sediment particles settling in the final deposit. Depositional processes are the main influence on the geometry and the extent of sediment units. The type of deposition can also determine sedimentary structures, grain size distribution and clast morphology. Additionally, sediments can be affected by post-depositional processes such as folding and faulting, frost-heaving, and leaching of fine material by wind and water (Evans and Benn, 2004). The sediments in glacial settings can be deposited in a variety of environments including subglacial, ice marginal, proglacial, glaciofluvial, glaciolacustrine, and glaciomarine.

1.6 Glaciofluvial systems and sediment transport

There are various routes for glacial meltwater to flow within the glacier system: supraglacially, englacially, or subglacially. The path’s location depends on pre-existing channels and subglacial cavities, or on crevasses within the ice. Additionally, the source and volume of meltwater influences the path of water flow through the glacier (Carrivick and Russell, 2007).

The thermal regime of a glacier also plays a role when it comes to the glacial drainage system (Hodgkins, 1997). Meltwater at the bed is absent in cold-based glaciers while temperate glaciers discharge most of their meltwater at the base near the glacier terminus. A well-developed basal glaciofluvial network is rare for polythermal glaciers and the meltwater usually follows supraglacial and englacial channels (Hambrey and Glasser, 2012).

Large-scale regular and irregular variability in runoff magnitude is characteristic of glaciofluvial systems (Maizels, 2002). Diurnal fluctuations of the meltwater discharge are regular and mainly controlled by daily temperature fluctuations. The lowest flow generally occurs during the night, with peak-flow during the day. However, the timing of peak-flow is dependent on the time it takes water to flow through the glacier system, which in turn is controlled by the size of the ablation zone and the extent of the englacial drainage network within the glacier (Maizels, 2002; Marren, 2005).

Long term discharge fluctuations include a seasonal cycle which closely follows the annual temperature curve (Marren, 2005). The seasonal cycle can be divided into four distinct stages (Maizels, 2002). The lowest flow is during the winter and is followed by the spring melting. In the beginning of the melt season, the majority of the meltwater comes from melting of river ice. Up to 25% of the melting within the glacier can be stored in the glacier drainage system and in snow and slush areas. As a result of this, discharge is much lower during this period than expected. In mid-summer when the temperature rises rapidly, both meltwater formed by snow- and ice melting and the stored meltwater from the spring season is released. As a result, more meltwater is released from the glacier than melted during this period and the englacial drainage system reaches its maximum capacity. In late summer, runoff is directly controlled by ablation and rainfall. The englacial channels are well-developed at that time and the water flows directly through without delay. With decreasing temperature, runoff decreases towards the end of the melt season, reaching the seasonal minimum with freezing temperatures (Maizels, 2002; Marren, 2005).

Previous work in Svalbard has suggested that meltwater discharge in cold-based glaciers in the region is mainly controlled by the seasonal pattern of meltwater storage and release. Hodgkins (2001), measured the meltwater discharge at Scott Turnerbreen, a cold-based glacier in central Spitsbergen, Svalbard. During the first half of the melt season, a significant volume of water was stored in the supraglacial snowpack; a greater volume than on temperate glaciers of the same size. The reason for this is the relatively flat and uncrevassed surface of the glacier (like many other glaciers in Svalbard), which is cold and impermeable. During mid-summer, this water is released rapidly because the water drains directly over the ice surface without flowing through the glacier as observed on temperate glaciers.

Irregular events also influence the discharge of glacial meltwater streams. The most common events are summer and autumn rainstorms, especially those after a warm period. During these storms, the meltwater rivers experience very high flow, and these events are often the main floods of the melt season (Maizels, 2002). Other high-magnitude runoff events which may also

occur in glacial meltwater rivers include glacier outburst floods and jökulhlaup events (Maizels, 2002). Long-term variation in runoff can also occur during glacier growth, with increased discharge, and during deglaciation, with decreased discharge. However, discharge can briefly increase during rapid deglaciation as more meltwater is available (Marren, 2005). In addition, glacial surges can significantly alter the glacial drainage system and meltwater discharge from a glacier (Björnsson, 1998). It has been suggested that when glaciers undergo a surge event, the basal drainage system shifts from an efficient conduit system to an inefficient linked cavity system (Kamb et al., 1985). During the termination of the surge event, when the ice flow velocity is slowing down, floods with high discharge can occur in the outflow streams at the terminus which are linked to the shift back to a basal conduit system (Kamb et al., 1985).

Glacial drainage systems can transport large volumes of sediments through glaciers. Rates of sediment transport depend on the availability of sediments in the glacial catchment and the characteristics of the flow. Generally, the largest particle carried by a stream and the total quantity of available sediments that can be transported increases with increased discharge and flow velocity (Benn and Evans, 2010).

Glacial rivers can transport sediments as bedload and suspended load (Benn and Evans, 2010). There are several factors which can cause suspended sediment concentration to be high in glacial meltwater rivers. This includes glacial advance, large discharge events (Hodson and Ferguson, 1999), rapid glacier growth as there is more sediment supply compared to periods of glacial stability, and deglaciation when glacial sediments which were stored in the glacier are released into the glaciofluvial system (Marren, 2005). Suspended sediment concentration is higher during the start of a cyclic event (e.g., diurnal- or flood event) and in the beginning of the melt season, than during the end of the season and the falling stage of a cyclic event (Maizels, 2002). This is due to the depletion of sediment supply towards the end of a cyclic event because all the transportable sediments available have already been moved away in the previous high discharge (Hodson and Ferguson, 1999). Hyperconcentrated flows, a transition between debris flows and normal stream flows, can occur in glaciofluvial rivers where the discharge is high and there is a high amount of available loose sediments (Benn and Evans, 2010).

Bedload refers to grains transported by sliding, rolling, and saltation along the bed of a stream. For bedload to occur, particles have to exceed the local threshold for entrainment and this depends on the force of the flow and resistance of the bed (Maizels, 2002). Grain size, rate of bedload, and the quantity of sediments which can be transported as bedload generally increases with higher discharge. In extreme flood events, even large boulders can be transported as bedload (Marren, 2005).

1.7 Glaciomarine environments and tidewater glaciers

The glaciomarine environment has been defined as a marine environment where glacial evidence can be found within the sediments (Powell and Domack, 2002). All sediments which are deposited in the ocean after being released from grounded or floating glacial ice are therefore defined as being located in the glaciomarine environment (Powell, 1984).

Marine-terminating glaciers can be divided into glaciers with ice-shelves (Fig. 1A), where floating ice tongues can extend up to several hundreds of kilometres away from the grounding zone, and tidewater glaciers (Fig. 1B) where floating ice is absent beyond the grounding zone (Batchelor and Dowdeswell, 2015). Marine conditions including water temperature, currents, salinity, sedimentary processes, and interactions between the marine and glacial environments vary between these two types of marine terminating glaciers (Powell and Domack, 2002).

The grounding zone, also referred to as a grounding-line, of a marine-terminating glacier is the boundary where the glacier is no longer in contact with the underlying ground (Fig. 1) (Batchelor and Dowdeswell, 2015). For ice-shelves, the grounding zone is where the glacier starts to float (Fig. 1A) whereas for tidewater glaciers the grounding zone occurs where the glacier ends in a nearly vertical cliff, where iceberg calving takes place (Fig. 1B) (Powell, 1984). The grounding zone is a crucial location concerning ice and meltwater transport from the glacier and into the marine environment (Batchelor and Dowdeswell, 2015).

Tidewater glaciers lose mass through iceberg calving, meltwater runoff and melting from tidewater cliffs (Batchelor and Dowdeswell, 2015). Luckman et al. (2015) found out that the rate of frontal ablation of tidewater glaciers in Svalbard is not dependent on glacier dynamics, rather the temperature of the fjord waters at depth. This implies that submarine melt is the dominant calving mechanism and therefore frontal ablation is controlled mainly by ocean temperature (Luckman et al., 2015; Slater et al., 2019). Climatically-forced changes can therefore have significant impact on tidewater glaciers such as changes in ocean temperature, sea level and ice thickness (Rignot et al., 2015; Wood et al., 2018).

Marine-terminating glaciers and ice caps produce a distinctive assemblage of submarine sedimentary landforms. These landforms are deposited by subglacial and proglacial sedimentary processes and can be well preserved, making them useful in reconstructing past ice dynamics (Robinson and Dowdeswell, 2011). These landforms include recessional moraines, terminal moraines, glacial lineations, glacigenic debris flows, crevasse-squeeze ridges, annual push moraines, grounding-zone wedges and grounding-line fans (sometimes referred to as ice-proximal fans) (Ottesen and Dowdeswell, 2006; Batchelor and Dowdeswell, 2015).

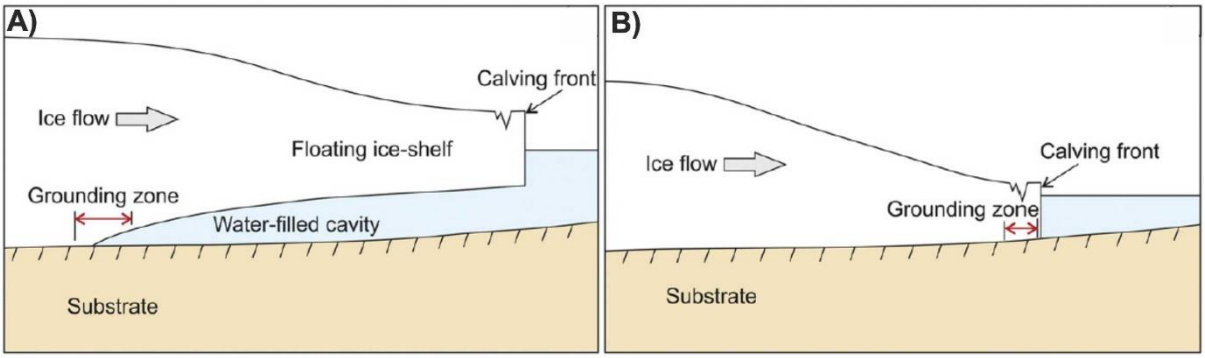

Figure 1. Schematic models of marine terminating glaciers and the position of the grounding zone. A) The ice margin of an ice sheet with a floating ice shelf. B) Ice margin of a tidewater glacier. Modified from Batchelor and Dowdeswell (2015).

1.8 Grounding-line fans

Grounding-line fans (also referred to as ice-proximal fans and ice-contact fans) can form at the mouth of subglacial and basal meltwater tunnels at the grounding-line of a marine-terminating glacier. High discharge can form a turbulent jet in front of the efflux, for example during melt season. The jet changes to a plume when the buoyancy force takes over, which can rise and produce a vertical plume of turbid meltwater which spreads out. Deposition of the coarse-grained particles occurs close to the point-source at the mouth of the subglacial channel due to rapid energy loss. The fine-grained material such as sands, silts and clays are transported further away with the buoyant upwelling plume and are deposited from suspension once the internal turbulence decreases (Powell, 1990; Bennett et al., 1999; Koch and Isbell, 2013; Batchelor and Dowdeswell, 2015; Dowdeswell et al., 2015). Where numerous subglacial tunnels are located along the grounding zone of a tidewater glacier, the fans can overlap each other and combine to form morainal banks (Batchelor and Dowdeswell, 2015).

Seramur et al. (1997) studied deposits within a morainal bank complex in Muir Inlet, Glacier Bay in Alaska. They observed that grounding-line fans were deposited along a stable ice terminus with two main depositional processes, gravity flows and settling of suspension. The difference in the sedimentary facies within the fans was suggested to be due to changes in depositional processes relative to the distance from the source.

Grounding-line fans may contain a variety of sediments, including sub-aquatic outwash, suspension settling of fine-grained material, and gravity-flow sediments. The sediment texture within grounding-line fans can vary significantly due to different sediment and water discharge, lateral movement of the efflux location across the grounding-line, and glacier terminus stability (Powell, 1990).

The presence of channelized meltwater system beneath a glacier is one of the main controls for the formation of grounding-line fans and these fans are therefore mainly produced where glaciers contain surface-derived meltwater, for instance in temperate glacial regions (Powell, 1990; Batchelor and Dowdeswell, 2015).

Additionally grounding-line fan formation is dependent on the type of the glacier terminus, ice velocity and sediment delivery rate, and grounding zone stability (Batchelor and Dowdeswell, 2015). These subglacial fans are usually formed when the grounding zone of a glacier is stable for some time. With sufficient time they can aggrade to sea level to form ice-contact deltas. Grounding-line fans are generally not produced in front of a glacier with a rapid retreating grounding-line as there will be insufficient time for them to build up. Grounding-line fans in front of an advancing glacier will not be well preserved as the glacier will override them with time (Powell, 1990; Batchelor and Dowdeswell, 2015). Large grounding-line fans are suggested to be formed under extreme meltwater discharge events with abnormally high rates of sediment transport to the ice margin. The "normal" meltwater discharge, at a still-standing glacier, is not enough to build up a large grounding-line fan (Batchelor and Dowdeswell, 2015).

Grounding-line fans formed during the last glaciation and interglacial have been described from, e.g., fjords of Alaska, Norway, and Svalbard (Powell, 1990; Lønne, 1993; Seramur et al., 1997; Lønne, 1997, 2005; Dowdeswell et al., 2015). Dowdeswell et al. (2015), presented schematic models of grounding-line fans in front of tidewater glaciers. The models represent different time periods of ice margin stability for a tidewater glacier (Fig. 2). The first model (Fig. 2A) presents the classical grounding-line fan, formed in front of an ice margin which has a stable position for one to several decades. Sediments from a meltwater plume are deposited in front of the ice margin to form a grounding-line fan. Fig. 2C, represents a quasi-stable ice terminus, where morainal banks are formed during glacier readvance, out of ice proximal deposit. The readvance will modify any existing fan, however part of the fan morphology and stratigraphy can be preserved. Slope failure and debris flows are a common feature on the ice-distal side of morainal banks. The last model (Fig. 2E) demonstrates a retreating ice margin with brief stillstands. This scenario does not allow a classical grounding-line fan to build up, rather small accumulations of ice-proximal deposit close to the grounding-line at the subglacial meltwater portal.

Future warming may impact the size of future grounding-line fans. Trusel et al. (2010), analysed the glaciomarine environment in front of Kronebreen and Kongsvegen glaciers in Kongsfjorden, Svalbard. Bathymetric profiles demonstrated a grounding-line fan next to a large submarine meltwater portal which was estimated to accumulate at more than 300 mm/year. They expect that with continued warming, meltwater volumes and sediment discharge will increase. This deposit may therefore aggregate above water to produce an ice-contact delta which can increase the stability of the ice margin and the ability of the terminus to readvance in the future.

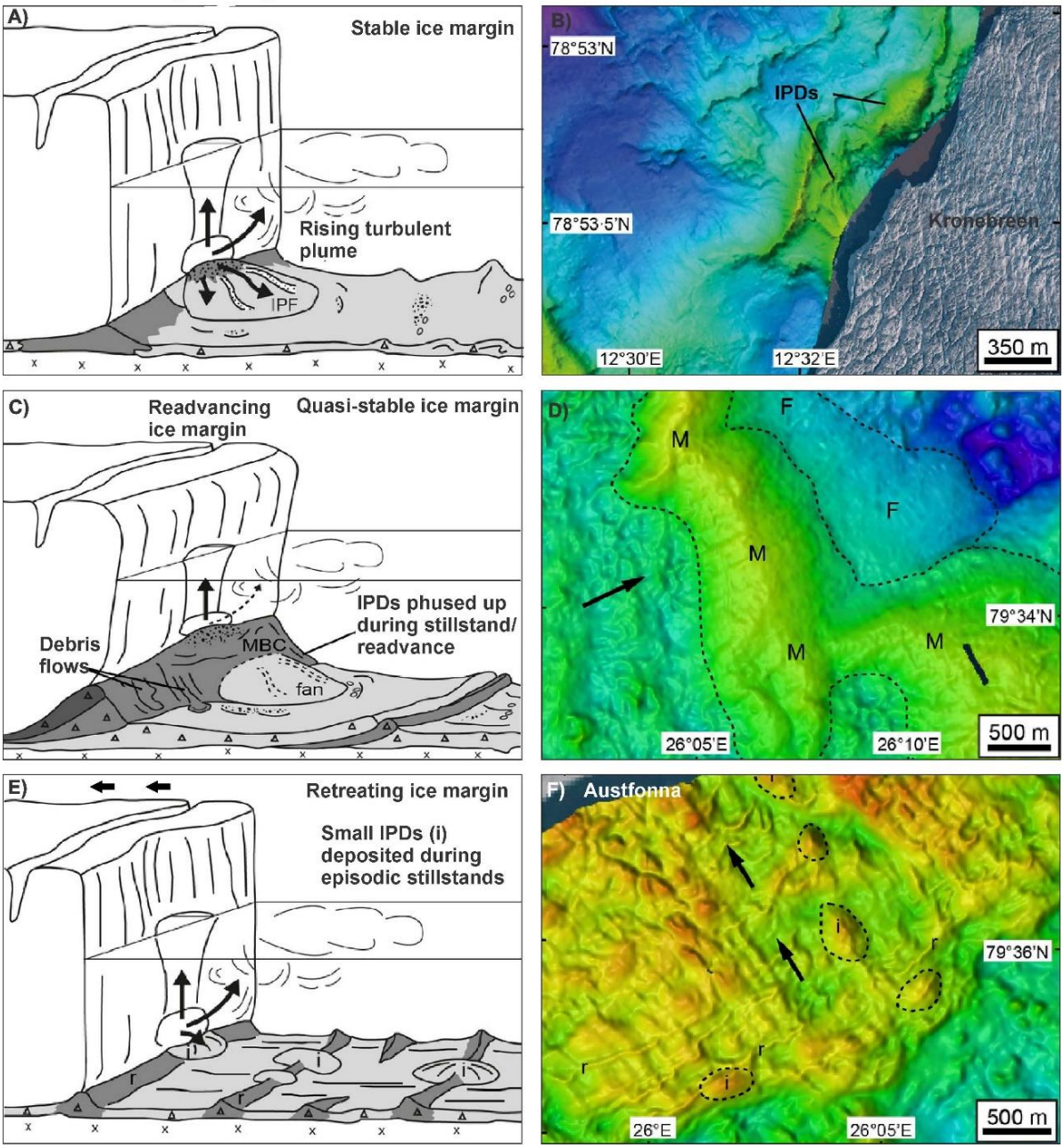

Figure 2. Schematic models of grounding-line fans in front of tidewater glaciers representing different time periods of ice margin stability and examples of ice-proximal deposits (IPDs) formed at marine terminating ice margins. A) A classical grounding-line fan formed at stable ice margin. B) Small grounding-line fans (marked as IPDs) actively building up offshore of Kronebreen, Kongsfjorden, Svalbard. C) Morainal bank formation in front of a quasi-stable ice terminus. D) Morainal bank complex in Hartogbukta, Svalbard, with morainal (M) and fan (F) components. E) Retreating ice margin forming small accumulations of ice-proximal deposit (i). F) Small ice-proximal deposits (i) close to the grounding-line in Hartogbukta. All images are modified from Dowdeswell et al. (2015).

2 Setting

2.1 Regional setting Svalbard

2.1.1 Landscape and glaciers

The Svalbard archipelago is situated on the boundaries between the Norwegian Sea, the Barents Sea and the Arctic Ocean (Fig. 3) (Humlum et al., 2005). The archipelago covers a total area of 60.667 km^2, between 74°N and 81°N and 10°E and 35°E. The largest island is Spitsbergen which occupies 62% of Svalbard's land area (Dallmann, 2015), with the other main islands being Nordaustlandet, Barentsøya, Edgeøya, Kong Karls Land, Prins Karls Forland and Bjørnøya. The western and the northern part of Spitsbergen is characterized by steep and rugged mountains while the mountains on the eastern side are more rounded or plateau-shaped. The coastal landscape of Svalbard is characterised by strandflats or coastal plains with marine deposits and raised marine beaches as common features (Dallmann, 2015). Numerous large fjord systems occur on west and north Spitsbergen, such as Wijdefjorden, Isfjorden and van Mijenfjorden. These fjords are all glacially eroded and cut far inland (Ingólfsson, 2011). Svalbard falls into the zone of continuous permafrost (Humlum et al., 2003). By definition, permafrost is ground which remains at or below 0°C for at least two years. Permafrost lies underneath at least 90% of the land surface in Svalbard, which is not covered by glaciers (Gilbert et al., 2018).

The archipelago is highly glaciated. In the late 2000s, about 57% of the total land area was covered with glaciers, corresponding to 33.775 km^2 (Nuth et al., 2013). Glacier types on Svalbard include cirque and valley glaciers, ice fields and ice caps. Some of these glaciers terminate on land. However the majority, or 65%, drain into the sea with a calving front (Nuth et al., 2013). The controlling factor for distribution of glaciers around the archipelago is the local climate as well as the topography (Hagen et al., 1993). Small cirque glaciers are common in high alpine mountain regions such as in western parts of Spitsbergen, while ice caps are more frequent in the flatter areas, such as in eastern Spitsbergen, Nordaustlandet, Barentsøya, and Edgeøya (Hagen et al., 1993). Most of the glaciers and ice caps in Svalbard are polythermal, a mixture of cold and temperate ice. Many of the smallest glaciers are below the pressure melting point, meaning that they are entirely cold-based and frozen to the substratum (Hagen et al., 1993). The glacier equilibrium-line altitude (ELA) in Svalbard reflects the precipitation pattern. The ELA is lowest in the west, only about 200 m a.s.l. where the precipitation is highest. The ELA rises to the north-eastern part of Spitsbergen up to more than 700 m a.s.l. where precipitation is relatively low (Hagen et al., 2003; Ingólfsson, 2011). Many of Svalbard's glaciers are surge type. When they surge, they undergo a fast increase in flow velocity over a period of a few months to a few years. Following this period of abnormally fast flowing ice, a much longer quiescent phase takes over when the glacier is stagnant and ice builds up in the upper part of the accumulation area. The quiescent period can last for more than 200 years (Dowdeswell et al., 1991; Lefauconnier and Hagen, 1991).

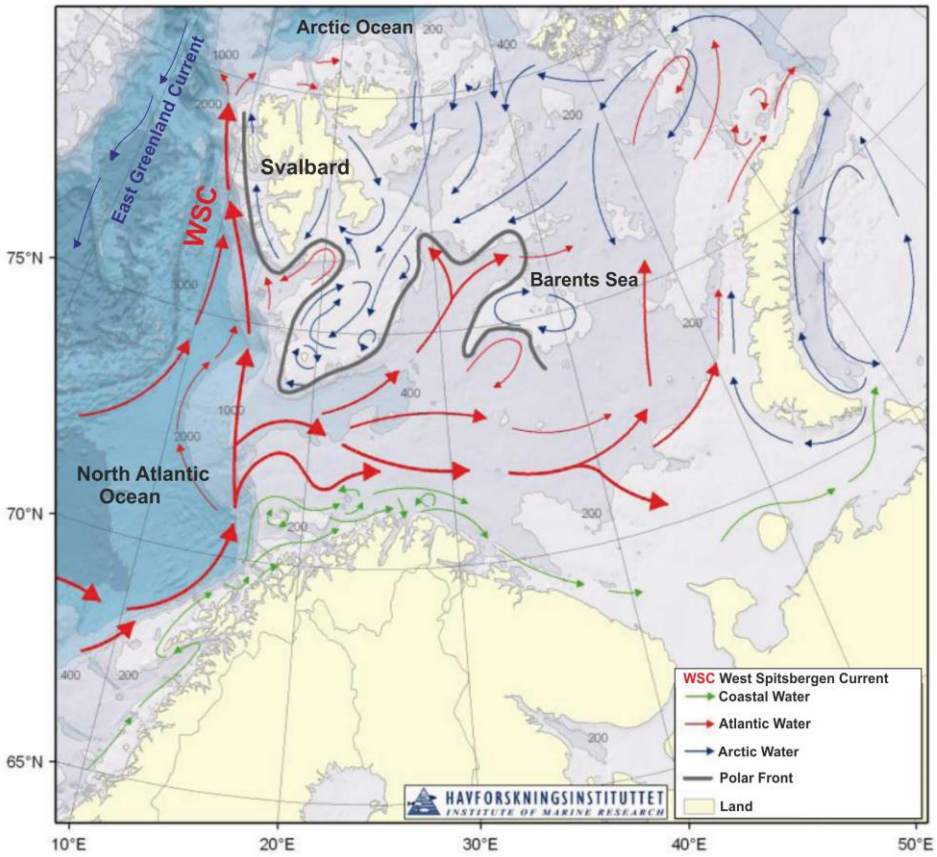

Figure 3. Location of Svalbard in the North Atlantic. The map illustrates the circulation of the main ocean currents in the Barents Sea and around Svalbard. Atlantic water flows along the west coast of Spitsbergen with the warm West Spitsbergen Current (WSC). Cold and fresh Arctic water from the Arctic Ocean flows along the east coast of Spitsbergen to the south. Modified from Hanssen-Bauer et al. (2019).

Svalbard has been highly glaciated most of the time since the onset of the Quaternary, 2.6 million years ago. During these glaciations, ice masses have repeatedly shaped the surface morphology of Svalbard. The characteristics of the modern Svalbard landscape, such as fjords, valleys, cirques and mountains are a result of a glacial erosion during these glaciations (Svendsen and Mangerud, 1997; Mangerud et al., 1998; Ingólfsson, 2011; Hormes et al., 2013).

2.1.2 Climate

The climate in Svalbard is described as a dry, high-Arctic climate with extreme low winter temperatures and periglacial conditions (Hanssen-Bauer et al., 1990; Hanssen-Bauer et al., 2019). Svalbard experiences a relatively milder and wetter climate compared to other places at similar latitudes. This is mainly due to Atlantic water that flows along the western coast of Spitsbergen with the warm West Spitsbergen Current, and influences weather and sea ice (Fig. 3) (Hanssen-Bauer et al., 2019). Fresh, cold Arctic water originating in the eastern Arctic Ocean flows south along the east coast of Svalbard (Hanssen-Bauer et al., 1990). The climate in Svalbard is generally controlled by large scale air currents in the northern part of the Atlantic Ocean, the low-pressure area near Iceland and high-pressure area over Greenland. Westerly and south-westerly winds transport mild air from lower latitudes up to Svalbard (Hanssen-Bauer et al., 1990).

The annual mean air temperature at Svalbard airport from 1991 - 2020 was -3.9°C (Fig. 4) with mean annual precipitation of 216 mm over the same period (Fig. 5) (Norwegian Meteorological Institute, 2021a; Norwegian Meteorological Institute, 2021b). However, the precipitation in Ny-Ålesund and at Isfjord Radio, which are both located on the west coast of Spitsbergen, is more than twice as high as at Svalbard Airport (Fig. 5) (Førland et al., 2011).

This regional difference is also visible in the air temperature (Fig. 4). Weather stations which are located more inland, such as Svalbard Airport, Longyearbyen, and Sveagruva, experience a more continental climate. These weather stations record winter temperatures of 2 - 5°C lower and summer temperatures of 1 - 2°C higher than the coastal station of Isfjord Radio, which is located on the west coast of Spitsbergen and is influenced by more maritime climate (Hanssen-Bauer et al., 1990; Førland et al., 1997).

The average air temperature in the Arctic and therefore Svalbard has been rising over the past two decades. In fact the rate of surface air temperature increase in the Arctic has more than doubled over the last two decades, compared to any other region on Earth (IPCC, 2019). This amplified temperature change in the Arctic is called "Arctic Amplification" and may be due to feedback mechanisms from decrease in snow and sea ice (Hanssen-Bauer et al., 2019).

The oldest weather station on Spitsbergen was established in 1911 in Grønfjorden, Green Harbour, about 2 km from Barentsburg. Both temperature and precipitation were measured there until 1930 when measurements began in Barentsburg. In 1937, meteorological observations started at Isfjord Radio and twenty years later a weather station was established in Longyearbyen. At Longyearbyen airport meteorological measurements have been carried out since 1975 (Førland et al., 1997).

In order to obtain two long temperature series from Spitsbergen and observe the long-term variation in the temperature, data from Barentsburg have been combined with values from Svalbard airport, to get a comprehensive temperature series for Svalbard airport from 1912 to present. The other series is from Ny-Ålesund with data from 1933 and additional data from Isfjord Radio. The Ny-Ålesund series represents different climate than the Svalbard airport series, a climate which is influenced by open water west of Spitsbergen (Førland et al., 1997).

From 1912 to 1930 an air temperature increase was observed in Svalbard when mean annual air temperature rose from -9°C to -5°C at sea level (Fig. 4) (Førland et al., 1997; Humlum, 2002). Mean annual air temperature decreased from the 1930s to the 1960s and since then the air temperature has been rising significantly (Førland et al., 1997). Precipitation (Fig. 5) has been increasing since 1912 at Svalbard airport for all seasons except winter. For other stations in Spitsbergen (Barentsburg, Isfjord Radio and Ny- Ålesund) the precipitation increase has been significantly more, or about 25% in the last 7-8 decades (Førland et al., 1997).

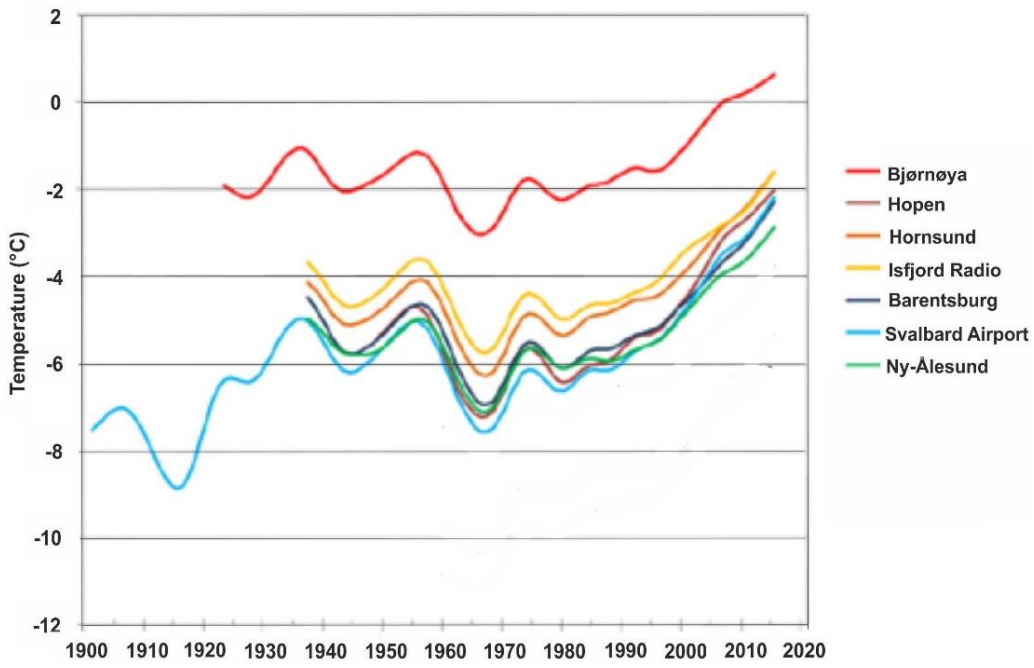

Figure 4. Annual mean air temperature (°C) for weather stations in Svalbard (Hanssen-Bauer et al., 2019).

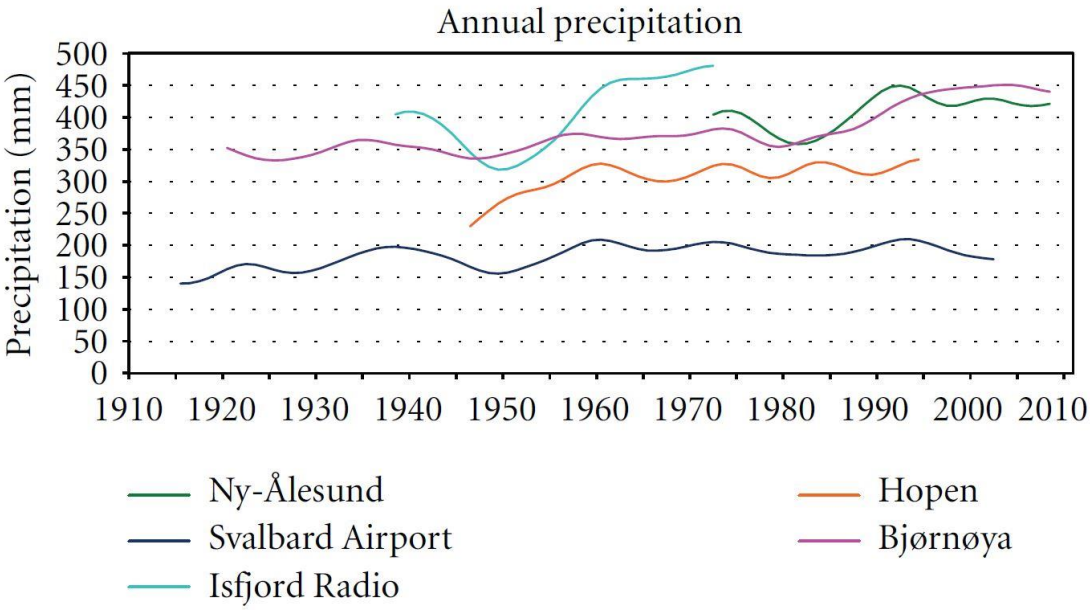

Figure 5. Annual mean precipitation for weather stations in Svalbard (Førland et al., 2011).

2.1.3 Glacial history

Knies et al. (2009) suggested that the initial growth phase of an ice sheet build up over the Svalbard and Barents Sea region occurred in the Pliocene-Pleistocene, or 3.6 - 2.4 Ma. During the last ~ 1 Ma, at least sixteen full scale ice sheet glaciations have been proposed over the Barents Sea and Svalbard, although this number is not fully reliable (Ingólfsson, 2011). The Svalbard and Barents Sea region is proposed to have been covered by an extensive ice sheet during the Saalian glaciation which culminated around 130 ka BP, when the Eemian interglacial period began (Mangerud et al., 1998). Mangerud et al. (1998), described three glaciations during the Weichselian that reached the continental shelf west of Svalbard. The peaks of these glaciations occurred in the Early Weichselian around 110 ka BP, Middle Weichselian around 70 - 50 ka BP and in the Late Weichselian ca. 24 ka BP (Mangerud et al., 1998).

Previous work suggests that the most recent marine-based Svalbard-Barents Sea Ice Sheet started to grow at 32 ka BP. A thin ice shelf advanced towards the western continental shelf edge during the Last Glacial Maximum, until 24 ka BP (Hormes et al., 2013). General warming occurred during the last deglaciation which has been related to changes in Earth's orbit and increase of greenhouse gas concentration (Reusche et al., 2014). As a result, the surface of the Svalbard-Barents Sea Ice Sheet started to thin around 26 ka BP in the northern and western part of Svalbard. Indications from west of Svalbard demonstrate a retreat of the ice sheet from the outer shelf to the inner shelf from 20.5 - 16.85 ka BP (Hormes et al., 2013). Marine sediment sequences show that the marine-based ice sheet became ungrounded and floating between 24 and 18 ka BP. From 15 to 14 ka BP, the deglaciation continued at a faster rate than before and the mouths and outer parts of Isfjorden, van Mijenfjorden, Kongsfjorden and Hinlopenstretet experienced deglaciation (Hormes et al., 2013).

The general warming during the deglaciation was interrupted by an abrupt cold event, the Younger Dryas cold period (12.9 - 11.7 ka BP) (Reusche et al., 2014). By that time, the ice sheet had retreated significantly and fjords had continued to deglaciate inwards until the ice was restricted to fjord-valley glaciers (Fig. 6A) (Farnsworth et al., 2020). It is still debated how valley glaciers in Svalbard responded to the Younger Dryas cold period, whether they advanced or retreated (Mangerud and Landvik, 2007; Hormes et al., 2013; Reusche et al., 2014). Farnsworth et al. (2020) suggested that fjords in Svalbard, including Isfjorden, were half-way deglaciated by 11.6 ka BP and 75 % ice free at 11.3 ka BP (Fig. 6B).

The Holocene is divided into three stages, Early, Middle and Late Holocene which represents the time from 11.7 - 8.2 ka BP, 8.2 - 4.2 ka BP and 4.2 ka BP to present, respectively. The Late Holocene is additionally divided into three periods which will be used in this study, Neoglacial (4.2 ka BP - 1920 AD), Little Ice Age (LIA, 1250 - 1920 AD) and Post-LIA (1920 AD - present) (Farnsworth et al., 2020).

The climate in Svalbard during the Early Holocene (11.7 - 8.2 ka BP) has been described as exceptionally warm. Thermophilous marine molluscs suggest that summer temperatures were 2°C warmer at 11.1 cal. ka BP than at present and 6°C warmer between 10.0 and 9.1 cal. ka BP (Mangerud and Svendsen, 2018). Consequently, glaciers in Svalbard continued to melt and retreat (Fig. 6). Some cirque glaciers disappeared entirely and marine-terminating glaciers retreated onto land (Svendsen and Mangerud, 1997; Farnsworth et al., 2020). Despite the ongoing warming during the Early Holocene, there are many indications for readvances of cirque, valley and outlet glaciers during this period in Svalbard (Salvigsen et al., 1990; Lønne, 2005; Farnsworth et al., 2017; Farnsworth et al., 2018; Larsen et al., 2018; Farnsworth et al., 2022). The majority of these readvances took place between 11 - 10 ka BP (Farnsworth et al., 2020).

There are indications for a cooling climate during the Middle Holocene (8.2 - 4.2 ka BP). Evidence from the marine environment imply a decrease in ocean temperatures from the Early Holocene to the end of Middle Holocene, when the sea surface temperature was close to the present (Hald and Korsun, 2008; Farnsworth et al., 2020). Despite this general cooling from the Early Holocene to the Middle Holocene, the climate was still warmer than present, until the latter part of the Middle Holocene, ca. 4.7 cal. ka BP, when the air temperature reached similar to modern levels (Mangerud and Svendsen, 2018). Some glaciers in north Spitsbergen have been described at their Holocene glacier minimum around ca. 7 cal. ka BP, when they retreated to innermost fjord position and onto land (Allaart et al., 2020), while some valley and cirque glaciers on western Spitsbergen are proposed to have melted entirely away during this time (Svendsen and Mangerud, 1997; Fjeldskaar et al., 2018). However, several ice caps on Nordaustlandet and in the east and south Spitsbergen are suggested to have survived the Middle Holocene warm climate (Fjeldskaar et al., 2018).

The Neoglacial was a period of air temperature decrease and ocean cooling around Svalbard during the Late Holocene. Increase in sea-ice cover and ice rafted debris (IRD) observed during this period suggests a cooling climate (Farnsworth et al., 2020). Glaciers in Svalbard readvanced as a response to this cooling, both during the Neoglacial and during the LIA (Werner, 1993; Svendsen and Mangerud, 1997; Reusche et al., 2014). The cooling intensified around 4 cal. ka BP and records demonstrate glacier growth as early as that (Miller et al., 2017; Mangerud and Svendsen, 2018). Glaciers in Svalbard have been experiencing negative mass balance with ice thinning and marginal retreat since the end of the Little Ice Age in the beginning of the 1900s (Nuth et al., 2007). Extrapolation of the volume loss has indicated that some valley glaciers in Svalbard will disappear in the next few decades (Holmlund, 2021).

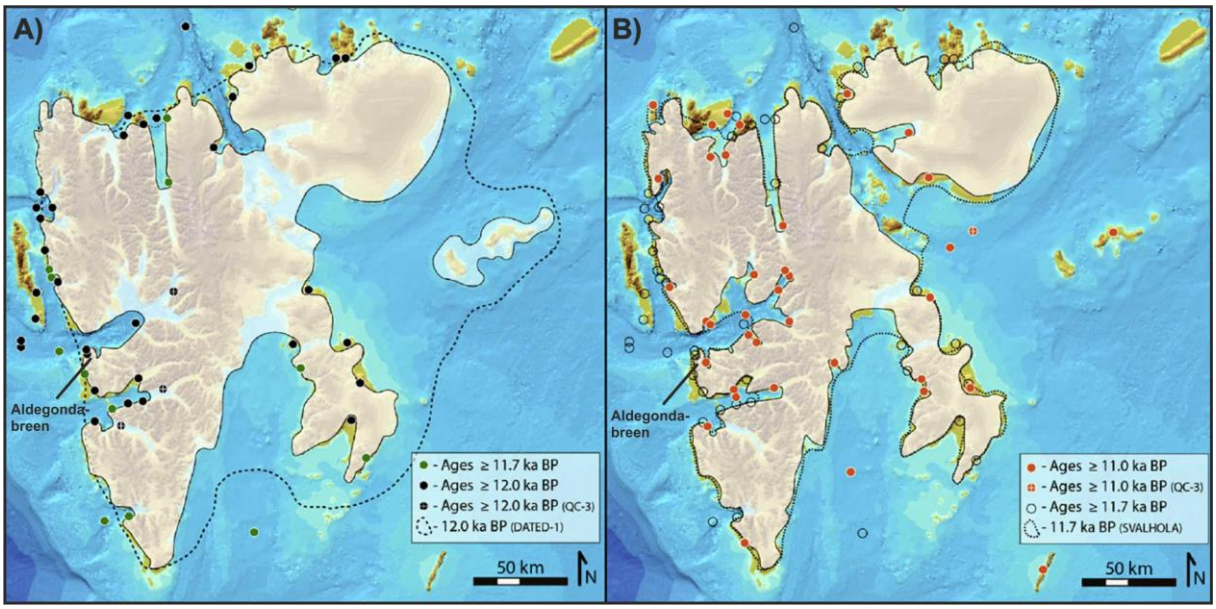

Figure 6. Ice cover over Svalbard during transition from Late Glacial into the Early Holocene. A) The regional ice cover in Svalbard from 12.0 ka BP to 11.7 ka BP. The dotted line demonstrates the ice around 12.0 ka BP and the semi-transparent white polygon demonstrates the regional ice cover at 11.7 ka BP. B) The map indicates the ice marginal retreat between 11.7 and 11.0 ka BP. The dotted line is the ice margin at 11.7 and the white semi-transparent polygon at 11.0 ka BP. Map modified from Farnsworth et al. (2020).

2.1.4 Holocene relative sea level change

Relative sea level since the last glaciation has been studied all over Svalbard (Forman et al., 2004). Relative sea level curves have been constructed for many regions in Svalbard which demonstrate a great variability from one location to another (Fig. 7). The reason for the variability is the isostatic uplift of the land which is controlled by the ice cover thickness during the last glaciation, and duration and timing of the last deglaciation (Forman et al., 1987; Sessford et al., 2015). Sea level curves show the range for the elevation of postglacial marine limits in Svalbard. The range is from around 20 m a.s.l. in south Spitsbergen to more than 100 m a.s.l. on Kong Karls Land in east Svalbard (Fig. 7) (Forman et al., 2004; Sessford et al., 2015; Schomacker et al., 2019).

A new study by Farnsworth et al. (2022) from Grønfjorden in western Spitsbergen suggests that rates of glacioisostatic emergence during the Younger Dryas (YD) were at least three times greater than previously thought. They propose that the relative sea level in Grønfjorden dropped at least 9 m, from >52 m a.s.l. to below 43 m a.s.l., in 600 years, from 12.8 and 12.2 ka BP, which corresponds to minimum 1.5 m/100 yr. However, this is only the minimum emergence rate and they suggest that it may have been up to 3 m/100 yr during this time (Farnsworth et al., 2022).

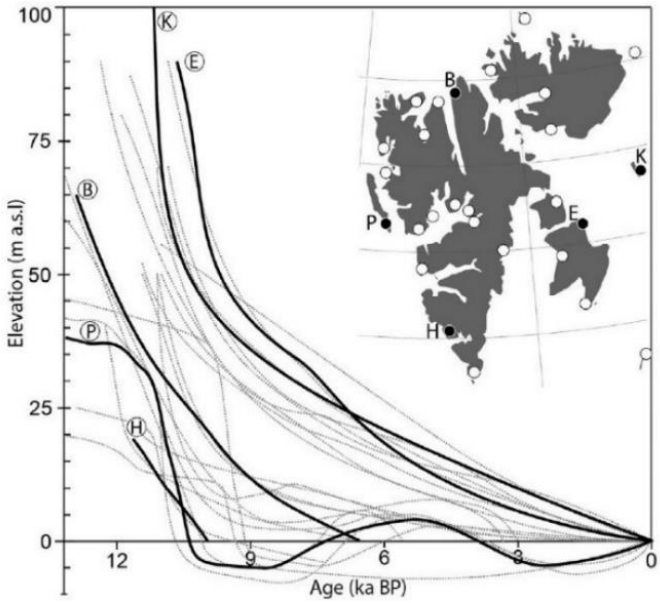

Figure 7. The plot shows variability in postglacial relative sea level from Svalbard. The sea level curves which have been highlighted in bold are: (P) Prins Karls Forland, (H) Hornsund, (B) Bangenhuk, (E) Edgeøya and (K) Kong Karls Land (Farnsworth et al., 2020).

The greatest isostatic uplift during the last 11.7 ka BP in Svalbard has been described from the Early Holocene. In Brøggerhalvøya on western Spitsbergen, the rate was around 2-3 m/100 yr during this period (Forman et al., 2004) and this rapid emergence of the land has been observed in other sites on western Spitsbergen including Erdmannflya and Bohemanflya (Salvigsen et al., 1990), and southern Prins Karls Forland (Forman, 1990). Throughout the Middle Holocene, the rate of the glacioisostatic uplift decreased and it has been suggested that the Middle Holocene sea level was similar or slightly higher than the present level (Forman et al., 2004). The northern and western coast of Svalbard are suggested to have exhibited a transgressive-regressive cycle during the Middle Holocene (Forman, 1990). Studies have demonstrated that the glacioisostatic uplift further decreased throughout the Late Holocene (Farnsworth et al., 2020).

2.2 Study area: Aldegondbreen

The largest fjord system of Svalbard is Isfjorden which extends from the west coast of Spitsbergen into the centre of the island. The fjord is oriented northeast-southwest, is around 100 km long, and 425 m deep. The Isfjorden system contains thirteen tributary fjords and bays, among these are Billefjorden and Sassenfjorden in the northeast, Adventfjorden in the southeast and Grønfjorden in the southwest (Forwick and Vorren, 2010). Numerous valley glaciers are located in the fjord system, with nine terminating into the fjord as tidewater glaciers. The fjord system has, however, the least glacier coverage on Spitsbergen, only about 40%. Both Arctic-type water and Atlantic Water from the West Spitsbergen current flow into the mouth of Isfjorden (Forwick and Vorren, 2009).

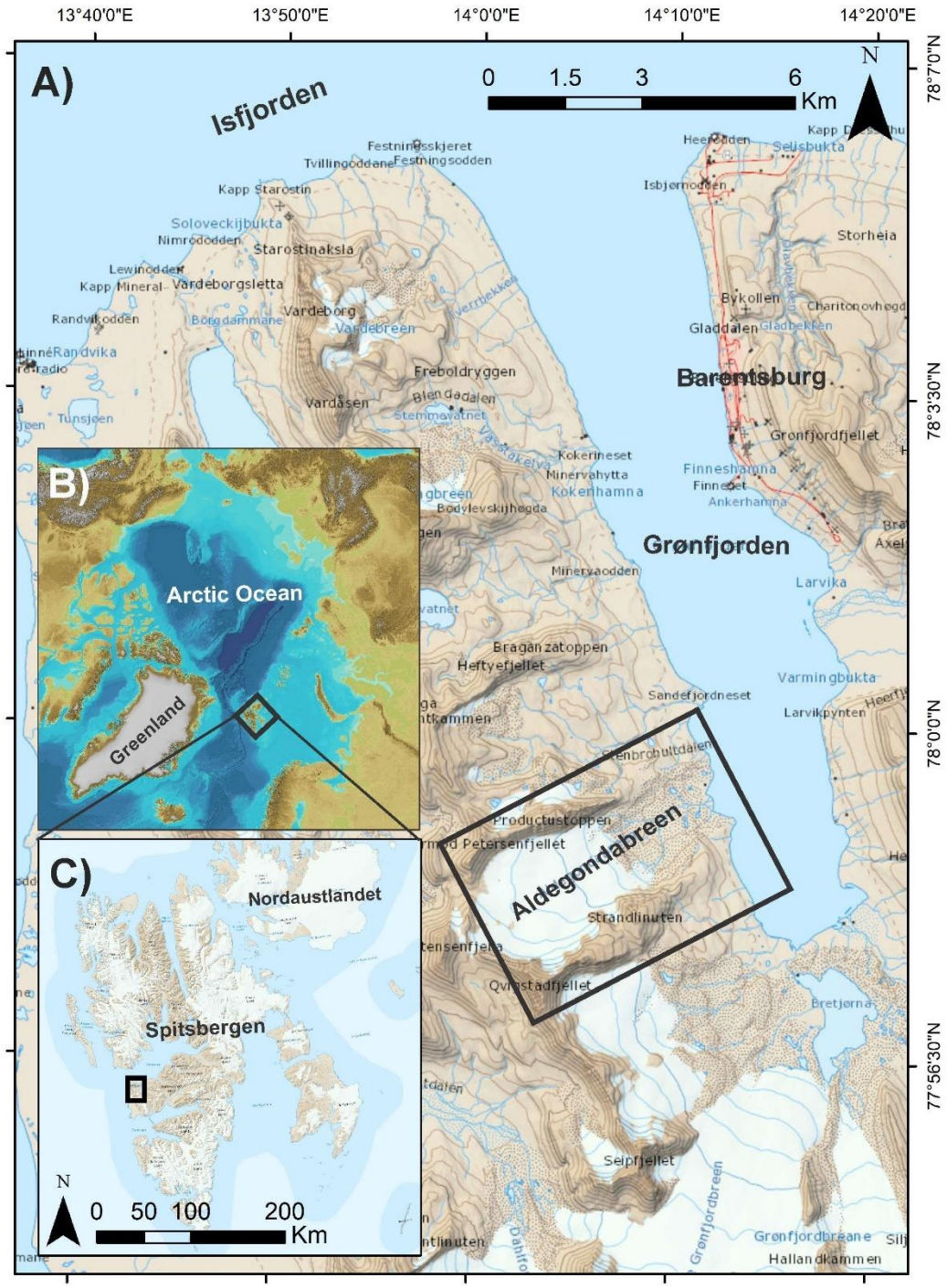

Figure 8. A) Topographic map of Grønfjorden with Aldegondabreen marked by black box. Base map modified from TopoSvalbard (2021) provided by the Norwegian Polar Institute (2021b). B) Location of Svalbard in the North Atlantic. Base map modified from IBCAO (Jakobsson et al., 2012). C) Location of the study area and Aldegondabreen, marked by black box, on the southwestern part of Spitsbergen. Base map modified from TopoSvalbard (2021).

Grønfjorden, is situated near to the mouth of Isfjorden in the south (Fig. 8A). The fjord is around 16 km long and has an NNW - SSE orientation. The fjord is widest in the north, around 6 km, and gets narrower to the south where it is ~2 km. The deepest part of the fjord is where it opens to Isfjorden in the north, around 170 m, and the depth decreases in the southern part where it is 50 m (Zhuravskiy et al., 2012). Five valley and cirque glaciers are located in Grønfjorden today. Those are Vardebreen, Vøringbreen, Aldegondabreen and Vestre and Austre Grønfjordbreen. Barentsburg, a Russian mining town, is situated on the eastern side of Grønfjorden. Mangerud et al. (1992) proposed that Grønfjorden was deglaciated prior to 11.5 cal. ka BP and that the postglacial marine limit at the mouth of Grønfjorden is ~70 m a.s.l. However, a new study from the Heftyebreen moraine in Grønfjorden suggests ice-free marine conditions in the fjord as early as 13.0 - 12.9 cal. ka BP or ca. 1.5 ka earlier than previously thought (Farnsworth et al., 2022). In inner Grønfjorden the highest raised marine deposit is situated around 52 m a.s.l., yet the relative sea level in the inner fjord is suggested to have been higher than 52 m a.s.l. during deglaciation (Mangerud et al., 1992; Farnsworth et al., 2022).

Aldegondabreen (~77°58'N, 14°04'E) is a small valley glacier, 2.6 km long and 2.1 km wide, located on the western side of Grønfjorden, Svalbard (Fig. 8A). The glacier extends from 200 - 600 m a.s.l. and covers around 5.7 km^2 (2019) (Holmlund, 2021). Steep mountains surround the glacier which is oriented northeast-southwest with an ice-flow to the northeast. Three main melt water streams emerge from the glacier front, two close to the northern glacier wall and another near the southern wall. These streams converge further down in the forefield where they flow in a braided meltwater river into the fjord, forming a fluvial outwash fan at the coast.

Aldegondabreen was surveyed in 1974/75 with a helicopter-based radio-echo sounder. The results revealed a body of ice with two-layered polythermal structure (Macheret and Zhuravlev, 1982; Navarro et al., 2005). In 1990, results from a study of Aldegondabreen demonstrated that the average thickness of the glacier was 73 m. In the same study, temperate ice with an overlying cold surface layer was observed in the southern part of the glacier, where it was thickest (Navarro et al., 2005). The glacier still had a small temperate core in 2017, demonstrated by unpublished radar data from the University Centre in Svalbard, however it has been decreasing rapidly (Holmlund, 2021).

Aldegondabreen has retreated drastically since the end of the LIA (Fig. 9) (Navarro et al., 2005; Holmlund, 2021). Aerial images from 1910/11 (Fig. 9) show that the glacier was a tidewater glacier terminating in the fjord and around 5 km long. Since then, the glacier has halved its length and surface extent (Holmlund, 2021). Holmlund (2021), demonstrated the retreat of the glacier from 1910/11 to 2016. He used photogrammetric analyses of photographs from 1910 and 1911 of Aldegondabreen to reconstruct the past shape and size of the glacier. Comparing that data with recent aerial imagery and satellite data from Aldegondabreen, he found that the glacier experienced around a 79% decrease in volume from 1910/11 to 2016. Comparison of elevation data for the study period revealed a volume loss rate of around 10.1×10^6 m^3/yr. By extrapolating the rate of volume change Holmlund (2021) proposed that the glacier may disappear within 30 years.

Other studies of Aldegondabreen include investigations of its hydraulic system, which have shown that the glacier contains a system of well-developed caves and englacial channels (Navarro et al., 2005). A master study by Kirkebøen (2018) focused on Aldegondabreen's glacial history since the Little Ice Age maximum extent, where a geomorphological map was produced of the whole forefield. A study of a sharp-crested ridge in the Heftye-catchment, a valley adjacent to Aldegondabreen in the north, has suggested that a surge event from Aldegondabreen prior to 12 ka BP, formed the ridge (Kokin and Mavlyudov, 2020). However a new study by Farnsworth et al. (2022) concludes that the ridge was formed as a moraine in a glacier readvance from Heftyebreen from 12.8 - 12.2 cal ka BP.

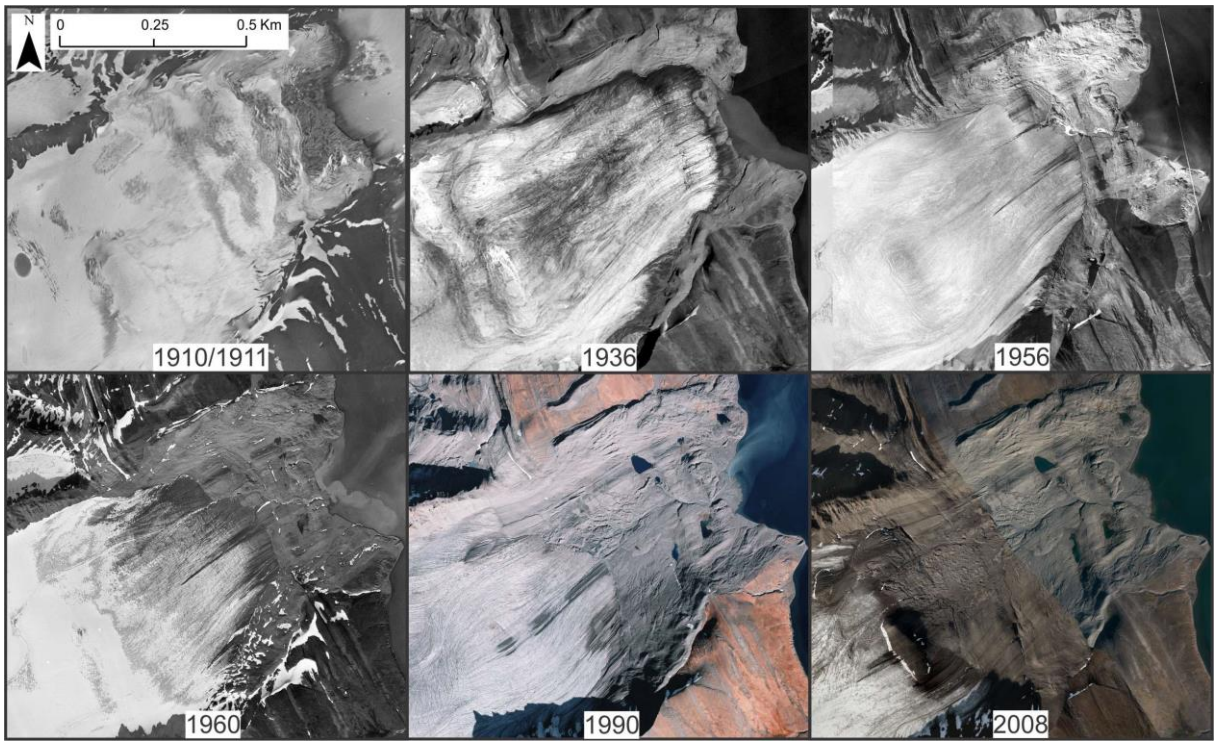

Figure 9. Aerial images of Aldegondabreen from 1910/1911, 1936, 1956, 1960, 1990 and 2008 demonstrating the retreat of the glacier since the end of the LIA. The images were provided by the Norwegian Polar Institute and processed by (Holmlund, 2021).

2.2.1 Bedrock geology

The bedrock surrounding Aldegondabreen is from upper Palaeozoic and Mesozoic time (Fig. 10) (Norwegian Polar Institute, 2021a). Western Spitsbergen, including the area around Aldegondabreen is situated within the West Spitsbergen Fold Belt, where the bedrock was affected by folding and thrusting in an east-northeast direction during the early Eocene (Dallmann, 2015). As a result, the bedrock is characterized by steep dipping and vertical beds.

The oldest bedrock surrounding Aldegondabreen is from the Carboniferous which consists of carbonate rocks such as limestone and dolostones, evaporites such as gypsum, and clastic sedimentary rocks; conglomerates, sandstone, siltstones and shales (Dallmann, 2015). Aldegondabreen is currently resting on top of bedrock from the Permian. It is composed of

marine clastic rocks, such as sandstone, siltstone and shale which are often fossil-rich, and deposits which contain abundant silica, as chert and siliceous shale. These rocks form hard layers which are not easily weathered or eroded (Hjelle et al.,1993; Dallmann, 2015; Norwegian Polar Institute, 2021a). The bedrock gets younger towards the northeast where the forefield of Aldegondabreen rests on top of Triassic strata. The westernmost part of the Triassic bedrock consists of soft shales which are susceptible to weathering and erosion. Eastwards, the Tvillingoddane formation forms two promontories in the north at the coast of Isfjorden. This formation is composed of harder siltstone and sandstone. These harder sedimentary rocks penetrate the forefield of Aldegondabreen with a northwest-southeast direction. Layers of calcareous sandstone occur further east, among the Triassic strata, which have been folded and faulted to a high degree (Hjelle et al., 1993). Soft and easily folded, dark grey and black shales underlaid by conglomerate, represents the Jurassic strata (Hjelle et al., 1993). The youngest bedrock surrounding Aldegondabreen is from the Cretaceous. The strata consist of marine sandstone and siltstone, and dark shale (Hjelle et al., 1993).

2.2.2 Meteorological observations

The average annual surface air temperature in Barentsburg demonstrates overall warming since 1911 (Karandasheva et al., 2021). The annual surface air temperature started to rise around 1910. A cooling period was observed from around 1940 to ca. 1970, whereafter air temperature rose again. Since 1990, warming has been increasing at a fast rate (Karandasheva et al., 2021). The mean annual air temperature for the period of 1931 - 1960 was -4.8°C. From 1961 - 1990 mean annual air temperature decreased to -6.1°C as a result of the cold period in the 1960s. The mean annual air temperature for the last 30 years, from 1991 - 2020, was -3.8°C (Karandasheva et al., 2021). Annual precipitation in Barentsburg (ca. 525 mm) is almost three times higher than at Svalbard airport, only 35 km away (Førland et al., 1997; Coulson et al., 2013). The annual mean value for surface water temperature in Grønfjorden increased by around 1°C from 1970 to 2008, from ca. 0°C to 1°C. Grønfjorden also experienced a trend towards less severe sea ice condition over the period from 1982 to 2012 (Zhuravskiy et al., 2012).

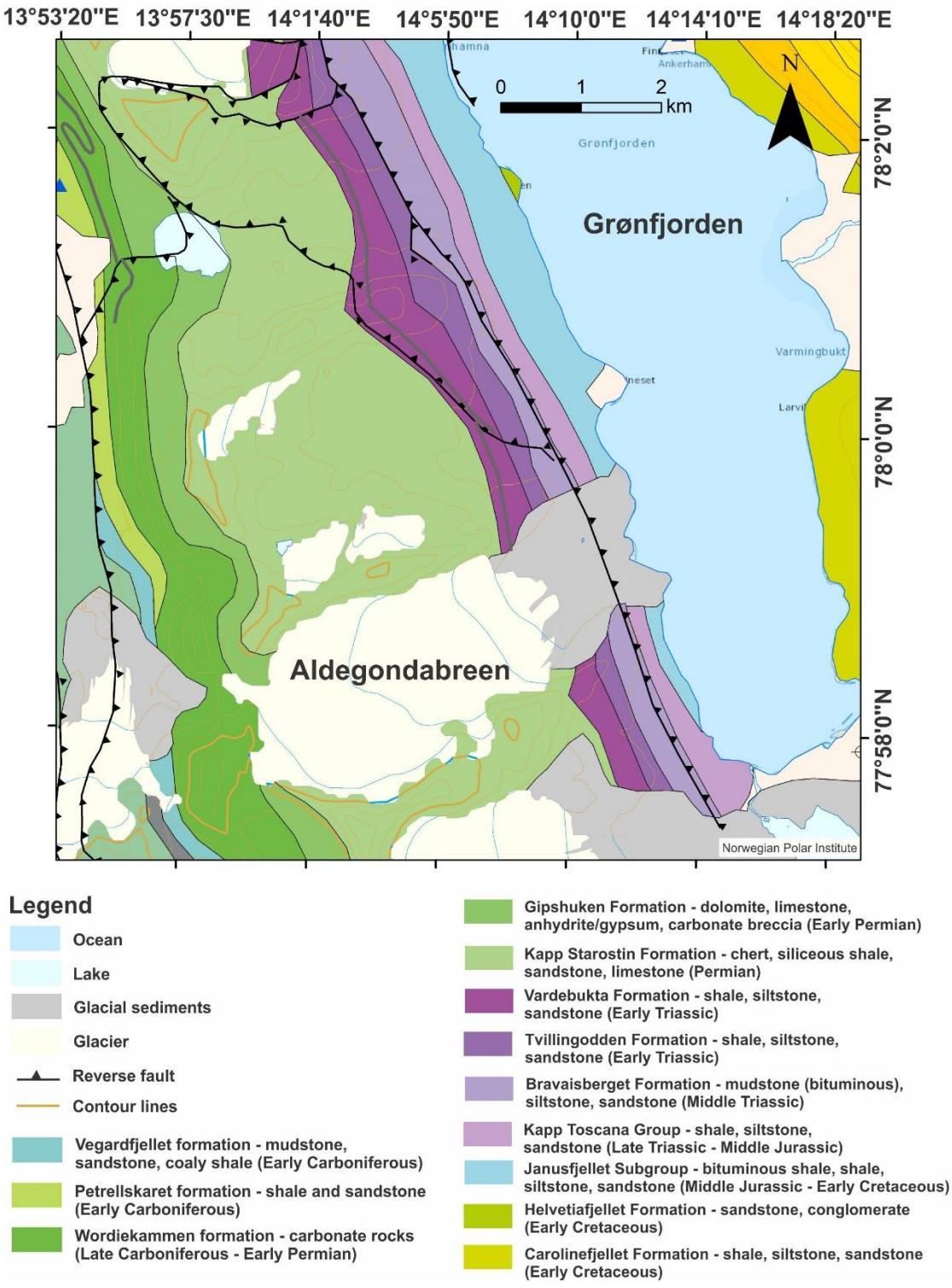

Figure 10. Bedrock map of the area surrounding Aldegondabreen in Grønfjorden. Base map modified from Svalbardkartet (2021) provided by the Norwegian Polar Institute (2021a).

3 Methods and Material

3.1 Methods

The glacial history of Aldegondabreen since around AD 1850 has been described and documented in written historical sources and in old aerial photographs (Dunér et al., 1867; Holmlund, 2021). Taking these historical sources into consideration, it is clear that the glacier has undergone drastic transformation since the end of the LIA, from a tidewater glacier calving into the sea (Holmlund, 2021) to a retreating land-terminating valley glacier. The forefield of Aldegondabreen has undergone significant erosion by glacial meltwater since the retreat of the LIA extent of the glacier. This has led to natural exposure of many sedimentary successions around the forefield, revealing archives of the glacial history of Aldegondabreen. The forefield of Aldegondabreen is therefore an ideal field site to investigate the Holocene glacial and sea level fluctuations in Grønfjorden and in west Spitsbergen.

In order to achieve the aims outlined in section 1.2, a combination of sedimentological and geomorphological methods were used in conjunction with radiocarbon dating.

3.1.1 Fieldwork

Field observations were conducted during three field campaigns: 6 days in August 2019, 2 days in August 2020 and 4 days in August 2021. The Russian settlement, Barentsburg, was used as a field base and a Polarcirkel boat was used for transport to the forefield of Aldegondabreen. Fifteen sites, in the glaciers lower forefield, were studied. However, the main focus was on two ridge-shaped cross-valley landforms in the lower forefield and sedimentary sections within these landforms. Earlier investigations from a UNIS course, AG-210, had demonstrated that these ridges contained bivalve shell fragments within stratified gravelly sediments overlayed by diamict sediments. Studying these landforms and dating the bivalve shells would provide an enhanced understanding of the glaciers forefield. Two sections (Sites A and D) were studied in a large ridge on each side of the active meltwater river and another section (Site G and H) was studied in a smaller ridge in the north-eastern part of the forefield, close to the coast. These sites were selected to document the lateral extent of sedimentary units (Fig. 11).

Three main sites (Sites A, D and G) were targeted with sedimentological logging and sampling. The outcrops were all naturally exposed due to meltwater erosion making them convenient sites to study the sedimentology and stratigraphy. The sections were excavated, cleaned, measured, and documented in the field. Individual stratigraphical units within sections were identified in the field based on their visual properties such as grain size, sorting, clast content, matrix composition, clast and matrix relationship, compaction, nature of contact between individual units and stratigraphical position. Each lithofacies unit was assigned a lithofacies code based on Alexanderson et al. (2018) for simple and effective description in sedimentary logs.

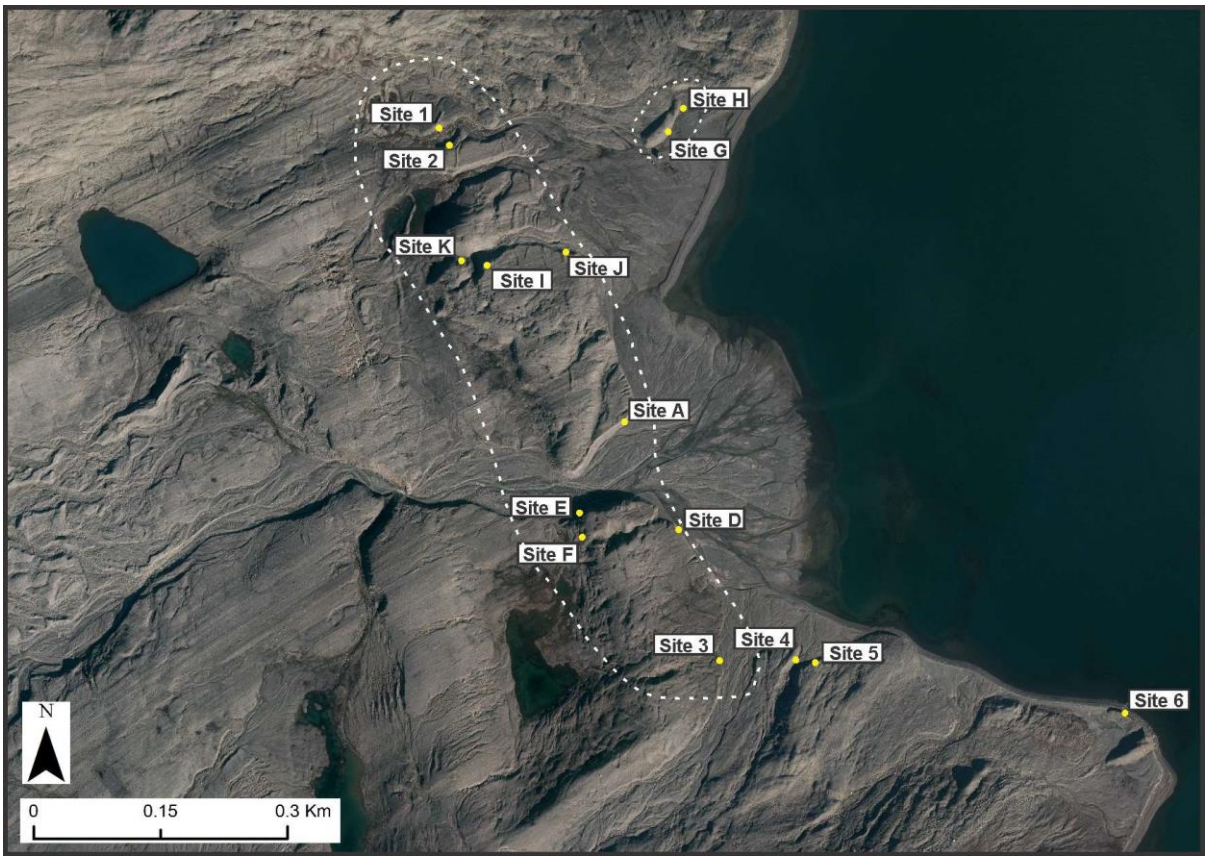

Figure 11. Map of the study sites in the lower forefield of Aldegondabreen. The white dotted lines demonstrate the large and the small sedimentary ridge. Base map from 2008, modified from TopoSvalbard (2021) provided by the Norwegian Polar Institute (2021b).

Bulk sediment samples, weighing around 1 kg, were collected from selected lithofacies units in the forefield in order to analyse the grain size distribution. To measure the clast morphology of selected lithofacies units, 50 clasts were randomly collected from each selected unit and the clasts shape, roundness and texture was measured. Marine mollusc shells and shell fragments were sampled from units within the sedimentary sections for radiocarbon (^{14}C) dating.

The large (Site A and D) and the small ridge (Site G and H) landforms and other study sites were photographed and notes were taken on the geomorphology, location, and orientation. Elevation above sea level was measured with a Nova Lynx 230 - M202 Handheld Digital Barometer - Altimeter.

3.1.2 Grain size analyses

The grain size measurements were done at the University Centre in Svalbard (UNIS). In total ten bulk samples were analysed. They were dried overnight at 105°C and weighed once dried. Subsequently, they were wet sieved to remove silt and clay smaller than 0.063 mm. Following the wet sieving, samples were dried once more overnight and sieved through a sieve stack from 0.063 mm to 20 mm. The sieved fractions were weighed to obtain the exact weight percentages (%) of clay and silt (<0.063 mm), fine sand (0.063 - 0.2 mm), medium sand (0.2 - 0.63 mm), coarse sand (0.63 - 2 mm), fine gravel (2 - 6.3 mm), medium gravel (6.3 - 20 mm) and coarse gravel (>20 mm) (Evans and Benn, 2004).

3.1.3 Clast analysis

Clast morphology was measured for selected lithofacies units on samples of 50 clasts of a massive mudstone lithology. The size range for sampled clasts was restricted to 35 - 125 mm for the long axes (a-axes) (Benn and Ballantyne, 1994; Evans and Benn, 2004). Seven clast samples were taken in total, four from selected lithofacies units and three control samples of known origin: supraglacial, subglacial, and from fluvial outwash fan. The control samples with known origins are used in comparison with samples from deposits of unknown origins.

The shape of each clast was defined by measuring the long, intermediate, and short (A, B, and C) axes. The clasts were assigned to three basic endmembers of clast shape: blocky shapes where $A \approx B \approx C$, elongate shapes where $A >> B \approx C$ and platy shapes where $A \approx B > C$ (Fig. 16A) (Benn and Ballantyne, 1993; Evans and Benn, 2004). The results for the shape characteristics for each sample are represented on ternary diagrams as introduced by Sneed and Folk (1958). On such ternary diagrams, the ratios of B/A and C/A are used to distinguish between the three end members of a clast shape. All clast shape data were plotted in TriPlot (Graham and Midgley, 2000). The C_{40}-Index, defined as the percentage of clasts with a C/A axial ratio less than or equal to 0.4, was calculated for each sample to distinguish blocky from elongated clast shapes (Benn and Ballantyne, 1994; Lukas et al., 2013).

Clast roundness was assigned to a category on the basis of a roundness scale from Powers (1953), (very angular, angular, subangular, subrounded, rounded and well-rounded). The results for each sample are translated into a percentage and presented as a frequency distribution. The RA index, which is the percentage of angular and very angular clasts in a sample, was calculated for each sample (Benn and Ballantyne, 1994). The proportion of clasts within a sample, which has not been edge-rounded during transport, can be estimated with the RA index (Benn and Ballantyne, 1994; Krüger and Kjær, 1999).

3.1.4 Radiocarbon (^{14}C) dating

Following field sampling, selected marine mollusc shells and shell fragments were sent for radiocarbon dating at the Radiocarbon Dating Laboratory at Lund University, Sweden. In total, five samples were dated with high-precision from the forefield of Aldegondabreen (Table 1). Each ^{14}C age was calibrated using the CALIB 8.2 program (Stuiver et al., 2021) applying the Marine20 calibration curve (Heaton et al., 2020) and a local reservoir correction 'Delta R'(ΔR) of -61 ± 37 (Pieńkowski et al., 2021). Radiocarbon dates from other previous studies, which are referred to in the text, are all re-calibrated accordingly. In this study, all ages are presented as calibrated median probability ages in calibrated years before present (cal. a BP, 0 BP = 1950 CE), with 2 sigma error ranges or in kiloyears (ka) BP where appropriate. Calibrated age ranges are presented in Table 1, as both 1σ and 2σ (68% and 95%) probability ranges respectively. Concerning the relatively smooth shape of the probability range curves (Fig. 12) and the time period for the dates in this study the 2σ age range will be used here.

When deciding on the local reservoir correction, it is imperative to consider the closest available correction locality to the sampling site, which is based on a collection of pre-bomb (prior to 1956) specimens with carbonate shells (Coulthard et al., 2010). Furthermore, it is important which species are used for these correction measurements. Some deposit feeding species, such as *Portlandia* and *Nuculana*, build up their shells from old carbon which can lead to problematic ^{14}C ages if they are used for the reservoir correction (Coulthard et al., 2010; Alexanderson et al., 2014).

The local reservoir correction used in this study is from Pieńkowski et al. (2021) where previously published pre-bomb ^{14}C dates from Mangerud et al. (2006) are used for local reservoir correction for west Svalbard, using the Marine20 and the IntCal20 calibration curve. The previously published radiocarbon dates used for the calculations, were collected over a short period of time. This is crucial as marine reservoir age varies constantly with time since the rapid fluctuations in the atmospheric ^{14}C content is attenuated within the large global ocean reservoir. If samples with different collection dates are measured for local reservoir correction, the variability in reservoir ages will additionally contain variation caused by this difference between the ^{14}C content in the atmosphere and in the ocean (Mangerud et al., 2006; Coulthard et al., 2010).

The calibration curve demonstrating the relationship between radiocarbon age and calendar age is not linear (Goslar et al., 1995; Goslar et al., 2000). There are some plateaus in the calibration curve such as at ~12 600, ~10 400, ~10 000 and ~9600 ^{14}C yr BP (Goslar et al., 1995; Gulliksen et al., 1998; Goslar et al., 2000; Walker, 2005). These plateaus correspond to periods of fluctuations in the ^{14}C production rate in the atmosphere and radiocarbon ages which intersect with such plateaus can therefore have affectedly long and low-precision age ranges (Walker, 2005; Levine and Stanish, 2014). However, the calibration curve where radiocarbon age is converted to calendar years is being updated and improved frequently with new studies such as in dendrochronology (Reinig et al., 2020). This has significantly increased the dating accuracy

during periods of ^{14}C plateaus such as the transition from the Late Glacial into the Early Holocene (Hogg et al., 2016; Reinig et al., 2020).

In addition to the five high-precision radiocarbon dates, two samples of shell fragments of blue mussels, *Mytilus edulis*, were sent to the Keck Carbon Cycle Accelerator Mass Spectrometer (AMS) facility at the Earth System Science department at the University of California, Irvine for low-precision estimates of their ages (Table 2). These samples received minimal cleaning and pre-treatment, consequently providing only low-precision ages of the shells. This method is simple and rapid with a lower-cost than the high-precision AMS measurements (Roberts et al., 2013). It has been suggested that this method is suitable for preliminary surveying of ^{14}C dating where many samples need to be dated quickly at low-cost and it has proved to be useful when selecting samples for further high-precision dating (Bush et al., 2013; Roberts et al., 2013). When interpreting the low-precision ages for the samples of *Mytilus edulis* in this study, it is important to not lose sight of the fact that these dates are possibly unreliable when suggesting ages of landforms and lithofacies units in the forefield of Aldegondabreen, as these dates can provide too old or young dates because they are less precise and accurate compared to the high-precision dating. However, results from this rapid dating method have been compared with results from high-precision measurements in order to evaluate the precision of the rapid method. The outcome has demonstrated that the average deviation between these methods for samples younger than 10 ka BP is ~1.8% (1σ) (Bush et al., 2013; Roberts et al., 2013). The samples of *Mytilus edulis*, from the forefield of Aldegondabreen that are dated with the rapid method, are calibrated and presented in the same manner as the high-precision dates from this study with the same local reservoir correction (Table 2).

3.2 Material

3.2.1 Digital Elevation Model (DEM)

A Digital Elevation Model (DEM) with a 2.6 cm resolution (Lundström, 2019), was used to create contour lines and hillshade for the large sedimentary ridge in the lower forefield. The DEM, derived from drone photogrammetry during fieldwork in 2019, was used to obtain accurate elevation above sea level for sedimentary sections and samples within the large ridge. Error analyses were made for the drone DEM by comparing pixel values with a DEM from 2010, provided by the Norwegian Polar Institute (Norwegian Polar Institute., 2014.). The error analyses for the drone DEM revealed a mean offset of 0.046 m with standard deviation of 0.68 m. These differences were observed to be caused by artefacts and actual signals as a result of erosion and deformation of the large ridge.

3.2.2 Aerial images and historical photos

Holmlund (2021), processed historical photos of Aldegondabreen from images by the Norwegian Polar Institute (NPI) by applying noise reduction, sharpening and contrast enhancement filters. These images were utilized in this study together with aerial photographs of Aldegondabreen from the Norwegian Polar Institute to examine the development of the forefield of Aldegondabreen since 1910/1911 to 2019 and to map geomorphological features of the landforms at present time (2019). The photographs used for this study are from 1910/1911, 1936, 1956, 1960, 1969, 1990, 2008 and 2020. Drone images collected in August 2019 by a student, Elias Lundström, on UNIS course AG-210, were used in this study to investigate the surface features of the large ridge and to create a detailed geomorphological map of it.

3.2.3 Software and other data

All data were handled in the WGS 1984/UTM 33 N reference system. Creation of maps and analyses of aerial images and historical photos was done in the ESRI ArcGIS 10.5 software. Composite logs and conceptual models were drawn using the software CorelDRAW 2017. A geomorphological map of the forefield of Aldegondabreen from Kirkebøen (2018) was used in addition to observations and interpretations from this study to create a more comprehensive and detailed map of the large ridge near the coast.

4 Results

4.1 Radiocarbon dating

Five shell samples collected in sediment units in the forefield of Aldegondabreen were radiocarbon dated with a high-precision method with the objective to provide maximum ages for the deposition of the units (Table 1). All radiocarbon dates are obtained from mollusc shell fragments which have been reworked, therefore only providing the maximum age of deposition of the units. Ages range from 9 995 +200/-244 cal. a BP to 11 380 +307/-231 cal. a BP and will be presented within descriptions of their sedimentological units. Relative probability age range curves for all the calibrated ^{14}C ages are presented in Fig. 12 with 1σ (68% probability) and 2σ (95 % probability).

Fig. 13 contains graphs with radiocarbon ages versus calibrated ages for dates with high-precision from this study. Sample A-01 and D-01 are not considered to be affected by ^{14}C plateaus. Sample F-01, G-01 and G-04 intersect with minor ^{14}C plateaus at ca. 9970, 9400 and 9500 ^{14}C yr BP respectively, which must be considered when interpreting the ages. However, the dates do not contain multiple peaks in the age range curves and the minor ^{14}C plateaus are not considered to cause large uncertainties.

The two samples of *Mytilus edulis*, contained shell fragments which were not *in situ* and were taken from the same lithofacies unit. These fragments were dated with low-precision radiocarbon dating (Table 2). The ages are 4 716 +367/-360 cal. a BP and 5 018 +302/-294 cal. a BP.

4.2 Geomorphological map

A detailed terrestrial geomorphological map has been created for the large sedimentary ridge and the area towards the sea, in the lower forefield of Aldegondabreen. The map was created based on a study from Kirkebøen (2018), augmented by observations and interpretations from this study. The mapped area covers approximately 0.3 km^2. The main focus is on the sediment cover and landform assemblages. The landforms are classified by origin; subglacial, supraglacial, glaciofluvial, and coastal. The map is presented in Fig. 14. Other landforms in the forefield of Aldegondabreen, situated outside of the mapped area for this study, have been described and mapped previously by Kirkebøen (2018). These landforms include flutes, medial moraines and hummocky moraines, and eskers.

Table 1. High-precision radiocarbon dates from Aldegondabreen. Dates corrected for marine reservoir age with ΔR = -61±37(Pieńkowski et al., 2021) and calibrated with Marine20 (Heaton et al., 2020) in CALIB 8.2. (Stuiver et al., 2021).

Laboratory No.	Sample No.	Site	Unit	Collection year	Elevation (m a.s.l.)	Latitude (°N)	Longitude (°E)	Sample	Lithofacies	^{14}C (a BP)	±	ΔR (a)	±	Cal. age (a BP) Median	Cal. age (a BP) 1σ	Cal. age (a BP) 2σ
LuS_15144	A-01	A	2	2019	5.9	77° 59.266	14° 11.574	Bivalve frag.	Gcm	10.310	70	-61	37	11.380	11 222 - 11 502	11 149 - 11 687
LuS_15145	D-01	D	1	2019	4.3	77° 59.197	14° 11.719	Bivalve frag.	Gcm	10.230	70	-61	37	11.273	11 145 - 11 392	11 052 - 11 591
LuS_15146	F-01	F		2019	11.3	77° 59.192	14° 11.445	*H. arctica* shell	D(G)mm	9.870	45	-61	37	10.785	10 644 - 10 921	10 560 - 11 055
LuS_15147	G-01	G	5	2019	5	77° 59.450	14° 11.696	Bivalve frag.	D(G)mm	9.290	45	-61	37	9.995	9 893 - 10 123	9 751 - 10 195
LuS_15148	G-04	G	3	2019	2.8	77° 59.451	14° 11.701	Bivalve frag.	SGcs	9.935	45	-61	37	10.881	10 753 - 11 013	10 645 - 11 116

Table 2. Low-precision radiocarbon dates from Aldegondabreen. Dates corrected for marine reservoir age with ΔR = -61±37 (Pieńkowski et al., 2021) and calibrated with Marine20 (Heaton et al., 2020) in CALIB 8.2. (Stuiver et al., 2021).

Laboratory No.	Sample No.	Site	Unit	Collection year	Elevation (m a.s.l.)	Latitude (°N)	Longitude (°E)	Sample	Lithofacies	^{14}C (a BP)	±	ΔR (a)	±	Cal. age (a BP) Median	Cal. age (a BP) 1σ	Cal. age (a BP) 2σ
UAL22384	G-LP-01	G	4	2019	3.5	77° 59.451	14° 11.698	*M. edulis frag.*	SGcs	4.620	120	-61	37	4.716	4 523 - 4 871	4 356 - 5 083
UAL22385	G-LP-02	G	4	2019	3.5	77° 59.451	14° 11.698	*M. edulis frag.*	SGcs	4.850	100	-61	37	5.018	4 853 - 5 167	4 716 - 5 312

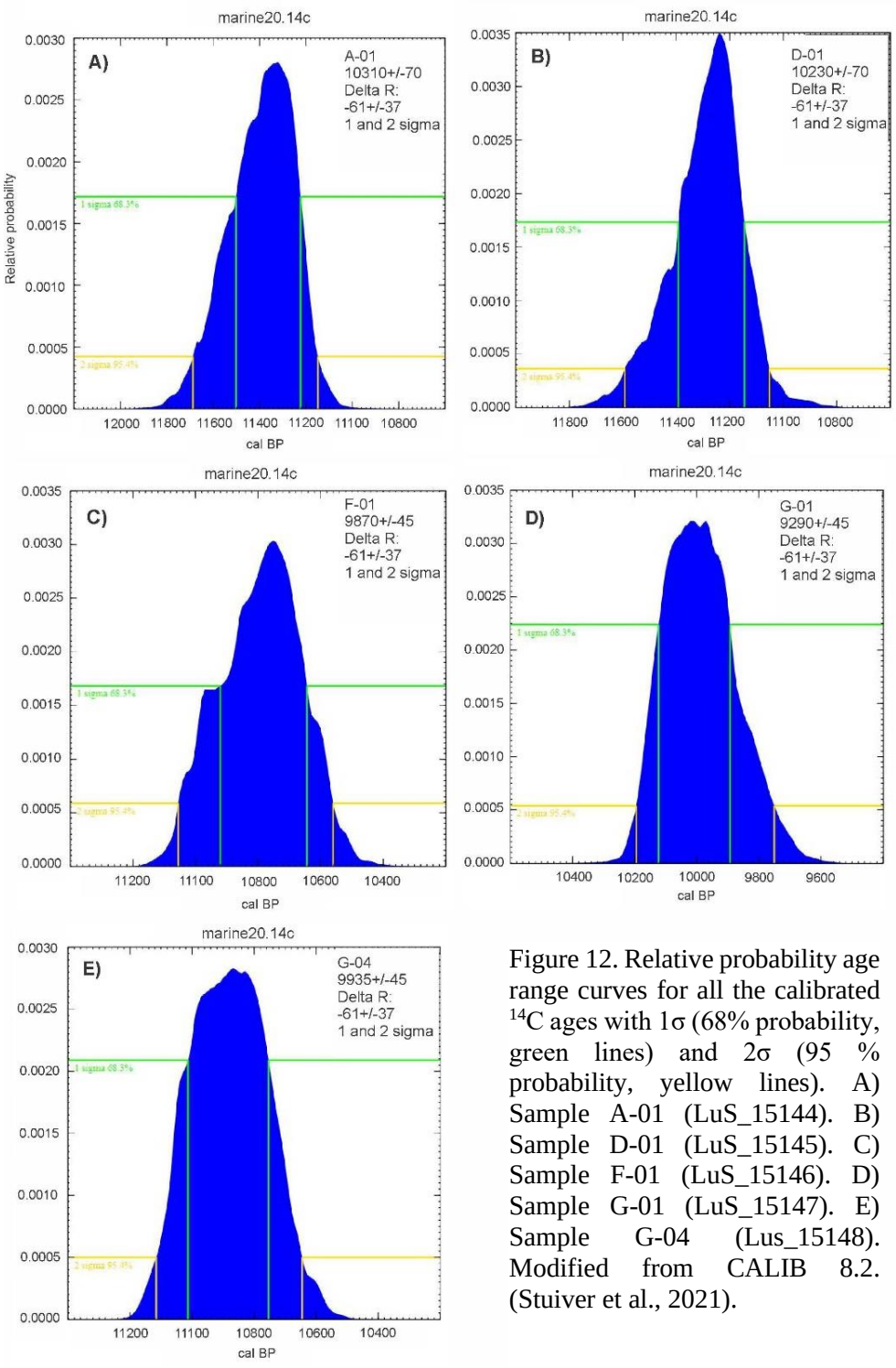

Figure 12. Relative probability age range curves for all the calibrated ^{14}C ages with 1σ (68% probability, green lines) and 2σ (95 % probability, yellow lines). A) Sample A-01 (LuS_15144). B) Sample D-01 (LuS_15145). C) Sample F-01 (LuS_15146). D) Sample G-01 (LuS_15147). E) Sample G-04 (Lus_15148). Modified from CALIB 8.2. (Stuiver et al., 2021).

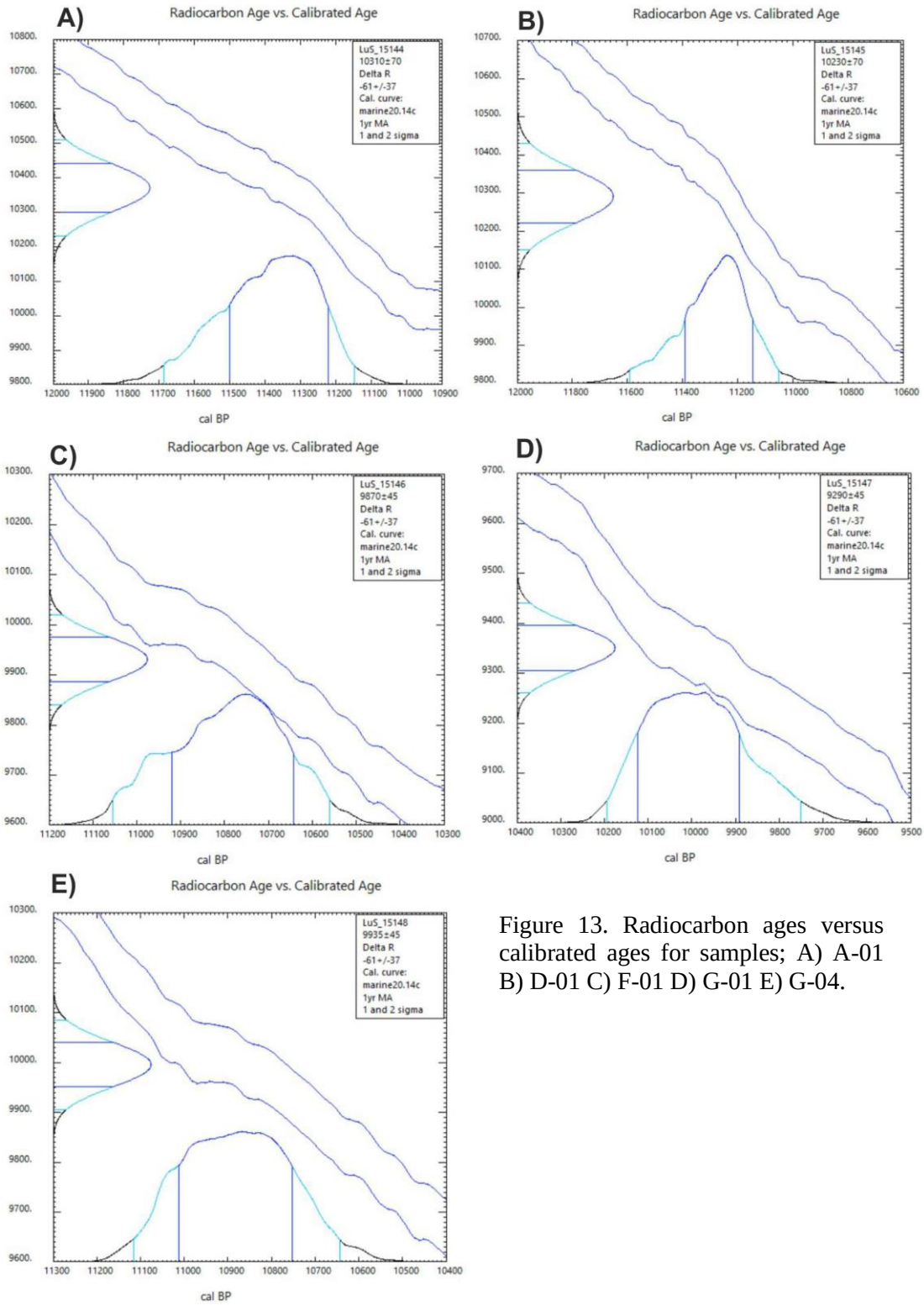

Figure 13. Radiocarbon ages versus calibrated ages for samples; A) A-01 B) D-01 C) F-01 D) G-01 E) G-04.

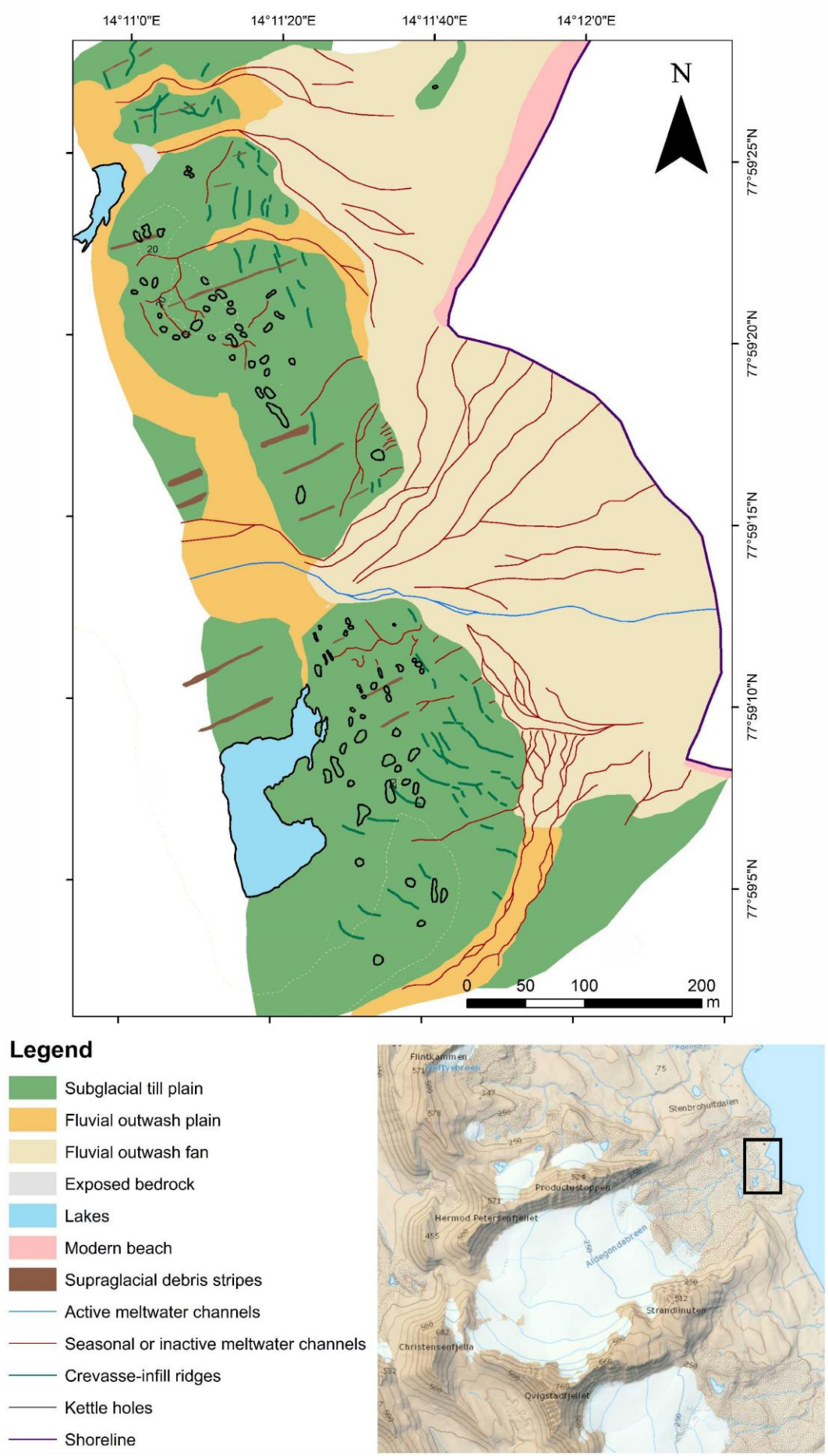

Figure 14. Geomorphological map of the large sedimentary ridge and the area towards the sea, at the forefield of Aldegondabreen. Base map modified from TopoSvalbard (2021) provided by the Norwegian Polar Institute (2021b).

4.2.1 Subglacial landforms

Diamict cover: Subglacial till plain

Description

Diamict sediments cover the majority of the forefield. Meltwater streams and associated outwash deposits, as well as lakes dissect this sediment cover. The diamict is composed of cobble-rich, matrix-supported sediments with some boulder-sized clasts. The matrix is mostly sand to medium and fine gravel. The clasts are mainly subangular to subrounded. Angular clasts, mostly dark shale, drape the surface cover of these deposits in some places. The large sedimentary ridge is mainly covered by these diamict sediments.

Interpretation

This diamict sediment cover is interpreted as a subglacial till plain (Fig. 14). An outcrop near the glacier front observed by Kirkebøen (2018) revealed clast-rich sediments with subrounded clasts, frozen onto the base of the glacier. The glacial ice in the outcrop is very clast-rich and the surface is covered with angular, supraglacial sediments. This suggests that the diamict sediment cover is a subglacial till with subrounded clasts. The angular clasts draping it is interpreted as supraglacial material which settled on top of the subglacial till as the glacier retreated and melted down (Kirkebøen, 2018). Lawson (1981), defined till as "sediment deposited directly by the glacier ice that has not undergone subsequent disaggregation and resedimentation". The main forming processes for a subglacial till are subglacial lodgement, deformation, subglacial melt-out, subglacial meltwater deposits, frictional retardation, and deposition by gravity (Evans et al., 2006; Benn and Evans, 2010). These processes can result in a range of till products such as glaciotectonite, subglacial traction till, deformation till and melt-out till (Evans, 2000; Evans et al., 2006). Based on sedimentological composition of the subglacial till plain observed in sedimentary units (unit 4 site A, unit 3 site D, and unit 5 site G), in stratigraphy sections from the forefield, it is suggested that these sediments are deformation till with inherited structure and sedimentary composition from the underlying sediments (Hart et al., 1990; Evans, 2000).

Bedrock: Exposed bedrock

Description

In two places surrounding the large sediment ridge, bedrock protrudes through the sediment cover. A small exposure of bedrock is situated within an active meltwater channel where it cuts through the ridge. This exposure was too small to be shown on the map. A larger bedrock exposure is situated within an old inactive meltwater channel on the northern part of the ridge (Fig. 14). Both of these exposures exist where fluvial meltwater has eroded the sediments away, uncovering the bedrock underneath. Larger outcrops of exposed bedrock are situated within the forefield, outside of the mapped area. The bedrock is sedimentary rock of siltstone and sandstone with very steeply dipping layers, and it breaks easily apart into smaller fragments.

Glacially scoured and moulded bedrock, and a small roche moutonnée formation were observed outside the study area, in the upper forefield of the glacier.

Interpretation

The exposed scoured and moulded bedrock and the small roche moutonnée formation indicate that the bedrock in the forefield has been shaped by glacial erosion. Historical photos from Aldegondabreen demonstrate that the whole forefield was covered by glacier in 1911 (Fig. 9) and as the glacier retreated the bedrock was exposed. The bedrock surrounding the large sedimentary ridge is situated within meltwater channels indicating that these exposures were more likely uncovered by fluvial meltwater erosion after or during glacial retreat (Brennand et al., 1996).

4.2.2 Supraglacial landforms

Debris stripes: Supraglacial debris stripes

Description

Debris composed of angular material accumulated in stripes, which are less than 50 cm thick, drape the subglacial till cover (Fig. 14). The debris stripes are oriented parallel to the ice flow direction and are deposited on top of other landforms in the forefield. The material within the stripes is of one lithology, mainly clasts of dark shale or light-coloured sandstone, and are therefore very prominent in the field and on aerial images (Fig. 15A). These stripes can be traced continuously from medial moraines melting out of the glacier surface, into the forefield (Fig. 15B). The debris stripes occur in all parts of the forefield, some of them are composed of very coarse debris while others are fine grained. The stripes situated on the large sediment ridge are up to 100 m long and 6 m wide. A clast control sample from a debris stripe located on the modern glacier surface showed a clast shape, C_{40} index of 52% and roundness, RA index, of 100% (Fig. 16C). The RA index demonstrates that the clasts within the debris stripe are all very angular and angular.

Interpretation

Because these debris stripes are both deposited on top of other landforms in the forefield and of angular and unilithological nature, it is suggested that these debris stripes are supraglacial lineations as described by Glasser and Hambrey (2003). The angular debris consisting of a single lithology is interpreted to be supraglacial debris, possibly as a result of a rockfall on to the glacier, transported supra- or englacially before it emerges at the glacier surface as a result of ablation near the snout. When the glacier retreats and melts away the angular debris is released from the ice as stripes in the forefield where it drapes the subglacial till below (Glasser and Hambrey, 2003). Some of the debris stripes can be traced back to their source areas at the valley sides in the ablation zone where rockfall is providing the stripes with debris material.

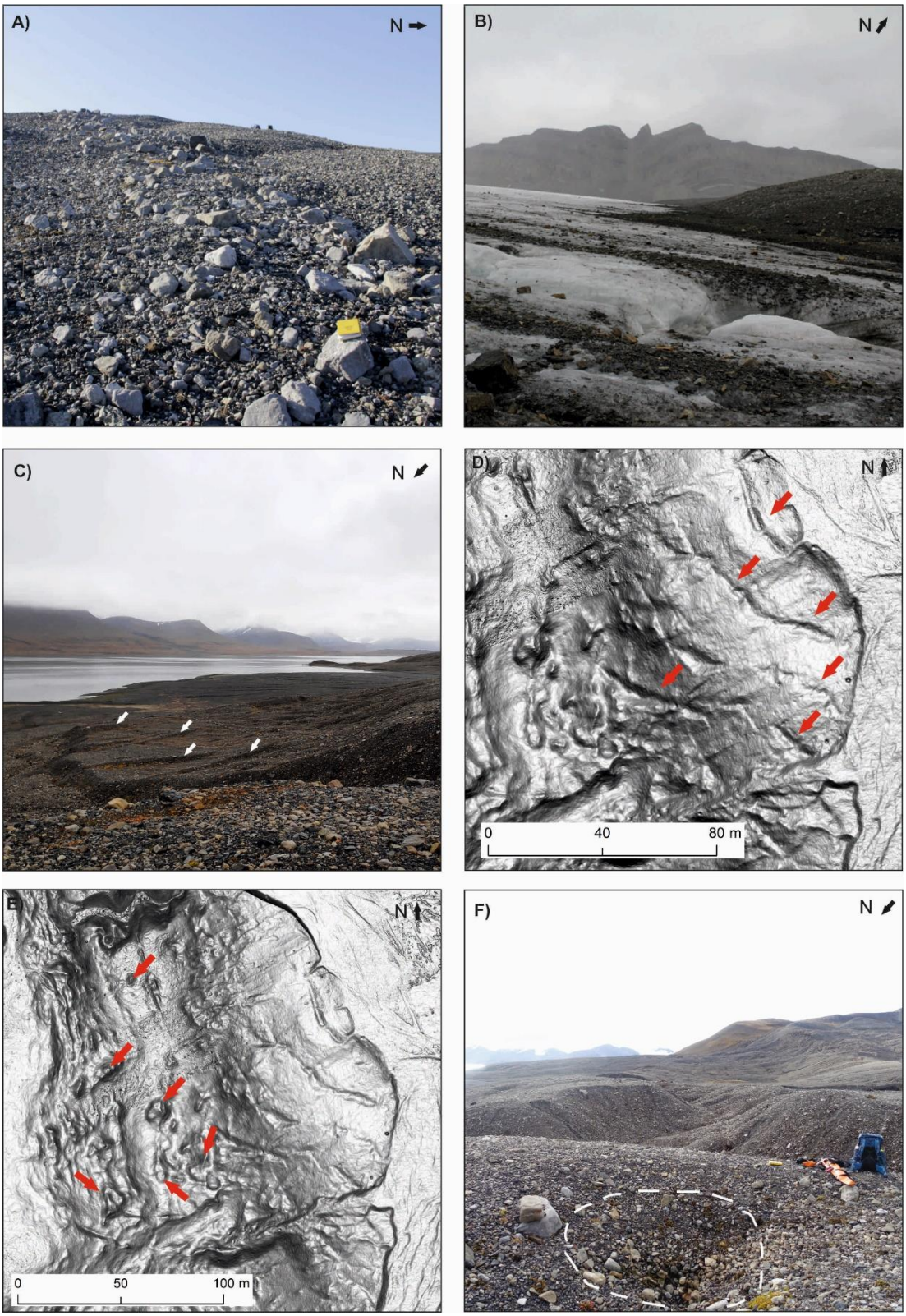

Figure 15. Supraglacial landforms in the forefield of Aldegondabreen. A) A debris stripe consisting of light-coloured, course sandstone. B) Angular medial moraines melting out of the glacier front. C) Crevasse-infill ridges, oriented transverse to ice flow direction, located on the ice distal slope of the large sedimentary ridge. D) Hillshade image of the large sedimentary ridge demonstrating the curvilinear shape of the crevasse-infill ridges. E) Hillshade image showing numerous kettle holes on the sedimentary ridge. F) A kettle hole situated on the large sedimentary ridge. Larger clasts have accumulated near the base of the hole.

Transverse ridges: Crevasse-infill ridges

Description

Sub-parallel transverse ridges are prominent on the large sediment ridge and in the north-eastern part of the forefield (Fig. 14). They occur predominantly on the ice-distal slope of the ridge and are generally oriented transverse to ice flow direction (Fig. 15C). 77 ridges have been mapped on the large sediment ridge. They are up to 45 m long, ~3 m wide and rise up to ~1 m above the surroundings. They are curvilinearly shaped (Fig. 15D). Observations from Kirkebøen (2018), demonstrate that the ridges are composed of gravel and sand, and contain higher concentrations of dark shale than the surrounding material. Unsorted, loosely packed material is also present within the ridges. Two transverse ridges, situated outside the mapped area for this study, drape flutes at a 90° angle (Kirkebøen, 2018).

Interpretation

Kirkebøen (2018) interpreted these ridges to be crevasse infills of glaciofluvial and supraglacial debris, based on the grain size distribution of the sediments within these ridges and their orientation and location on the sedimentary ridge. As the glacier flows over an obstacle, crevasses can form on the lee side where the glacier flows downhill due to tensile stress, which pulls the walls of the crack apart (Benn and Evans, 2010). Supraglacial material can fall into these crevasses, resulting in crevasse infills which will form ridges transverse to ice flow when the glacier melts away. Meltwater can flow into these crevasses and deposit sorted glaciofluvial material (Bennett et al., 2000; Kirkebøen, 2018). The transverse ridges are therefore a result of a supraglacial infill into crevasses influenced by glaciofluvial processes, leaving behind both sorted and unsorted material. The two transverse ridges draping the subglacial flutes support this hypothesis, indicating that the material within the ridges is not a result of subglacial deposition.

Depressions in the subglacial till plain: Kettle holes

Description

Clusters and single depressions with various shape and size were observed on the large sedimentary ridge and on the fluvial outwash plain in front of it (Fig. 15E). In total 80 depressions were mapped (Fig. 14). The landforms situated on the large sedimentary ridge occur predominantly on the ice proximal side of it, within the subglacial till plain. They are up to 26 m long, ~10 m wide and ~2 m deep, and are both U- and V- shaped. No water was observed within them. Some appear with vegetation at the bottom, while others contain larger clasts which have accumulated near the base of the depression (Fig. 15F). Two larger water-filled depressions were observed on the outwash plain in front of the ridge. Old aerial images of the forefield (Fig. 17) reveal that all of these depressions have increased in size with time since they were exposed, after the glacier retreated.

Interpretation

Kirkebøen (2018) interpreted these depressions to be kettle holes. The same interpretation is used here based on the depressions shape and increase in size since exposure. The kettle holes were formed by melting of ice, buried beneath a cover of outwash or till deposits (Maizels, 1977). As the glacier retreats, it can leave behind a stagnant ice terminus or blocks of isolated ice, which have become detached from the major ice body and buried beneath a debris cover. When the ice has melted completely, depressions are left behind. Some of the kettle holes have undergone gravity sorting while the ice was melting from below, seen by larger clasts accumulated at the bottom of the depressions which have slumped or rolled down during subsidence (Kjær and Krüger, 2001). Kirkebøen (2018) observed that the water level in the larger kettle holes lowered during the summer season and she suggested that these water-filled kettle holes were still water fed during the melt season due to snowmelt, rainfall or from groundwater in the forefield.

4.2.3 Glaciofluvial landforms

Outwash plain

Description

The surface material of the outwash plains consists of sorted subangular to subrounded cobbles, gravel and sand which has a gentle down-glacier sloping surface of around 2°. The surface is characterized by networks of inactive and active braided meltwater channels. Longitudinal sand bars appear in some places between channels with some up to 15 m long and 3 m wide.

Interpretation

Due to the network of inactive and active braided channels and sorted material, these plains are interpreted to be glaciofluvial outwash plains. They are formed when braided proglacial streams erode and carry large amounts of bedload and some suspended sediments, which are then deposited by aggradation in these large outwash plains. These outwash plains are generally gently sloping (Krigström, 1962; Benn and Evans, 2010). Bar formation occurs between channels with sorted sand and gravel which are very unstable landforms and may change form and position from day to day (Benn and Evans, 2010).

Fan shaped outwash plain: Fluvial outwash fans

Description

Four outwash fans have been mapped. They build out from the fluvial outwash plain and into the fjord (Fig. 14). The surface of these fan systems is characterised by braided channels, both inactive and active, as on the outwash plains. The surface material on these fans is sorted, from silt to boulders. One out of the four fan systems was active during fieldwork. It is the largest one in the forefield and it dissects the large sediment ridge where meltwater streams have cut

through it before flowing into the fjord.The meltwater streams transport debris into the fjord across the large outwash fan, seen on aerial images by a suspended sediment plume in the fjord, in front of the fan-shaped outwash. A clast sample, taken from the large active outwash fan demonstrates that the clasts are predominately subangular and subrounded with RA index of 0% and C_{40} index of 66% (Fig. 16B). Old aerial images (Fig. 17) show how the meltwater activity has migrated between fans since the glacier retreated. Before 1936, the meltwater activity was limited to the north-eastern most outwash fan. After 1936, the large outwash fan became active and started to build up into the fjord and has since dominated the meltwater activity.

Interpretation

These fan-shaped outwash landforms are interpreted to be the topsets of small deltas that build out into the fjord (Postma, 1990). They are described separately from the outwash plains to underline the different depositional environment. Old aerial images support the delta interpretation, demonstrating how the largest fan-shaped outwash in the forefield of Aldegondabreen has been growing and extending into the fjord with time since the glacier retreated (Fig. 17). The deltas are formed when subaerial meltwater streams transport debris by suspension and bedload into a basin. Once the streams meet the water body, they decelerate and lose their energy resulting in rapid deposition of the sediments they carried (Postma, 1990; Benn and Evans, 2010). With time, the deltas prograde into the water, extending the shoreline.

Active and seasonal or inactive meltwater channels

Description

Numerous channels were observed in the forefield (Fig. 14). Only one channel was active during fieldwork, with water running from the glacier across the forefield following the topography. It cuts into the large sediment ridge before entering the fjord, modifying its shape and eroding it. The channels migrate laterally over the forefield and several of them initiate in a single channel which then spreads out to form a braided system. Four inactive channels are observed to cut into the large sedimentary ridge. They are situated up to 8 m above the fluvial outwash plain below.

Interpretation

The channels are interpreted as meltwater channels (Kirkebøen, 2018). The dry channels are suggested to be inactive or seasonally active meltwater channels. The meltwater has actively reshaped and eroded the forefield since glacier retreat and the channels have migrated across the forefield depending on source location of meltwater from the glacier.

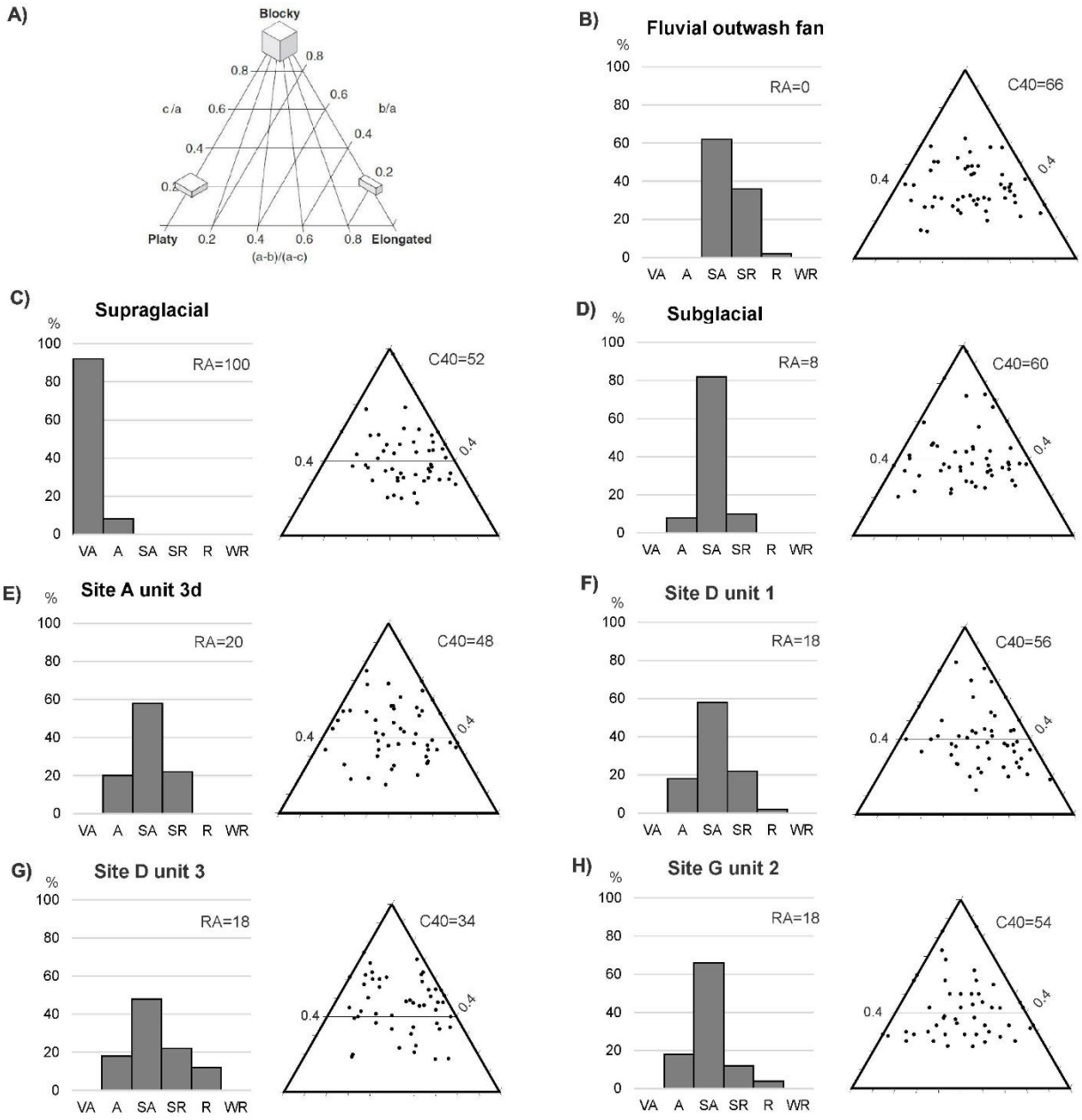

Figure 16. Ternary diagrams for clast shape data and frequency distribution histograms for roundness data. A) Schematic ternary diagram showing axial scales and the three clast shape endmembers. Shape and roundness data of massive mudstone lithology for: B) Control sample from fluvial outwash fan. C) Control sample from supgraglacial environment. D) Control sample from subglacial environment. E) Unit 3d at site A. F) Unit 1 at site D. G) Unit 3 at site D. H) Unit 2 at site G.

An aerial image from 1936 (Fig. 17) demonstrates that while the glacier was retreating, glacial meltwater streams emerged from the glacier in several places onto the large sediment ridge below, cutting into the sediments within it. This can be seen today with the four inactive channels on the ridge. The streams have not had enough time to erode into the base of the ridge, suggesting that the glacier front was only standing on top of the sedimentary ridge for a short period before it retreated further up-valley.

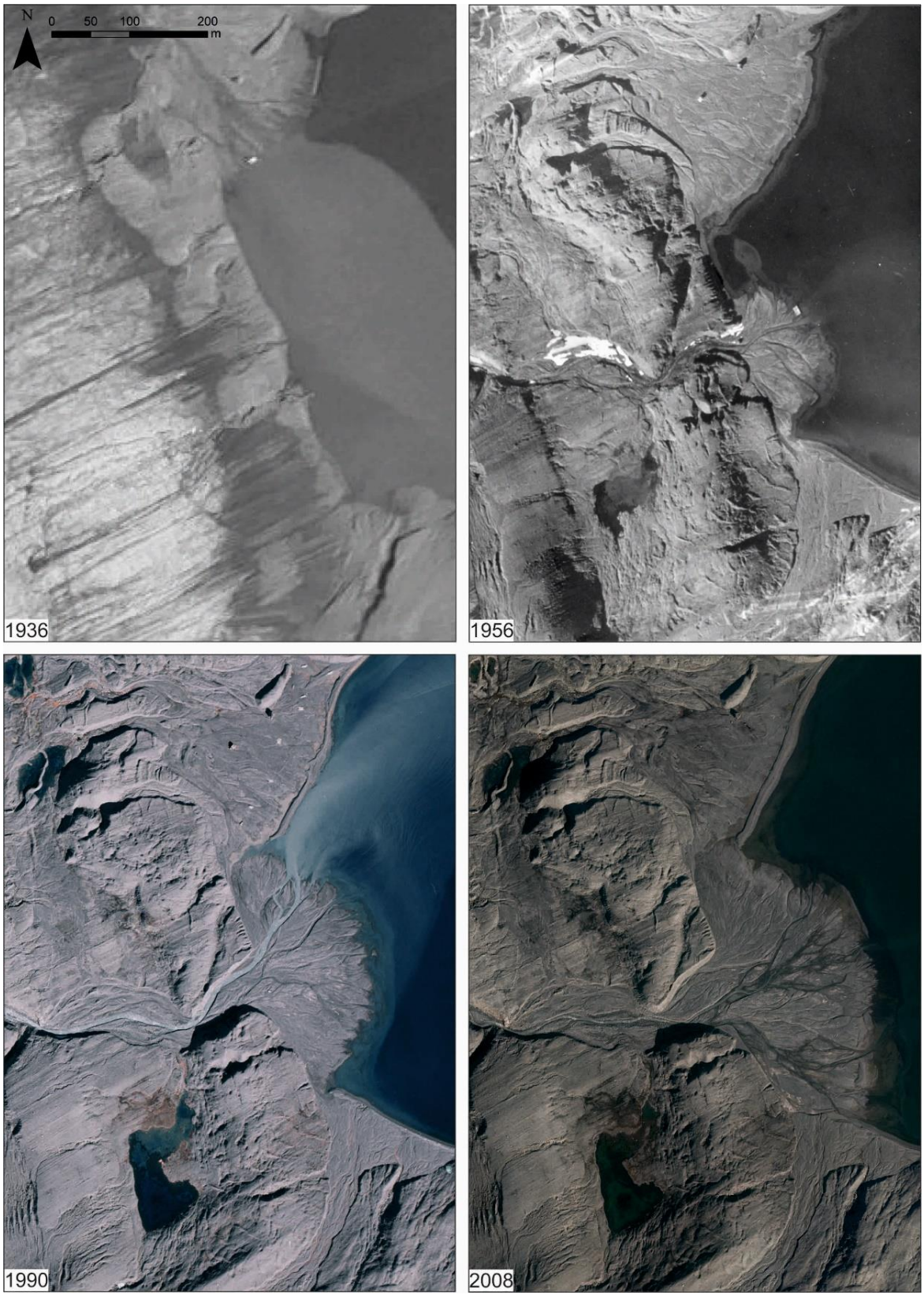

Figure 17. Old aerial images demonstrating the development of the large sediment ridge and the fluvial outwash fan near the shore in the forefield of Aldegondabreen, from 1936-2008. The images were provided by the Norwegian Polar Institute and processed by Holmlund (2021).

4.2.4 Coastal landforms

Modern beach

Description

These deposits consist of sorted, washed gravel and sand with shells and shell fragments, dipping towards the fjord. They are situated along the coastline of the forefield, except where the active fluvial outwash fan meets the fjord.

Interpretation

These deposits are interpreted to be sorted beach material. The beach material is a combination of reworked glacial deposits, transported to the coast with meltwater streams and material deposited on the shore by wave action (Kirkebøen, 2018). This beach material is suggested to be modern, as the beaches are situated at the present sea level. Images of Aldegondabreen from 1911 show that the tidewater glacier extended further into the fjord than the current coastline, indicating that these beach deposits accumulated after the glacier retreated from the coast, after 1911.

4.3 Study sites and sediment lithofacies units

Descriptions of studied sites and lithofacies units in the forefield of Aldegondabreen are presented below together with an interpretation of each unit. Three main lithofacies associations were identified at the main sites A, D and G, and in the minor sections E, F, H, I, J, K, 1, 2, 3, 4, 5, 6. Facies 1; gravel units formed in a shallow glaciomarine environment in a grounding-line fan, facies 2; glaciotectonised gravel units, formed in a subaerial glaciofluvial outwash plain, facies 3; glaciogenic facies, including subglacial till with supra and englacial components and glaciotectonised marine sediments. These lithofacies associations are summarized in the end and the variance within each association is discussed.

4.3.1 Main sites

Site A

Site A is located on the northern flank of the glacial meltwater river (Fig. 11) which flows from the glacier, across the forefield where it cuts through the large sedimentary ridge before it enters the fjord. An exposed sedimentary section, about 100 m long, with a northeast-southwest orientation was documented in detail in one log at the site (Fig. 18A). The sedimentary section is situated in a small terrace that forms from the large sedimentary ridge, on its glacier-distal side (Fig. 18B). The ice-proximal side of the section is more massive and contains a higher concentration of bigger clasts and boulders while the distal part of the section is stratified and contains finer material (Fig. 18C). The surface of the previously mentioned terrace slopes about 5° towards the fjord to the northeast and the surface cover is composed of clast-rich diamict. Particle size ranges from gravel up to boulders of 50 cm. The clasts are mainly subangular to subrounded. The surface is weathered where smaller clasts and fine material have settled into

empty spaces between larger clasts. Two small transverse ridges, which are partly eroded, and debris stripes composed of angular clasts are observed on the surface of the terrace (Fig. 14). Several seasonal or inactive small fluvial channels are found on the terrace and a small kettle hole. No water was present within these landforms during fieldwork. The grain size within the channels and the kettle holes was observed to be finer than in the surrounding area and small vegetation is growing within them. The largest channel extends along the margins between the large ridge and the terrace.

Log A

The sedimentological section which was logged at site A is situated on the fjord side of the ridge. It is 4.7 m high, extending from 4.3 to 9 m a.s.l. The sedimentary section was naturally exposed as a result of erosion from the glacial meltwater river, which flows along it. Fig. 19 demonstrates the erosion of the large ridge at sites A and D, since 1956. The river has been flowing through the ridge, eroding it on each side. Consequently, debris from the upper part of the section has slumped down, forming concave shaped slopes on each side (Fig. 18D). The sedimentary section at site A has preserved its shape since around 1990, and the exposure of the logged slope occurred somewhere between 1990 and 2019 (Fig. 19). The sedimentary section at site A was divided into five stratigraphic units. Unit 1A - 3 all dip at 5° towards northeast (Fig. 20).

Unit 1A

Description

Unit 1A is minimum ~30 cm thick, ranging from 4.3 to 4.6 m a.s.l. It is a massive medium to fine gravel, rich in pebbles which are up to 7 cm. Small bivalve shell fragments are scattered in the unit (Fig. 21A). The unit is sorted and unconsolidated with washed appearance and collapses easily when excavated. No indications for post-depositional sediment disturbance or deformation are found within the unit.

Interpretation

Sedimentological properties, small shell fragments, and the elevation of unit 1A closely resembles unit 1 at site D, which has been dated to a maximum 11.27 cal. ka BP and interpreted as subaqueous grounding-line fan sediments. Because of the similarities between the two units, unit 1A is interpreted in the same way as unit 1 at site D. Unit 1A has also been influenced by wave- or current reworking, indicated by its washed appearance, where finer sediments have been transported away, sorting the sediments, and decreasing the cohesion (Powell, 1984, 1990; Lønne, 2005). These sediments are assigned to lithofacies association 1 (LFA1).

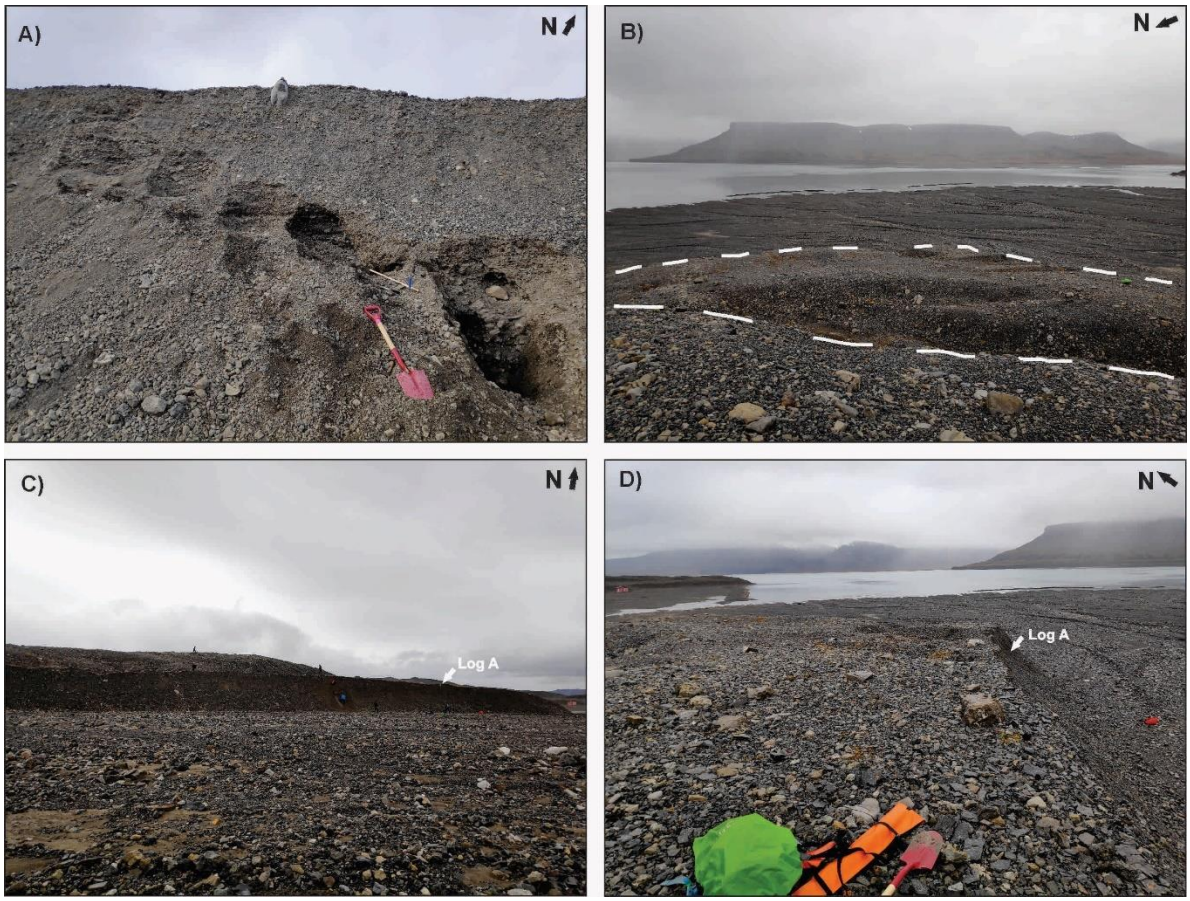

Figure 18. A) The sedimentary section studied at site A. B) The small terrace at site A, which forms from the glacier-distal side of the large sedimentary ridge. C) Overview image of the whole sedimentary section located at site A. D) The sedimentary section at site A, where debris from the upper part of the section slumps down forming concave slopes.

Unit 1B

Description

Unit 1B is a 115 cm thick, massive cobbly gravel. The unit is poorly sorted and unconsolidated (Fig. 21B). The matrix is predominantly composed of coarse sand and medium to fine gravel (Fig. 22). The unit ranges from 4.6 up to ~5.75 m a.s.l. and its lower boundaries are gradual. It contains abundant subrounded, imbricated cobbles which are more prominent in the upper part. Clasts are up to 23 cm in size and their surfaces is draped with thin mud coat. The unit dips 5° towards the fjord, to the northeast. There are no observable evidence of post-depositional sediment disturbance or deformation within the unit.

Interpretation

Because of clast surfaces being draped with mud and the location of the unit in the stratigraphy section, below sediments dated to maximum 11.38 cal. ka BP when sea level was around 43 m a.s.l. (Forman et al., 2004), the unit is suggested to be formed in a subaqueous environment.

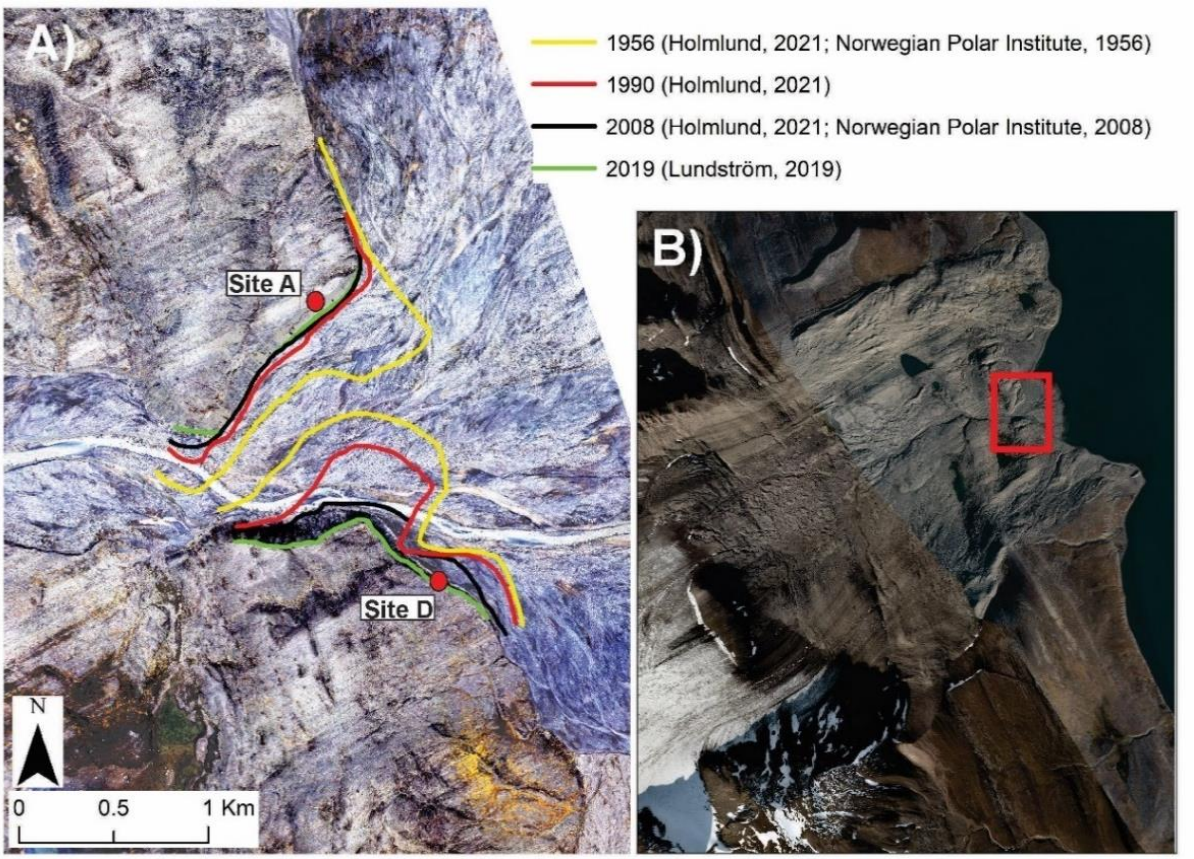

Figure 19. A) Erosion of the large ridge at sites A and D, since 1956. Coloured lines mark the outline of the ridge each year. Image modified from Lundström (2019). B) Location of the erosion site (red square) in the forefield of Aldegondabreen. Image modified from TopoSvalbard (2021) provided by the Norwegian Polar Institute (2021b).

The sediments are interpreted to be deposited in an ice-proximal, shallow glaciomarine grounding-line fan, based on the grain size, gentle dip and dip direction of the unit (Powell, 1990; Lønne, 2005). The unit is more precisely suggested to be formed near the tunnel efflux where the discharge can be very high and fully turbulent, indicated by imbricated cobbles (Powell, 1990). The grain size variation within the unit, from mud to cobbles suggests high fluctuation in water discharge. The presence of mud draping the surface of clasts indicates sedimentation within an environment in which suspension settling is occurring while the discharge is low, in this case from a vertical buoyant plume (Powell, 1990; Bennett et al., 1999). Mud and silt drape deposits can also be formed in a subaerial glaciofluvial environment, in pools of standing water. However, fluvial mud drapes form usually massive beds or lenses that blankets the underlying deposit (Miall, 1977). It is therefore more likely that the mud draping clast surfaces in unit 1B is a result of glaciomarine suspension settling from a vertical buoyant plume. Unit 1B forms part of LFA1.

Unit 2

Description

Unit 2 consists of a clast-supported, medium to fine gravel with shell fragments which dips 5° towards northeast (Fig. 21C, Fig. 22). The unit is ~30 cm thick, ranging from ~5.75 to 6.05 m above sea level. The unit is poorly sorted and rich in cobble and pebble clasts with a maximum size of 10 cm. A 10 cm thick, well-sorted sand lens composed of massive, coarse sand is situated within the unit at ~5.85 m a.s.l. (Fig. 21D). The basal contact is gradual and there is no evidence for post-depositional deformation in the unit.

Interpretation

Due to the coarse grain size of the unit, it is interpreted to be deposited close to the mouth of a subglacial tunnel which discharges high volumes of sediment-charged meltwater into the shallow marine environment at the grounding-line of a tidewater glacier. Furthermore, the sediments are interpreted to be deposited within a grounding-line fan (Powell, 1990; Bennett et al., 1999) indicated by the gentle dip of the unit towards the fjord, when the meltwater discharge was high, enabling fine grained sediments to be transported further away by suspension, leaving the coarse-grained particles behind (Dowdeswell et al., 2015). A radiocarbon age from a bivalve shell fragment from unit 2 at 5.9 m a.s.l. yielded 11 380 +307/-231 cal. a BP (Sample A-01; Table 1) which is interpreted to be the maximum age of deposition of the unit as the shell fragments are not *in situ* rather suggested to be reworked. The glacier might have advanced over pre-existing marine sediments containing these shells further up the valley. The shells were transported subglacially or englacially with sediment-charged meltwater, where they broke up into fragments, and finally deposited in the fjord in a grounding-line fan. The well-sorted sand lens is interpreted as being deposited during low water discharge with sediment-rich meltwater (Powell, 1981). The relative sea level in the area around Grønfjorden was ca. 43 m a.s.l. at 11.38 cal. ka BP (Forman et al., 2004), which further supports the idea of the unit being formed in a subaqueous grounding-line fan. This unit is classified as a part of LFA1.

Unit 3

Description

Unit 3 is 155 cm thick, ranging from ~6.05 to 7.6 m a.s.l. with no indications of post-depositional sediment deformation. The unit is divided into five subunits. 3a is 35 cm thick, consisting of fine to medium gravel. The maximum particle size is 5 cm. 3b is a coarse to medium gravel bed, 10 cm thick (Fig. 21E). The bed is well-sorted and the largest clast size is 3 cm. Its lower boundaries are sharp. Subunit 3c is 30 cm thick. It is composed of sandy gravel in the upper part and silty gravel in the lower part. Sand and silt particles are present between clasts and form a thick coat around them. The unit is massive and unconsolidated, however with more cohesion than other subunits (Fig. 21E). Maximum particle size is 7 cm.

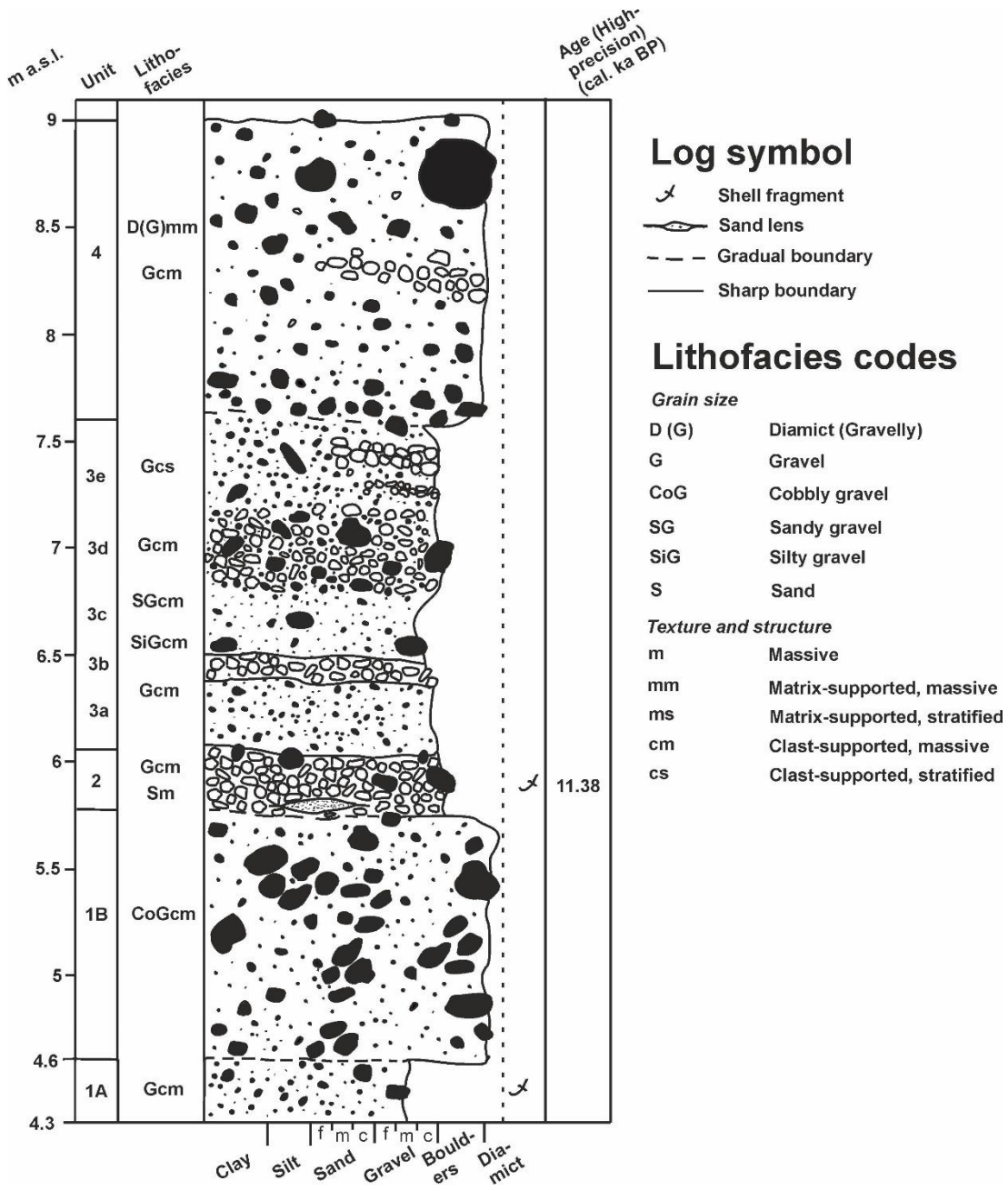

Figure 20. Lithostratigraphic log A from site A. Explanation of lithofacies codes and symbols for all the logs in the study are presented on the right side.

Subunit 3d is a coarse gravel, ~40 cm thick and has undergone some sorting. It is cobble-rich with the largest clast size being 12 cm. The clasts are predominately subangular with a RA index of 20% and C_{40} index of 48% (Fig. 21F, Fig. 16E). In subunit 3e, beds of sorted fine to medium gravel alternate with well-sorted, pebbles- and coarse gravel lenses. The unit is nearly horizontally bedded, around 40 cm thick and the lenses within it are from 3 to 4 cm thick. Largest clast size is ~8 cm in diameter (Fig. 21G).

Interpretation

This unit is assigned to LFA1. The sediments within unit 3 are interpreted in the same way as the underlying unit (unit 2, dated to 11.38 cal. ka BP) based on resembling sediment composition and lack of evidence for post-depositional disturbance or deformation of the stratigraphy section. Unit 3 is therefore suggested to be deposited in a shallow marine environment in a grounding-line fan in front of a tidewater glacier (Powell, 1990; Bennett et al., 1999). Different characteristics of subunits represent different environmental conditions during time of deposition. Moderate meltwater discharge is proposed to have deposited subunit 3a based on its grain size. Subunit 3b and 3d, consisting of coarse gravel, are suggested to be deposited under high water discharge, where finer particles were washed away in suspension and deposited further from the grounding-line. The sandy and silty gravel deposit in unit 3c is interpreted to represent redistributed sediments deposited in a gravity-flow on the fan, indicated by its poor sorting, and thick sand and silt coating around clasts (Powell, 1981, 1990; Ó Cofaigh et al., 1999; Dowdeswell et al., 2015). Well-sorted, pebbles- and coarse gravel lenses from subunit 3e are interpreted as having been deposited during pulses of increased discharge, sorting the sediments and forming lenses (Powell, 1990).

Unit 4

Description

Unit 4 consists of alternating, matrix-supported diamict and clast-supported, pebbles- and coarse gravel lenses (Fig. 21H). The unit is 140 cm thick, from 7.6 to 9 m a.s.l. The matrix of the diamict is a sandy- medium to fine gravel (Fig. 22). The clean clast-supported, coarse gravel lenses are well-sorted and up to 10 cm thick. The lenses become more visible towards the base of the unit. The unit is unconsolidated and is more compacted than the upper part of unit 3. The upper part contains some angular clasts and also boulders up to 25 cm in size with few that are subrounded and striated. A large subrounded boulder, 50 cm in size, with striations, is situated on the surface of the unit.

Interpretation

Unit 4 is categorised as lithofacies association 3 (LFA3). The unit is interpreted to be formed in a subglacial environment as a mixture of debris from unit 3 (sandy and silty gravel formed in a grounding-line fan), and subglacial till with some englacial and supraglacial components. Historical photos from 1911 (Fig. 9) demonstrate that this top unit was covered by the glacier which suggests that some of the material within the unit derives from the subglacial environment, supported by the subrounded striated clasts.


A)
Unit 1A
B)
Unit 1B
C)
Unit 2
D)
Sm
E)
Unit 3c
Unit 3b
F)
Unit 3d
G)
Gcm
Gcm
Unit 3e
H)
N
Unit 4

Figure 21. Images of units from log A, site A. A) Unit 1A. Gravel with small shell fragments deposited in a grounding-line fan in front of a tidewater glacier. B) Cobbly gravel from unit 1B with imbricated cobbles. C) Clast-supported gravel from unit 2 deposited in a groundling-line fan. D) A massive sand lens from unit 2. E) Boundaries between subunit 3b, a coarse gravel and subunit 3c. The image demonstrates the lower part of subunit 3c, silty gravel. F) Subunit 3d, a coarse gravel formed under high water discharge in a grounding-line fan. G) Subunit 3e, gravel with some well-sorted, pebbles- and coarse gravel lenses. H) Unit 4, matrix-supported, gravelly diamict.

The clast-supported, pebbles- and coarse gravel lenses observed within the layer are more prominent towards the base of the unit. Because unit 3 contains very similar clast-supported, pebbles- and coarse gravel lenses and is a clast-rich gravelly unit, it is suggested that the base of unit 4 contains some reworked pre-existing sediments from unit 3, such as the coarse gravel lenses, which were only partly eroded when the glacier advanced across it. Because of this inherited structure and sedimentary composition from the underlying unit, unit 4 is suggested to be a deformation till (Hart et al., 1990; Evans, 2000). Angular clasts within the unit suggest that it contains material from englacial and supraglacial environments (Krüger and Kjær, 1999). This idea is supported by the presence of debris stripes with angular debris on top of, and in some places draping, the unit. Fig. 17 demonstrates the melting of the glacier on top of the large sedimentary ridge in 1936. The snout of the glacier is very thin and englacial and supraglacial debris is observed to melt out from the ice and drape the sediments below as the glacier degrades from underneath. Abundant kettle holes situated on the ice proximal side of the glacier indicate that this uppermost unit has likely been affected by dead-ice processes followed by a re-sedimentation.

Unit 4 represents the subglacial till plain presented in the geomorphological map of the large sediment ridge (Fig. 14). Kirkebøen (2018) described an outcrop close to the glacier where clast-rich, subrounded striated sediments were frozen onto the base of the glacier. These sediments are further up-valley and closer to the glacier than site A. The reason for the few subrounded clasts within unit 4 at site A compared to the outcrop near the glacier described by Kirkebøen (2018), is likely due to close proximity of site A to the shore. In the centre of the forefield, where the glacier was thickest and possibly warm-based, the subglacial sediments at the base of the glacier were likely affected by active transport, where clasts are effectively edge rounded. The sediments situated near the shore where the ice margin was situated, such as site A, may have been less likely to undergo effective edge rounding compared to sediments further up valley in the centre of the forefield, as the glacier was thinner close to the ice margin and possibly cold-based (Hambrey and Glasser, 2012; Hanáček et al., 2021). The two sites are also provided with sediments from different sources. The site near the glacier contains sediments likely derived from erosion of bedrock or supraglacial debris from mountain sides while the lower part of the forefield also contains sediments derived from reworking of existing materials, including glacimarine-deposited material and glaciofluvial sediments. These different factors will result in highly variable characteristics of the subglacial till cover across the forefield.

To summarize, unit 4 was deposited as a response to a glacier advance across a pre-existing gravelly, grounding-line fan deposit from unit 3, representing the LIA advance. Subsequently followed by a stagnation and degradation of thin cold-based ice that finally melted away and left a cover of sediments of supraglacial and englacial environments resting on a bed consisting of a mixture of subglacial material from the LIA advance and older pre-existing gravelly grounding-line fan sediments from LFA1.

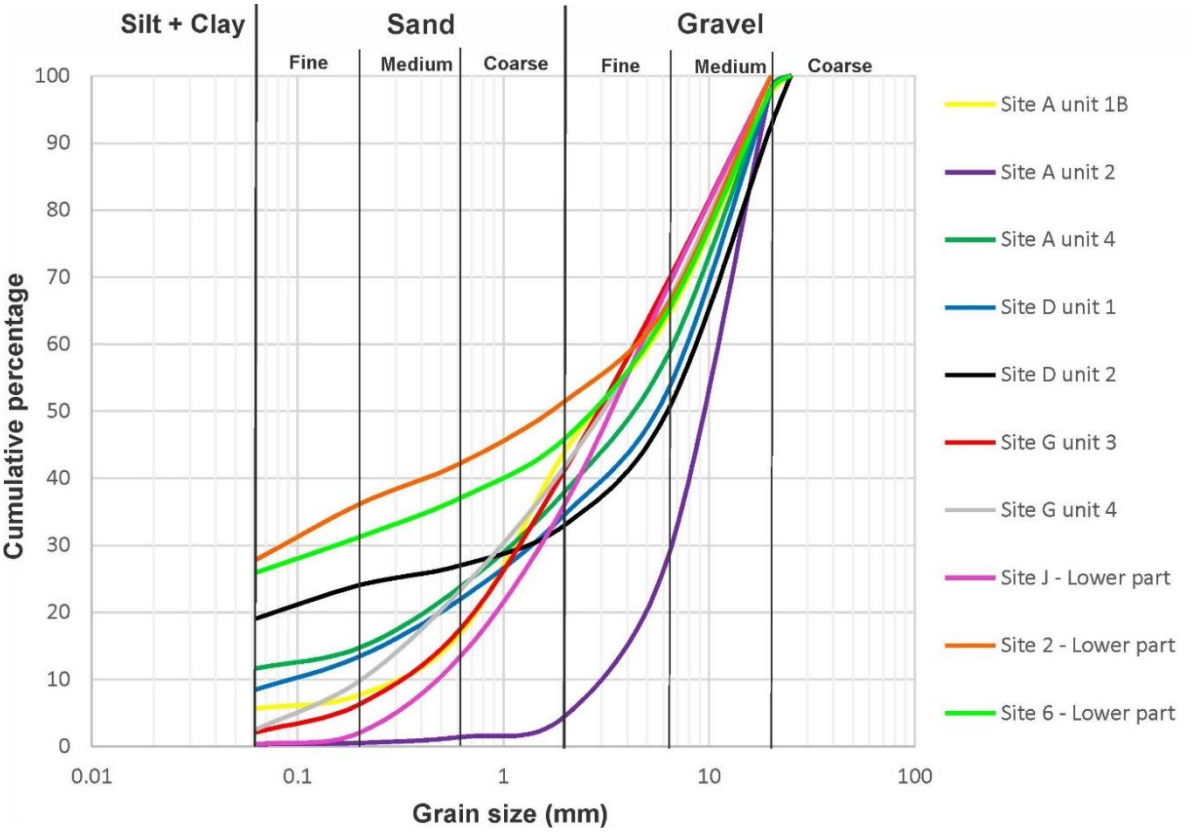

Figure 22. Grain size distributions for sediment samples in cumulative percentage.

Site D

Site D is situated in the distal side of the large cross-valley sedimentary ridge (Fig. 11), on the southern flank of the main glacial meltwater river. Site D was documented in detail with one log (Fig. 24). The surface cover at the top of the section is composed of clast-rich, matrix-supported diamict, with clasts ranging in size from boulders of 25 cm to gravel and sand. The surface debris is weathered and finer material has settled in between larger clasts. The clasts on the surface are mainly subangular and subrounded. Small seasonal or inactive fluvial channels were observed on the surface, with a northeast-southwest direction. The grain size within the channels is finer than the area surrounding it and no water was observed inside of them during fieldwork. The surface is overall undulating with little vegetation scattered around.

In some places, the surface is draped with debris stripes composed of angular clasts such as darker shale and lighter sandstone. Small kettle holes, up to 3 m long, 2 m wide and 0.5 m deep, and small transverse ridges, up to 17 m long, 1 m wide and 0.5 m high, are situated on the surface in close proximity to the site (Fig. 23A).

Log D

The sedimentological section at site D is ~270 cm high, ranging from 3.8 - 6.5 m a.s.l. It is naturally exposed due to erosion from the glacial meltwater river, which flows on the outwash fan beneath. Erosion of sediments in the lower part of the section has led to slumping of debris from above, forming a concave slope (Fig. 23B). Fig. 19 demonstrates that site D has undergone heavy erosion since mid-last century and exposure of the sedimentary section occurred recently, somewhere between 2008 - 2019. Three sedimentary units are defined in the section at site D (Fig. 23C; Fig. 24).

Unit 1

Description

Unit 1 is at least 70 cm thick, reaching up to 4.5 m a.s.l. (Fig. 25A). It is a pebble-rich, massive medium to fine gravel with a washed appearance (Fig. 22). The maximum particle size is 10 cm and the clasts are mainly subangular with an RA index of 18% and C_{40} index of 56% (Fig. 16F). The unit is unconsolidated and collapses easily when excavated. Small fragments of bivalve shells are found within the whole unit. There is no evidence for post-depositional deformation within the unit.

Interpretation

A radiocarbon date from the unit, obtained from a bivalve shell fragment at 4.3 m a.s.l., yielded an age of 11 273 +318/-221 cal. a BP (Sample D-01; Table 1) which represents maximum age for deposition of the unit. The relative sea level at that time was around 43 m a.s.l. (Forman et al., 2004) and these sediments are therefore suggested to be formed in subaqueous environment rather than as a washed beach gravel. The sediments in the unit are further interpreted as being deposited in a shallow glaciomarine environment, on the distal side of a grounding-line fan in front of a tidewater glacier (Powell, 1990; Lønne, 2005). Only small shell fragments were found within the unit, implying reworking in a high energy environment, for instance in subglacial meltwater streams which supports the grounding-line fan suggestion. The washed appearance of the unit implies wave- or current reworking, where fine-grained material is winnowed, leaving coarse grained material behind and decreasing the cohesion of the unit (Powell, 1984). Unit 1 is suggested to represent LFA1.

Unit 2

Description

Unit 2 consists of alternating sorted, silty gravel beds and well sorted, coarse gravel lenses (Fig. 25B). The unit is ~130 cm thick, from 4.5 to 5.8 m a.s.l. The coarse gravel lenses are from 1 to 3 cm thick and the boundaries between them and the silty gravel are sharp (Fig. 25C). The silty gravel is stratified with less fine material in the lower part (Fig. 22). The maximum particle size is 6 cm, and the surface of larger clasts is draped with thin mud coat. The unit is unconsolidated, although with greater cohesion and compaction than unit 1. The unit's lower boundary is sharp and no observable evidence of post-depositional sediment disturbance are found.

Interpretation

Unit 2 is interpreted to represent sediments deposited in a subaqueous, grounding-line fan in front of a tidewater glacier (Powell, 1990; Batchelor and Dowdeswell, 2015). The deposit is not suggested to have formed in close proximity to the mouth of the subglacial meltwater tunnel, rather along the runout distance of the jet on the fan, indicated by the relatively fine grain-size and mud draped surfaces of larger clasts. The well-sorted, coarse gravel lenses indicate meltwater discharge pulses which can sort the sediments and wash the fines away in suspension (Powell, 1990). Mud draping on surfaces of larger clasts imply rain-out of fine particles from suspension during low discharge. The particles were deposited and settled on surfaces of larger clasts (Bennett et al., 1999). Unit 2 is assigned to LFA1.

Unit 3

Description

Unit 3 is around 70 cm thick, from 5.8 to 6.5 m a.s.l. It is a massive, matrix-supported diamict with a gravelly matrix (Fig. 25D). The diamict is clast-rich, with a maximum particle size up to 25 cm in diameter. Few, 1 - 3 cm thick, pebbles and coarse gravel lenses are present within the unit with sharp boundaries with the diamict. The clasts are generally subangular and subrounded with an RA index of 18% and C_{40} index of 34% (Fig. 16G). Larger clasts are more abundant in the upper part of the unit. The unit is unconsolidated, however more compacted than the lower units within the section. The uppermost 5 cm of the unit forms a weathered surface cover, where finer material has settled in between larger clasts. Roots from vegetation penetrate from the surface and into this weathered material. The basal contact of the unit is gradual.

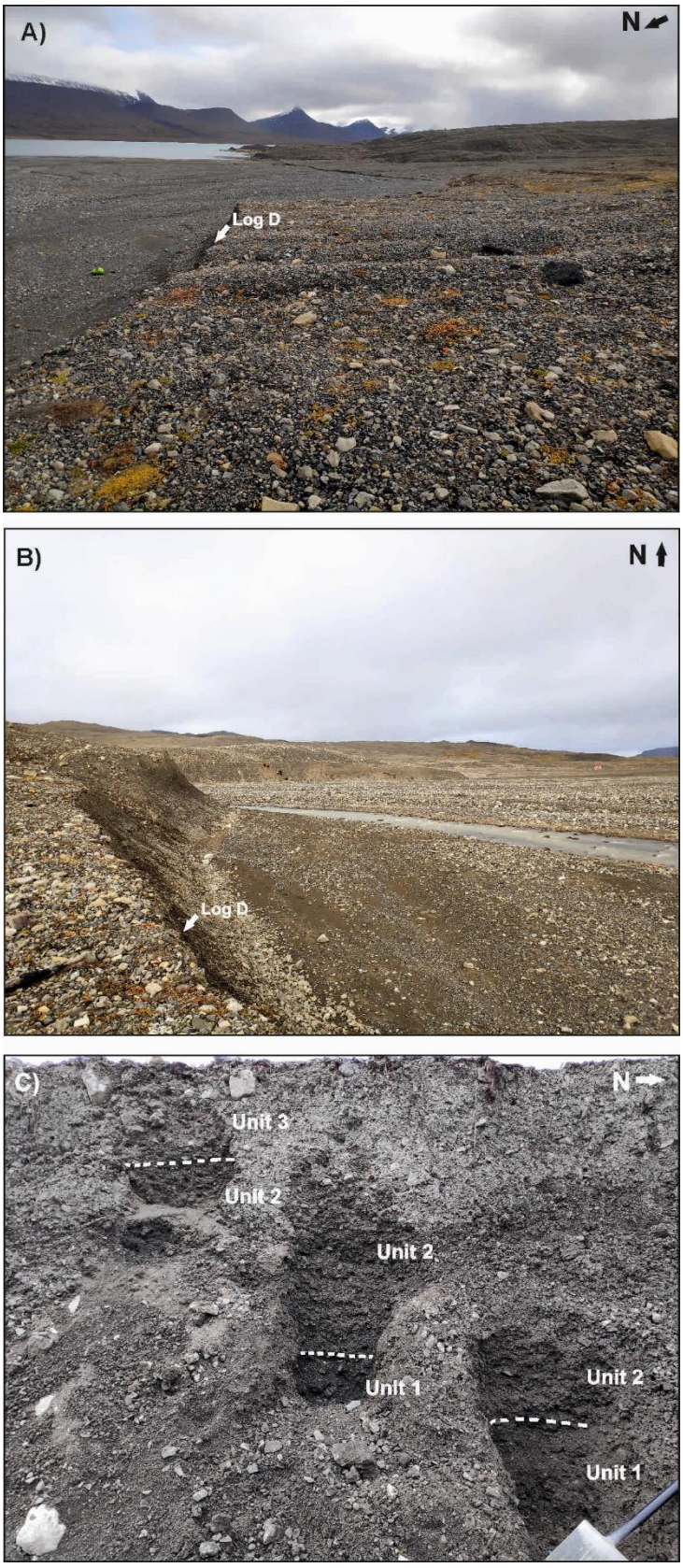

Figure 23. Overview of site D and log D. A) Location of log D at site D on the large sedimentary ridge, on the southern flank of the active glacial meltwater river. B) Image demonstrating the glacial meltwater river which flows on the outwash fan beneath the section. The river has eroded the lower part of the section which has led to slumping of debris from above, forming a concave slope. C) The three sedimentary units at site D.

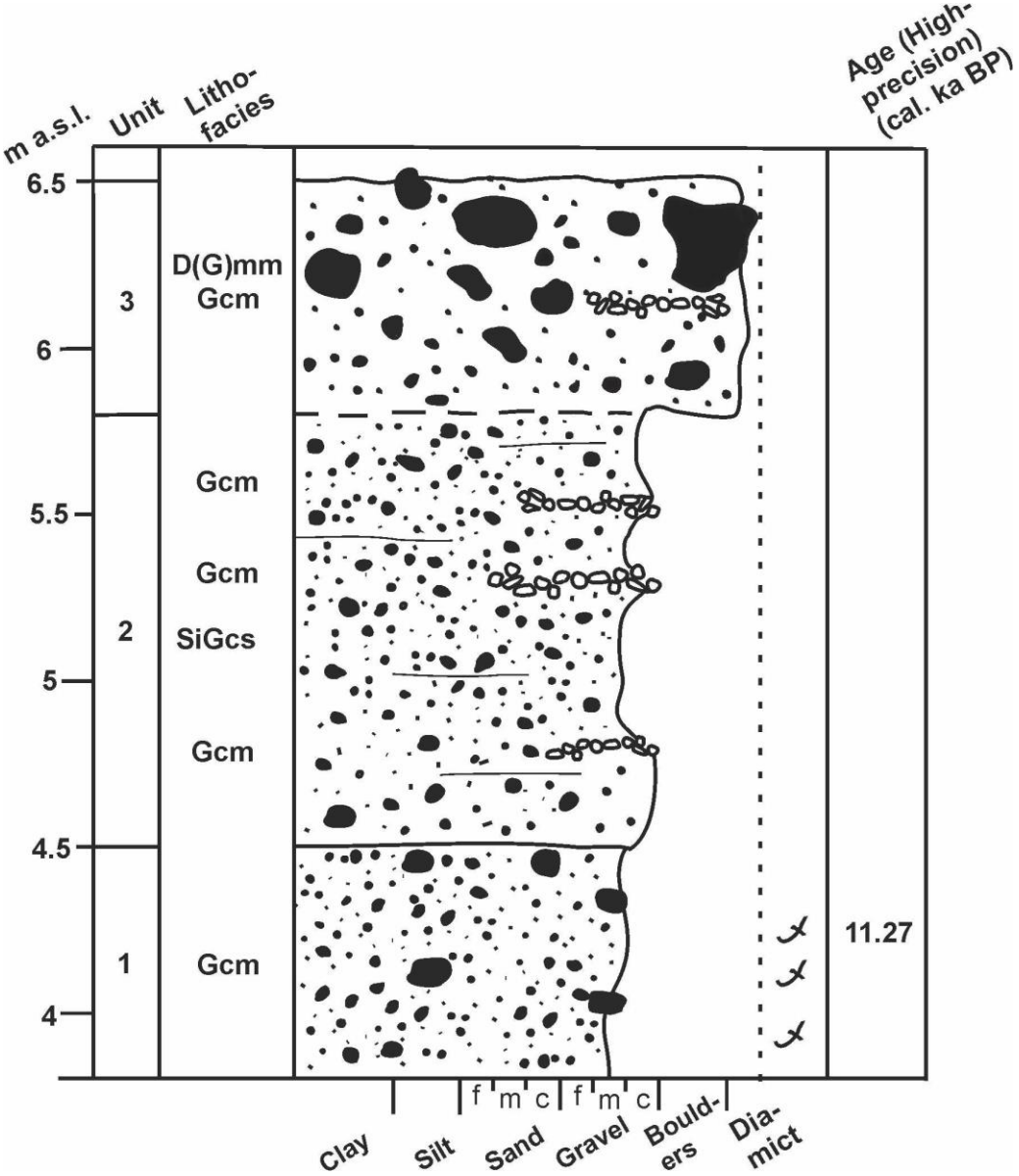

Figure 24. Lithostratigraphic log D from site D. Explanation of lithofacies codes and symbols for the log are presented in Figure 20.

Interpretation

The gravelly matrix-supported diamict in unit 3 is interpreted to be formed in a subglacial environment with a mixture of debris from unit 2 (shallow, glaciomarine deposit from a grounding-line fan), and subglacial till with some englacial and supraglacial components. The interpretation is based on the compaction of the unit, weak sorting, and appearance of subrounded boulders. This unit is further suggested to be a deformation till (Hart et al., 1990; Evans, 2000), based on the sedimentary composition and structure inherited from the underlying unit. Photos from 1911 show how the glacier covered this uppermost unit supporting the subglacial origin. Angular material is suggested to come from supraglacial and englacial environments (Krüger and Kjær, 1999).

Due to the fact that unit 2 contains similar lenses of pebbles and coarse gravel, it is suggested that the gravel lenses in unit 3 have been incorporated from unit 2 when the glacier advanced across it and formed unit 3. Unit 3 represents the subglacial till plain presented in the geomorphological map of the large sediment ridge similar to unit 4 at site A. The unit is categorised as LFA3.

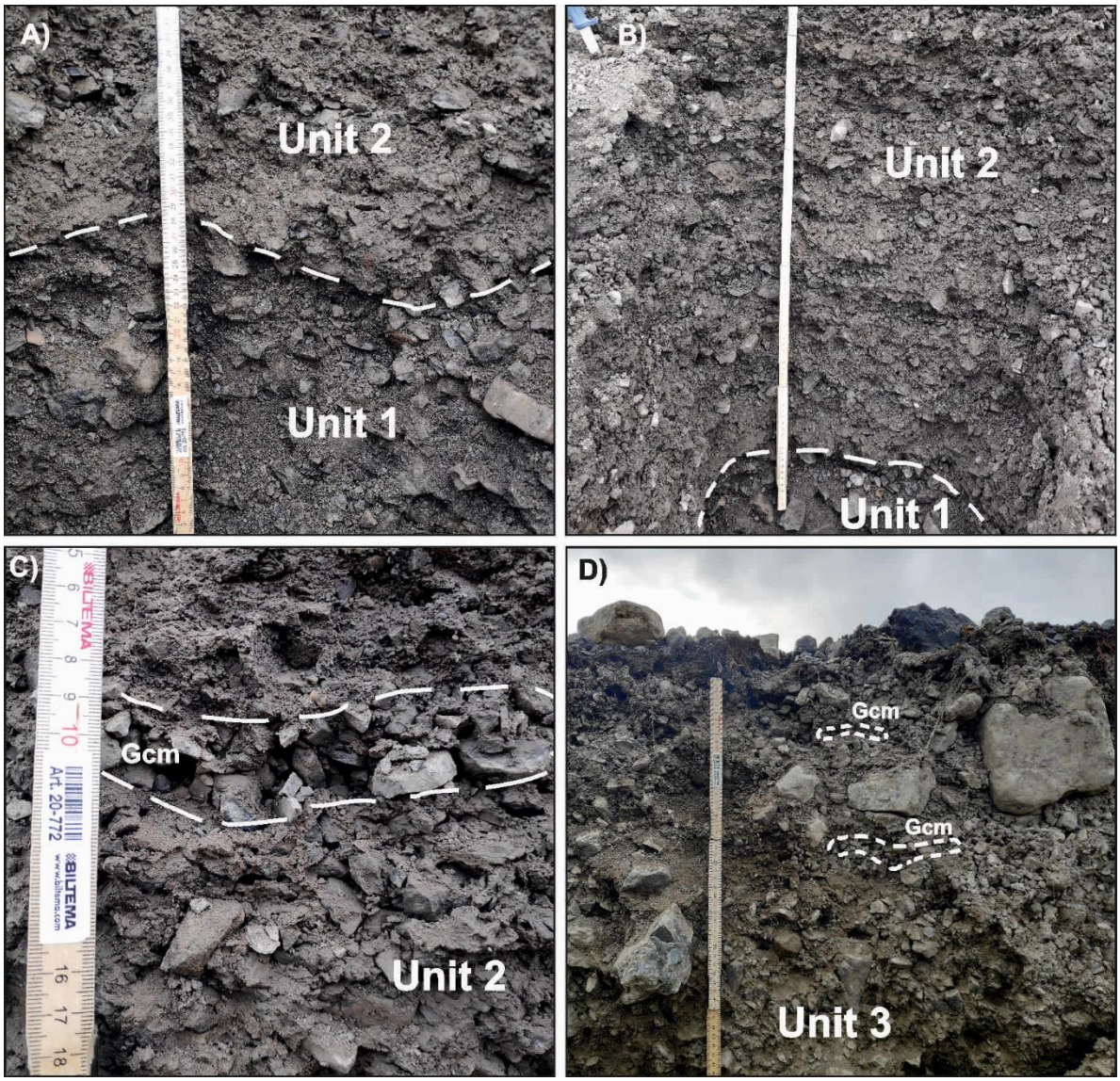

Figure 25. Images of units from log D. A) Boundaries between the medium to fine gravel in unit 1 and the silty gravel in the lower part of unit 2. B) Image of unit 2 at site D showing stratification of silty gravel beds. C) A coarse gravel lens from unit 2, surrounded by the silty gravel. D) The matrix-supported, gravelly diamict from unit 3 with some coarse gravel lenses.

Site G

Site G is located in a small ridge in the north-eastern part of the forefield, ~100 m from the coast (Fig. 11). The ridge is curve-shaped with northeast-southwest direction and is situated adjacent to a small cabin (Fig. 26A). It measures ~70 m long, ~18 m wide and the highest point reaches up to around 7 m a.s.l. The ridge is highest on the southwestern point, thinning towards the north-eastern side (Fig. 26B). The surface cover of the ridge consists of clasts from 1 m in size down to gravel and sand. The surface is weathered where finer particles have settled in between larger clasts. A small kettle hole is observed on the surface of the ridge, where gravity sorting has occurred, resulting in bigger clasts slumping down into the depression. A glaciofluvial outwash fan with inactive fluvial channels surrounds the ridge on all sides separating it from other landforms in the forefield.

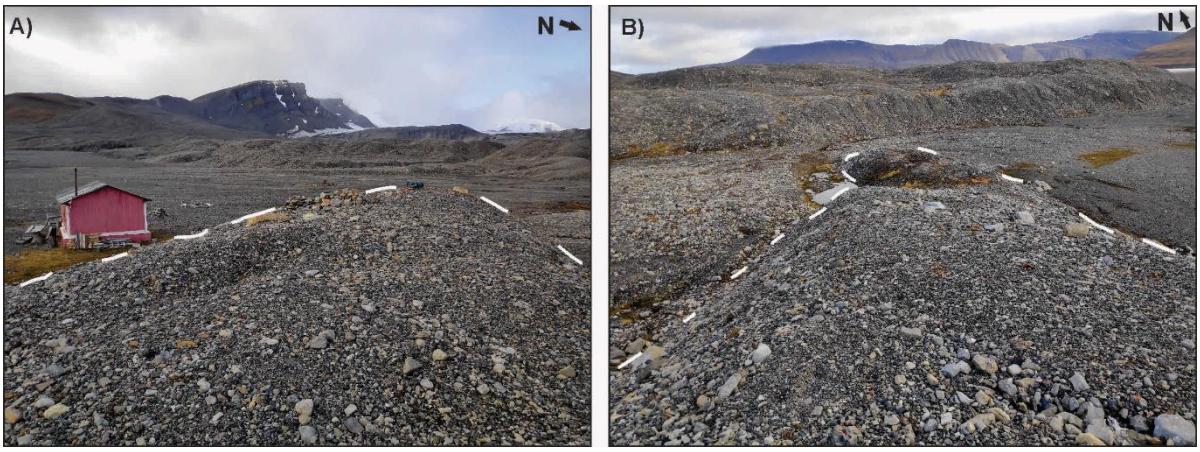

Figure 26. Overview of the small ridge at site G. A) The small ridge situated adjacent to the small cabin, Aldegondabreen is located behind the large ridge in the background. B) Looking to the northern side of the small ridge where it is lowest. The glaciofluvial outwash fan with inactive channels can be seen surrounding the ridge.

Log G

A sedimentary outcrop was excavated on the sea side of the ridge in order to log the succession. The sedimentary outcrop is located in the centre of the ridge and is ~5 m high, reaching from 0.5 to 5.5 m above sea level. Five different lithofacies units were distinguished within the section (Fig. 27).

Unit 1

Description

Unit 1 is minimum 1 m thick, reaching from ~0.5 to 1.55 m above sea level (Fig. 27). The unit is composed of stratified, sandy gravel with a maximum particle size of 4 cm. The unit is pebble-rich and contains small bivalve shell fragments (Fig. 28A). The beds within the unit dip ~38° up glacier, towards the southwest. The grain size decreases towards the base of the unit.

Interpretation

The gravel in unit 1 is interpreted to be deposited within a glaciofluvial outwash plain formed by meltwater from Aldegondabreen. Sediments in glaciofluvial outwash are built up in large aggradational plains by number of meltwater streams that carry sediments both as bedload and in suspension (Krigström, 1962; Maizels, 1993). The small shell fragments are interpreted to originate from older marine sediments, which were reworked with glaciofluvial meltwater and finally deposited in the glaciofluvial outwash plain. The difference in the grain size of the unit represents discharge fluctuations where the coarser grain size in the upper part was deposited during a period of higher discharge while the fine grained sediments in the lower part were deposited by low-energy streams (Maizels, 1993). The unit is suggested to represent lithofacies association 2 (LFA2). The steep up-glacier dipping of the unit suggests that the unit has been modified after deposition. However, data from this study are insufficient to validate whether the unit was deposited with this steep dip or if it was modified after deposition. A hypothesis has been made as a suggestion for the steep dipping of the unit. After the glaciofluvial outwash plain was formed, the sediments within it were overridden by ice during a glacier advance which consequently glaciotectonised the outwash plain, with a thrust block formation (Fig. 29). As a result, the sediments from the glaciofluvial outwash plain in the thrust block were pushed higher up forming the ridge at site G. This could potentially explain the steep up glacier dipping of the unit (Evans, 2000). Glaciotectonism has been defined as deformation of bedrock or sediments due to glacier overriding or pushing and glaciotectonic structure and landforms can occur in a wide range of scales (Aber and Ber, 2006). To be able to further confirm the exact formation of the ridge, more detailed studies of the ridge are needed including investigation of a sediment section which provides a profile view into the sediments to examine if any glaciotectonic structures are present.

Unit 2

Description

Unit 2 is an 85 cm thick, cobbly gravel with few boulder sized clasts, up to 45 cm in size (Fig. 28B). The unit ranges from 1.55 to 2.4 m above sea level. It is unconsolidated and collapses easily when excavated. The largest clasts are located in the middle of the unit and the grain size decreases towards the base where the maximum particle size is 7 cm. Some imbricated cobbles and boulders are found within the unit. A clast sample from unit 2 demonstrates that the clasts are predominately subangular with an RA index of 18% and a C_{40} index of 54% (Fig. 16H). Small bivalve shell fragments are scattered around the unit. The unit has a gentle dip, ~3 - 5° down glacier, towards the sea in the opposite direction to the dip of unit 1. The basal contact is sharp.

Interpretation

The unit is interpreted as glaciofluvial sediments deposited in a high energy flow indicated by the coarse grain size, imbricated cobbles and roundness of clasts (Maizels, 1993). The sediments were deposited in a glaciofluvial outwash plain formed with meltwater from Aldegondabreen (Krigström, 1962; Maizels, 1993; Evans, 2000). The boulders are suggested to have been transported as bedload under high-discharge, possibly during the peak of the meltwater season (Maizels, 1993). The small shell fragments indicate that they have been reworked from their original deposition. The glaciofluvial meltwater is suggested to have cut into older marine sediments with shells deposited higher up in the forefield. These sediments were then reworked with the meltwater and transported further downstream until it was deposited in a glaciofluvial outwash plain close to the coast. Unit 2 is categorised as LFA2. The gentle dip of unit 2 in the opposite dip direction to unit 1 could potentially support the hypothesis that the glaciofluvial sediments were deformed with a thrust block formation when a glacier overrode them during an advance which formed the ridge at site G.

Unit 3

Description

Unit 3 consists predominantly of sorted, sandy medium to fine gravel, containing small bivalve shell fragments (Fig. 22). The unit is nearly horizontally bedded with moderate clast content and the maximum clast size is 7 cm. The unit is 80 cm thick, reaching from 2.4 to 3.2 m a.s.l. with gradual basal boundaries (Fig. 28C). The unit is unconsolidated, and it slumps easily down when excavated. The beds within the unit dip ~3 - 5° down glacier, towards the sea like unit 2.

Interpretation

These sediments are interpreted to be deposited within a glaciofluvial outwash plain formed by meltwater from Aldegondabreen (Krigström, 1962; Maizels, 1993). The fine grain size of the sediments suggest deposition during low discharge, possibly during the beginning of the ablation season or towards the end of it (Krigström, 1962). The shell fragments found in the unit imply reworking of older marine sediments by meltwater as described for unit 2, which were re-deposited within a glaciofluvial outwash plain. A radiocarbon age from one of the shell fragments from unit 3 at 2.8 m above sea level, was dated 10 881 +235/-236 cal. a BP (Sample G-04; Table 1) which provides the maximum age of the deposition of the unit. The unit is suggested to represent LFA2. The similar gentle dip and dip direction of unit 2 and 3 which is the opposite dip direction of unit 1, is suggested to support the hypothesis that the glaciofluvial sediments were deformed when a glacier overrode and pushed them up to a higher elevation forming the ridge at site G. This is in accordance with the interpretation from unit 2.

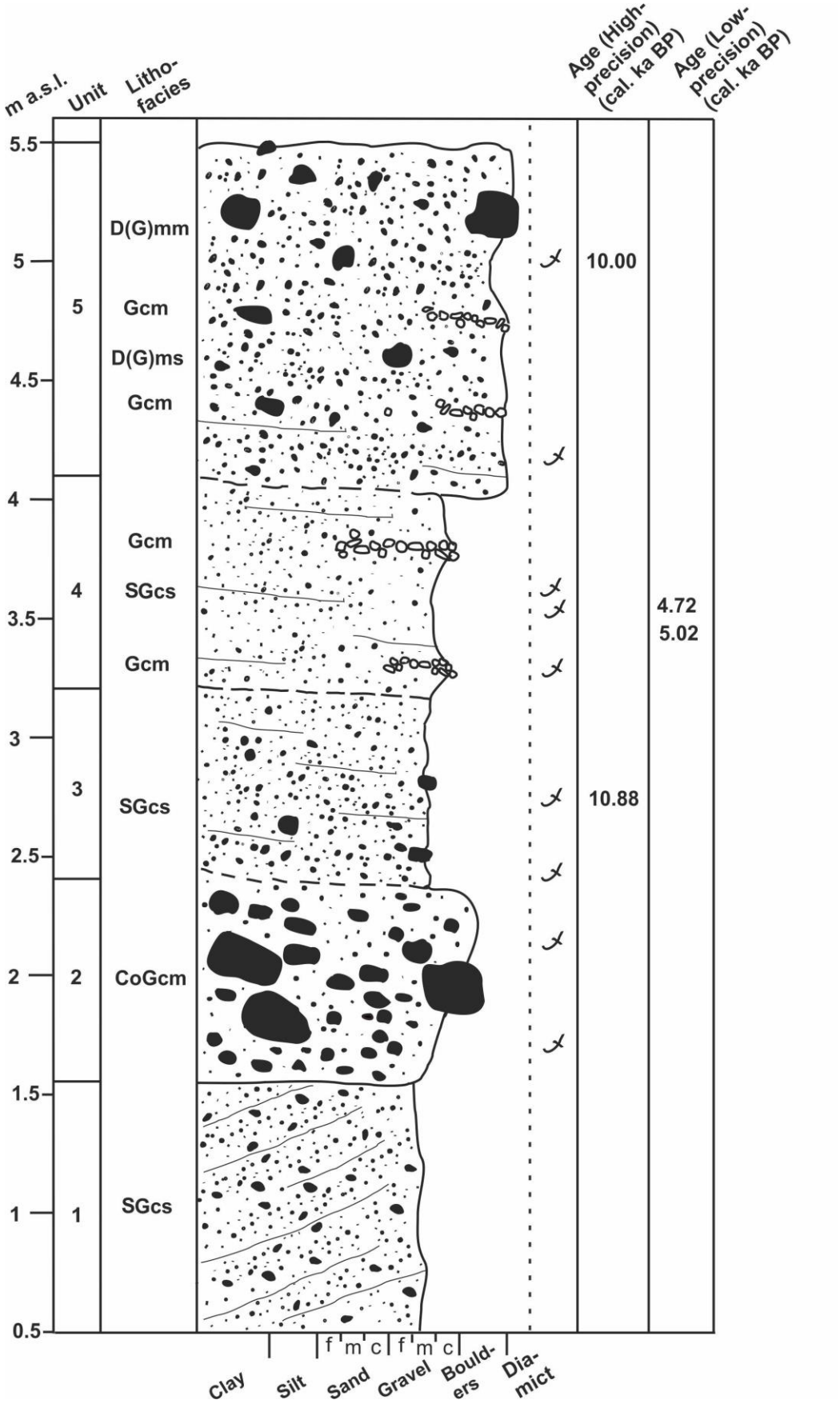

Figure 27. Lithostratigraphic log G from site G. Explanation of lithofacies codes and symbols for the log are presented in Figure 20.

Unit 4

Description

Within unit 4, stratified sandy medium to fine gravel beds (Fig. 22) alternate with medium gravel lenses. The unit is 85 cm thick, ranging from 3.2 to 4.05 m a.s.l. (Fig. 27). It contains small bivalve shell fragments and the maximum clast size is 3 cm. The unit is unconsolidated, however it exhibits greater cohesion than unit 3. The medium gravel lenses are from 1 to 3 cm thick, well sorted and contain small shell fragments. The beds within the unit dip ~3 - 5° down glacier, to the northeast which is the opposite dip direction to unit 1. The basal contact of the unit is gradual. Blue bivalve shell fragments were identified among other unidentified bivalve shell fragments within the unit. The blue shell fragments are *Mytilus edulis* shell fragments, also known as blue mussel (Mangerud and Svendsen, 2018).

Interpretation

The sandy medium to fine gravel is interpreted to be deposited in a glaciofluvial outwash plain (Krigström, 1962; Maizels, 1993) and subsequently deformed in a thrust block formation, lifting the sediments to a higher elevation during a glacier advance. This is in accordance with the hypothesis suggested for the interpretation of unit 1. This idea is supported by the gentle dip of units 2 - 4, down glacier, which is the opposite dip direction than of unit 1, which is up glacier. The coarse gravel lenses within the unit represent periods of higher discharge. The small shell fragments found within unit 4, indicate that they have been transported from their original deposition and reworked. It is proposed that glaciofluvial meltwater cut into pre-existing marine sediments which contained whole shells. The meltwater transported the marine sediments and the shells down-stream, where the shells broke up into fragments and were eventually re-deposited in a glaciofluvial outwash plain near the coast. Two shell fragments of *Mytilus edulis* were dated with low-precision radiocarbon dating from unit 4. The results yielded ages of 4716 +367/-360 cal. a BP and 5018 +294/-302 cal. a BP (Table 2). These ages could potentially provide the maximum age of deposition for the unit. However, these ages were dated with low-precision dating which must be considered when interpreting the ages of the sediments containing the shells. For more reliable age results, these shells must be re-dated with high-precision radiocarbon dating. Unit 4 is interpreted to be LFA2.

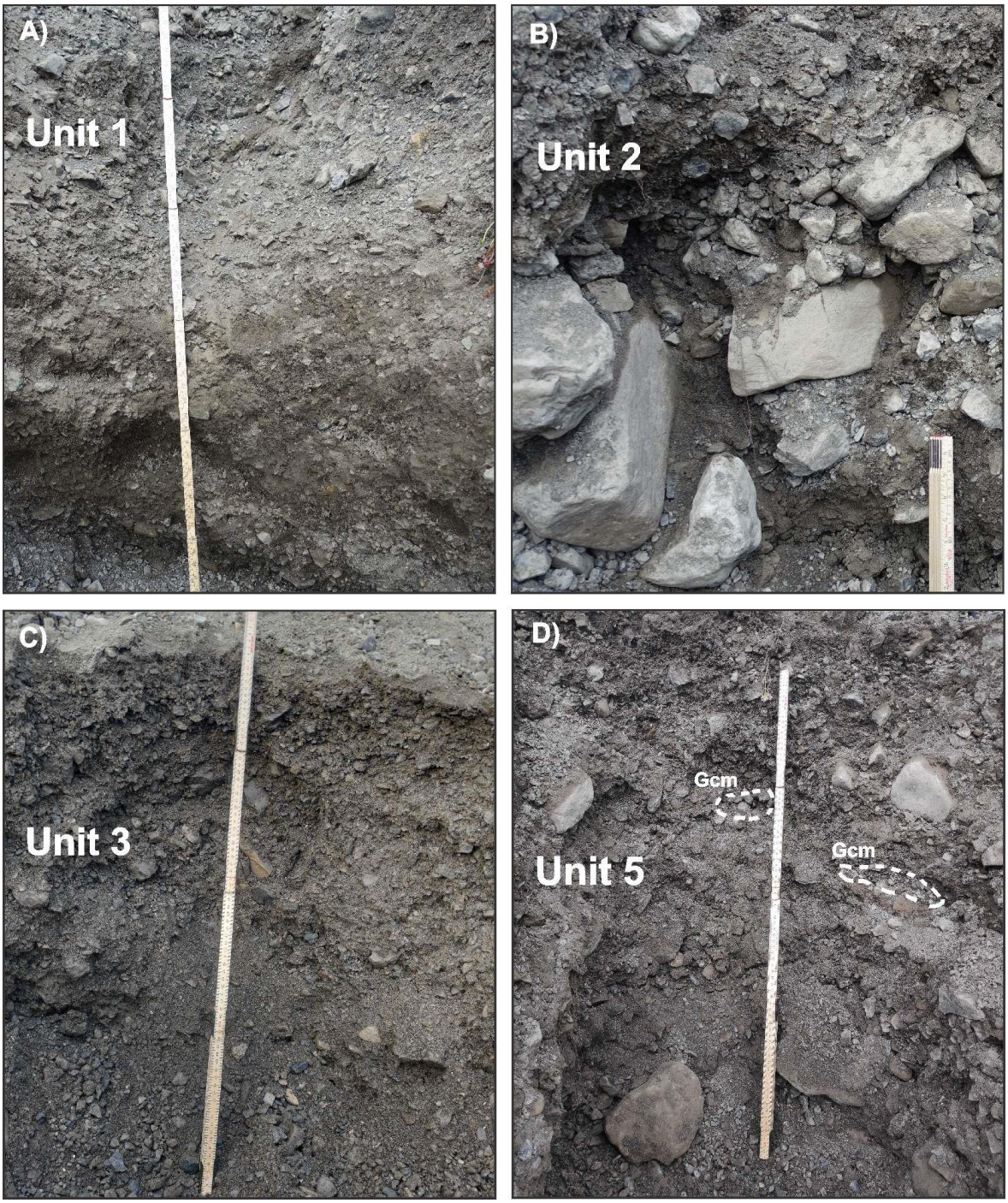

Figure 28. Units from log G. A) Image of unit 1 demonstrating the glaciofluvial sandy gravel. B) Unit 2 with cobbly gravel and some imbrication. C) The sandy gravel from unit 3. D) Unit 5 with the gravelly diamict.

Unit 5

Description

Unit 5 is a clast-rich gravelly diamict with small bivalve shell fragments (Fig. 28D). The unit is 145 cm thick and its top reaches 5.5 m above sea level. Medium gravel lenses occur within the unit. The lenses are about 1 - 3 cm thick and are well sorted. The diamict is matrix-supported with maximum particle size up to 25 cm and larger subrounded clasts are more abundant in the upper part. A striated clast was found on the surface of the unit. The unit is unconsolidated and weak stratification is visible in the lower part. The top 5 cm of the unit is weathered and smaller grains have settled in between larger clasts. Thin roots extend from the surface down into the top part of the unit. The lower boundary of the unit is gradual.

Interpretation

Unit 5 is interpreted to be formed in a subglacial environment as a result of a glacier advance over pre-existing sandy gravelly sediments from unit 4, formed in a glaciofluvial outwash plain. The unit is therefore interpreted to be a deformation till (Hart et al., 1990; Evans, 2000) with mixture of sediments from unit 4 and subglacial till with some englacial and supraglacial components. The interpretation of a subglacial origin is based on large subrounded clasts in the uppermost part of the unit and a striated clast at the surface. Aerial images from 1911 (Fig. 9) demonstrate that this top unit was covered by the glacier, further supporting a subglacial origin. Angular clasts within the unit are suggested to be of englacial and supraglacial origin. Medium gravel lenses, shell fragments and the weak stratification in the lower part are interpreted as inherited sediments from unit 4, which were poorly modified when the glacier advanced across it. A radiocarbon date from unit 5 yielded 9 995 +200/-244 cal. a BP, obtained from shell fragments at 5 m a.s.l. (Sample G-01; Table 1). As only small shell fragments were found within the unit it is interpreted that the shell fragments are not *in situ*, rather reworked shell fragments which can only provide maximum depositional age of the unit. The unit is assigned to LFA3.

A hypothesis for the formation of the small ridge at site G

Based on the observed structure and sedimentary composition of the small ridge at site G, a mechanism for its origin can be hypothesized. The hypothesis assumes that the low-precision radiocarbon dates are reliable for interpretation of the age for the formation of the ridge. It should be noted that data from this study shows no direct evidence of glaciotectonism at site G.

Units 1 - 4 at site G are suggested to be deposited in a glaciofluvial outwash plain near the coast as a result of meltwater activity from Aldegondabreen. Dates from these sediments yielded ages from both Early and Middle Holocene, the youngest age is 4.72 cal. ka BP and the oldest is 10.88 cal. ka BP. Both of these ages are derived from shell fragments which indicates that they have been reworked. It is suggested that meltwater from Aldegondabreen has reworked several kinds of sediments from the forefield, including marine sediments from both Early and Middle Holocene. These sediments were then transported down to the coast where they were re-

deposited, forming a glaciofluvial outwash plain. This could explain the age difference of shell fragments within the units in the ridge at site G.

The youngest radiocarbon date from the ridge is 4.72 cal. ka BP which is suggested to be the maximum age for the formation of the ridge. The relative sea level in Svalbard during that time has been described as a maximum of 3 m above present sea level (Salvigsen et al., 1990; Forman et al., 2004) and it has been lowering since that time, until it reached the present-day level (Forman et al., 2004; Ingólfsson and Landvik, 2013). Based on sedimentological properties and composition of sediments within units 1 - 4 in the ridge, they are proposed to be formed in a subaerial environment, in a glaciofluvial outwash plain, after the relative sea level had lowered to similar level as today. Unit 1 - 4 were than lifted to a higher elevation after deposition in the glaciofluvial outwash.

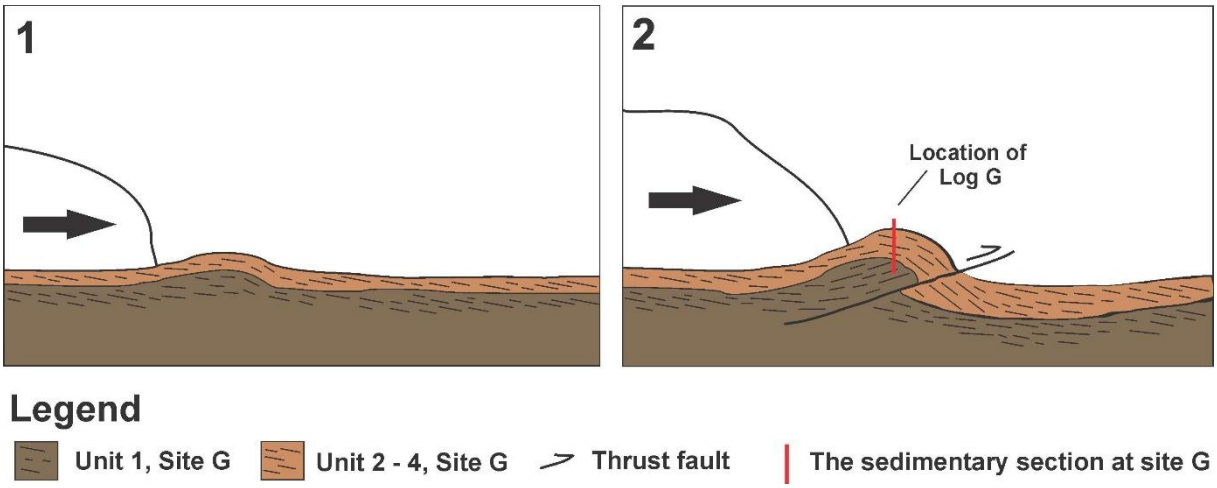

Figure 29. A sequential model showing the hypothesis for the formation of the small ridge at site G. 1: The glacier advances into the glaciofluvial outwash sediments which starts to deform. 2: As the glacier advances further into the outwash plain the glaciofluvial sediments are glaciotectonised with a thrust block formation, lifting the sediments in the thrust block to a higher elevation. The red line indicates the sedimentary section at site G where log G was drawn, demonstrating how unit 1 dips steeply towards the glacier while units 2 - 4 dip gently in the opposite direction, towards the sea.

It is proposed that after 4.72 cal. ka BP, when the sea level had lowered to modern day level, Aldegondabreen advanced into the glaciofluvial outwash plain (Fig. 29). The glaciofluvial deposit was consequently glaciotectonised and deformed with a thrust block formation which pushed the sediments up to a higher elevation, forming the ridge at site G. This could potentially explain the two opposite dip directions of the sediments within the ridge and their elevation above sea level.

Aerial images from 1911 (Fig. 9) demonstrate that Aldegondabreen rests on top of the ridge at site G. It is suggested that during the LIA advance of Aldegondabreen, the glacier overrode the ridge and formed unit 5 subglacially. This would explain the striated clasts on the surface of unit 5 at site G. Since the culmination of the LIA, the area around the ridge has been heavily influenced by meltwater activity from Aldegondabreeen, adding sediments to the glaciofluvial outwash plain surrounding the ridge at site G.

4.3.2 Minor sections

Site E

Description

A small window was excavated into a sedimentary section in the large ridge, adjacent to the glacial meltwater river on its southern flank (Fig. 11). A pebble-rich, sandy gravel with small shell fragments and washed appearance was observed at 7 m above sea level, resembling to unit 1A at site A and unit 1 at site D (Fig. 30A). The unit falls easily down when excavated. It is situated at the base of the sedimentary section on top of a diamict. A small bedrock exposure is situated below the diamict.

Interpretation

Because of the similarities of site E to units 1A at site A and 1 at site D, site E is interpreted as being deposited in subaqueous environment, in a grounding-line fan in front of a tidewater glacier (Powell, 1990; Lønne, 2005) rather than as a washed beach gravel. The small shell fragments are not *in situ* within the unit and no large shell fragments or whole shells were found, suggesting reworking of the shells in a high-energy environment. The shells are proposed to have been reworked and transported with subglacial meltwater streams into the shallow glaciomarine environment and deposited in a grounding-line fan. The washed appearance of the sediments and the absence of fine-grained material implies wave- or current reworking which winnows the fine-grained sediments and leaves coarser material behind (Powell, 1984). The unit is assigned to LFA1.

Site F

Description

Site F is situated on the ice-proximal side of the large sedimentary ridge, at 11.3 m above sea level (Fig. 11). Abundant shells and shell fragments of *Hiatella arctica,* were observed on the surface and within the sediments below (Fig. 30B). The sediments are composed of greyish, clast-rich, and matrix-supported gravelly diamict. These sediments appear in small, sorted polygons on the surface, where coarser material surrounds the finer debris of the polygons (Fig. 30C). The surface surrounding the shells is very hummocky with several kettle holes, debris stripes and inactive fluvial channels (Fig. 30D).

Interpretation

These sediments were only observed on the surface as no natural exposure into these sediments exists, therefore the internal structure of the sediment is unknown. However, the sediment at this site was overridden by the LIA glacier advance of Aldegondabreen (Fig. 9) and following retreat and degradation of the ice after 1911 the area was affected by dead-ice melting indicated by abundant kettle holes in and around the site.

The fact that the sediments appear on the surface in sorted polygons indicates that these sediments have undergone some frost-heave and thaw settlement, after the LIA retreat of the glacier, possibly in an active layer of permafrost (Humlum et al., 2003). This has been described as a result of convection in fine-grained centre of the polygons and subduction in the contact between the fine and coarse grained material on the sides of the polygons (Hallet and Prestrud, 1986). The large number of whole shells and large shell fragments indicate that the shells have not been transported for a long distance and are located close to their depositional position. The diamict sediments are therefore interpreted as glaciotectonised rafts and pods of displaced shallow marine sediments incorporated into subglacial till, as a result of a glacier advance. However, the glacial erosion and reworking of the sediments were insufficient to break all the shells into small fragments. A radiocarbon age of a *Hiatella arctica* shell from this site was dated 10 785 +270/-225 cal. a BP (Sample F-01; Table 1) which represents the maximum age of this glacier advance. Eventually, the LIA advance of Aldegondabreen, overrode these sediments. Following melting and retreat of the glacier, after 1911, they were influenced by dead-ice and possibly permafrost, frost and thaw processes. The shelly diamict sediments at site F are classified as LFA3.

Site H

Description

Site H is situated in the same small, curve-shaped sediment ridge as site G. A little section was excavated on the sea side of the north-eastern part of the ridge where it is lowest (Fig. 11). The sediments within the section consist of pebble-rich sandy gravel. Small shell fragments were observed within the whole section. The lowest 60 cm of the section, from ~2.1 m a.s.l. to 2.7 m a.s.l. has a maximum particle size of 5 cm. It has undergone some sorting and is stratified. Larger clasts become more abundant in the middle part with some clasts up to 20 cm in size. The top ~1 m of the section, reaching up to 4.3 m above sea level, is more clast-rich than the sediments below and the clasts are up to 30 cm in size, with some which are subrounded. This upper part is unsorted and more compacted than the lower part (Fig. 31A). On the glacier side, of this lower part of the ridge, brownish, gravelly silt and clay with whole shells and large shell fragments were observed on the surface (Fig. 31B). A striated clast was found within this deposit. These sediments appear similar to the sediments at site F.

Figure 30. A) The sandy gravel with small shell fragments at site E. B) Shell and shell fragments within the diamict at site F. C) Demonstration of the shelly sediments at site F, sorted in small polygons at the surface. D) Overview of the hummocks surrounding site F.

Interpretation

The top part of the section is interpreted to be deposited in a subglacial environment as a mixture of sediments from the lower part and subglacial till with some supraglacial and englacial components. This interpretation is based on the compactness of the upper part and the presence of large subrounded clasts. The upper part is suggested to be LFA3. The lower part of the section is interpreted in the same way as sediments at site G or sediments deposited in a glaciofluvial outwash plain and classified as a LFA2 (Krigström, 1962; Maizels, 1993). The silt and clay with whole bivalve shells and fragments, observed on the surface on the glacier side of the ridge, are suggested to be rafts and pods of glaciotectonised marine sediments similar to the deposit at site F. These sediments have been displaced during an ice advance and transported to a higher elevation. They are assigned to LFA3. It is suggested that these sediments were located below the outwash plain and lifted up to the surface of the ridge during the same glacial advance as described in the hypothesis for the formation of the ridge at site G. Striated clasts within these sediments indicated that they have been overridden by a glacier which supports the idea that the top part of the section is a mixture of sediments from the lower part and subglacial till, representing LFA3.

Site I

Description

Two small sections were excavated in the sides of an inactive fluvial channel on the large ridge. The site is situated on the northern part of the large sedimentary ridge where meltwater has cut deep into the ridge leaving natural exposures behind (Fig. 11). The top section is 80 cm thick, extending from ~20.5 to 19.7 m above sea level. The sediments in the top part consist of a matrix-supported, clast-rich, sandy-gravely diamict. Larger clasts occur in the upper part with a maximum particle size of 30 cm (Fig. 31C). Clasts on the surface are from subrounded to angular. Kettle holes, debris stripes and small transverse ridges are observed on the surface surrounding the site. The lower section was excavated at about 13.5 m above sea level. The sediments are composed of gravel, rich in clasts which are up to 6 cm in size. A few small shell fragments were found within the sediments, particularly towards the base.

Interpretation

The gravel from the lower section is interpreted to be LFA1 deposited in a shallow glaciomarine environment, near the grounding-line of a tidewater glacier (Powell, 1990; Batchelor and Dowdeswell, 2015). The small shell fragments indicate that they are not *in situ* within the unit but have been reworked. The sandy-gravely diamict in the top part is classified as LFA3. This unit is interpreted to be a mixture of the gravelly marine sediments from the lower part, and subglacial till with components of supraglacial- and englacial debris. Historical photos from 1911 demonstrate how this upper part was covered by the LIA glacier. Photos from 1936 show where supra- and englacial material melts out from the ice as it retreats, draping the subglacial surface underneath (Fig. 17).

Site J

Description

Site J is situated within the large sediment ridge, on its northern part on the ice distal side. The section studied is situated in an inactive fluvial channel where meltwater has exposed the sediments (Fig. 11). On the surface, at the top of the section, a small ridge, oriented transverse to ice flow is observed. The sediments within the upper part of the section are composed of clast-rich gravelly diamict. Sorted, sandy medium to fine gravel sediments are situated in the lower part which appear to be washed, similar to unit 1A at site A, unit 1 at site D and the sediments at site E (Fig. 22; Fig. 31D). The sandy gravel is at around 7.5 m above sea level and contains small shell fragments. The lower part is less cohesive than the upper part and falls easily down when excavated.

Figure 31. A) The top part of the section at site H. Sandy gravel with some clasts up to 30 cm in size. B) The brownish, gravelly silt and clay with whole shells found on the surface on the glacier side of site H, the dotted line demonstrates the outline of the small sediment ridge. C) The sediments from the top part of site I, classified as lithofacies association 3, sandy gravelly diamict. D) Boundaries between the upper and the lower part of the section at site J.

Interpretation

The gravelly diamict in the top part of the section is interpreted to be a subglacial till with some components of supra- and englacial debris. The upper part is categorised as a LFA3. The sediments and the small shell fragments in the lower part resemble units 1A at site A, 1 at site D and site E. The sediments in unit 1 at site D have been dated to maximum 11.27 cal. ka BP, when relative sea level was around 43 m a.s.l. These units have therefore been interpreted as deposited in subaqueous environment, within a grounding-line fan in front of a tidewater glacier

(Powell, 1990; Lønne, 2005). This interpretation is also suggested for the lower part of site J. The washed appearance of the lower part indicates current- or wave washing, sorting the sediments by transporting finer particles away (Powell, 1984). These sediments are categorised into LFA1.

Site K

Description

Site K is situated in the same inactive fluvial channel as site I, on the northern part of the large ridge (Fig. 11). A small section was dug into the sediments, 80 cm thick, with its top at ~15 m above sea level. The sediments are stratified and consist of sorted sandy gravel. Maximum particle size is 10 cm and thin mud coat was observed to drape clasts surfaces, similar to unit 1B at site A and unit 2 at site D.

Interpretation

The sediments are interpreted to be deposited in a subaqueous environment based on the thin mud coat draping clasts surfaces, which indicates settling out of suspension during a period of low discharge (Powell, 1984). The stratification and the grain size of the sediments implies that they were deposited along the runout distance of a jet in a grounding-line fan, which originates from subglacial and basal meltwater tunnels that transport sediments into the marine environment (Powell, 1990). The sandy gravel at site K is a part of LFA1.

Site 1

Description

A small section was excavated at site 1. The site is located within an inactive fluvial channel on the northernmost part of the large sediment ridge (Fig. 11). The sedimentary section is situated on the northern side of the channel. Above the sedimentary section, on the surface of the ridge, a small transverse ridge and debris stripes are observed. The top of the sedimentary section is at ~13 m a.s.l. The uppermost 150 cm of the section is a matrix-supported, gravelly diamict. The diamict is clast-rich with the maximum clasts size being 20 cm. Beneath the diamict is a sandy gravel layer with abundant large shell fragments (Fig. 32A, B). The sandy gravel is at least 60 cm thick, from 11.5 to 10.9 m a.s.l.

Interpretation

The section at site 1 is assigned to LFA3. The 150 cm thick gravelly diamict in the upper part is interpreted to be a mixture of the shelly gravelly unit from below and subglacial till with some debris from supra- and englacial environment. The sandy gravel in the lower part with abundant large shell fragments is interpreted similarly as the shelly diamict at site F, or pre-existing sediments, deposited in a shallow marine environment and brought to a higher elevation during a glacier advance. These sediments have only been transported several hundred

meters with the glacier and are therefore close to their original depositional environment, demonstrated by the number of large shell fragments.

Site 2

Description

Site 2 is situated on the large sediment ridge, in the same inactive fluvial channel as site 1, however on its southern side (Fig. 11). Two small sedimentary exposures were excavated into the sediments. The lower exposure, at 10 m a.s.l., revealed at least 30 cm thick silty-clayey, medium to fine gravel unit with whole shells and numerous large shell fragments (Fig. 22; Fig. 32D). Clast size is up to 20 cm and clay and silt form a thick coat around clasts. The upper exposure was excavated at ~12 m a.s.l., adjacent to the other one. The sediments in this upper exposure are composed of sandy gravel, at least 60 cm thick. Maximum particle size is 20 cm and some shell fragments were found within the unit, although they are less abundant and smaller than in the lower exposure (Fig. 32C). Debris stripes and small transverse ridges are found on the surface of the ridge, above the section.

Interpretation

Section at site 2 is interpreted to represent LFA3. The sediments in the top part of the section are suggested to be a mixture of the shelly gravelly unit from below and subglacial till with some debris from supra- and englacial environment. The lower part is interpreted as shallow marine deposits which have been overridden by a glacier advance and lifted to a higher elevation. This idea is supported by coarse clasts found within the sediments, the high amount of silt and clay, and the number of large shell fragments, which indicate that these sediments have not been transported a long distance, only several hundred meters, from their original deposition.

Site 3

Description

A sedimentary section was dug at site 3. The site is in an inactive fluvial channel on the southern edge of the large sedimentary ridge (Fig. 11; Fig. 33A). The upper part of the exposure consists of a gravelly diamict with clasts of up to 30 cm in size. Below, is a stratified, sorted sandy gravel with maximum particle size of 7 cm. Small shell fragments are scattered around the lower part (Fig. 33B). It is at least 50 cm thick and is situated at ~6.5 m a.s.l. Small transverse ridges and inactive fluvial channels are situated on the surface of the ridge, around the site.

Figure 32. A) The boundaries between the gravelly diamict from the upper part and the sandy gravel with large shell fragments from the lower part at site 1. B) Example of shell fragments from the lower part at site 1. C) The upper exposure at site 2, composed of sandy gravel with some large clasts up to 20 cm in size. D) Silty-clayey gravel from the lower exposure at site 2 with large shell fragments.

Interpretation

The diamict, situated in the upper part is interpreted to be a combination of debris with sub-, supra- and englacial origin and the sorted sandy gravel from the unit below. This upper part is categorised as LFA3. The sandy gravel and the small shell fragments in the lower part of the section in site 3, resembles the deposit which has been interpreted as sediments from a shallow glaciomarine environment near the grounding-line of a tidewater glacier. The lower part of section 3 is therefore also classified as LFA1, possibly deposited along the runout distance of a jet in a grounding-line fan (Powell, 1990; Batchelor and Dowdeswell, 2015).

Site 4

Description

Site 4 is located in a narrow inactive fluvial channel in the southern part of the forefield, approximately 70 m from the coast (Fig. 11). A sedimentary section was excavated on the northern side of the channel. The uppermost 150 cm of the section is a clast-rich, matrix-supported gravelly diamict with clasts up to 15 cm in size. Sorted sandy gravel was observed below, at least 30 cm thick with a maximum particle size of 10 cm. The gravel contains very small and few shell fragments and is situated at 6 m a.s.l. (Fig. 33C).

Interpretation

The upper part of the section is interpreted to be LFA3, subglacial till with englacial and supraglacial components, combined with sandy-gravelly material from the lower part of the section. The lower part of the section has a similar sediment composition and small shell fragments as deposits which represent LFA1. The sandy gravel at site 4 is therefore also interpreted to be deposited in a shallow glaciomarine environment, along the runout distance of a jet in a grounding-line fan in front of a tidewater glacier (Powell, 1990). The shell fragments indicate reworking of pre-existing marine sediments.

Site 5

Description

Site 5 is situated on the southern side of the same inactive fluvial channel as site 4 (Fig. 11). A small sedimentary section was excavated at 5 m a.s.l. The sediments within the exposure are silty-clayey gravel. Few shell fragments were found within the sediments.

Interpretation

The sediments and the small shell fragments at site 5 resemble the grounding-line fan deposit in LFA1 and are therefore interpreted as sediments deposited in a grounding-line fan. The fine grain size suggests deposition along the runout distance of a jet in front of a tidewater glacier (Powell, 1990).

Site 6

Description

Site 6 is situated on the southernmost tip of the forefield in a coastal sedimentary section (Fig. 11). The section is ~1 m thick, from 2 to 3 m a.s.l. The uppermost 50 cm consists of a clast-rich gravelly diamict. Below, a pebble-rich, silty-clayey medium to fine gravel unit was observed (Fig. 22). The gravel contains an abundance of white and orange coralline algae. Several shell fragments were found as well within the gravel (Fig. 33D).

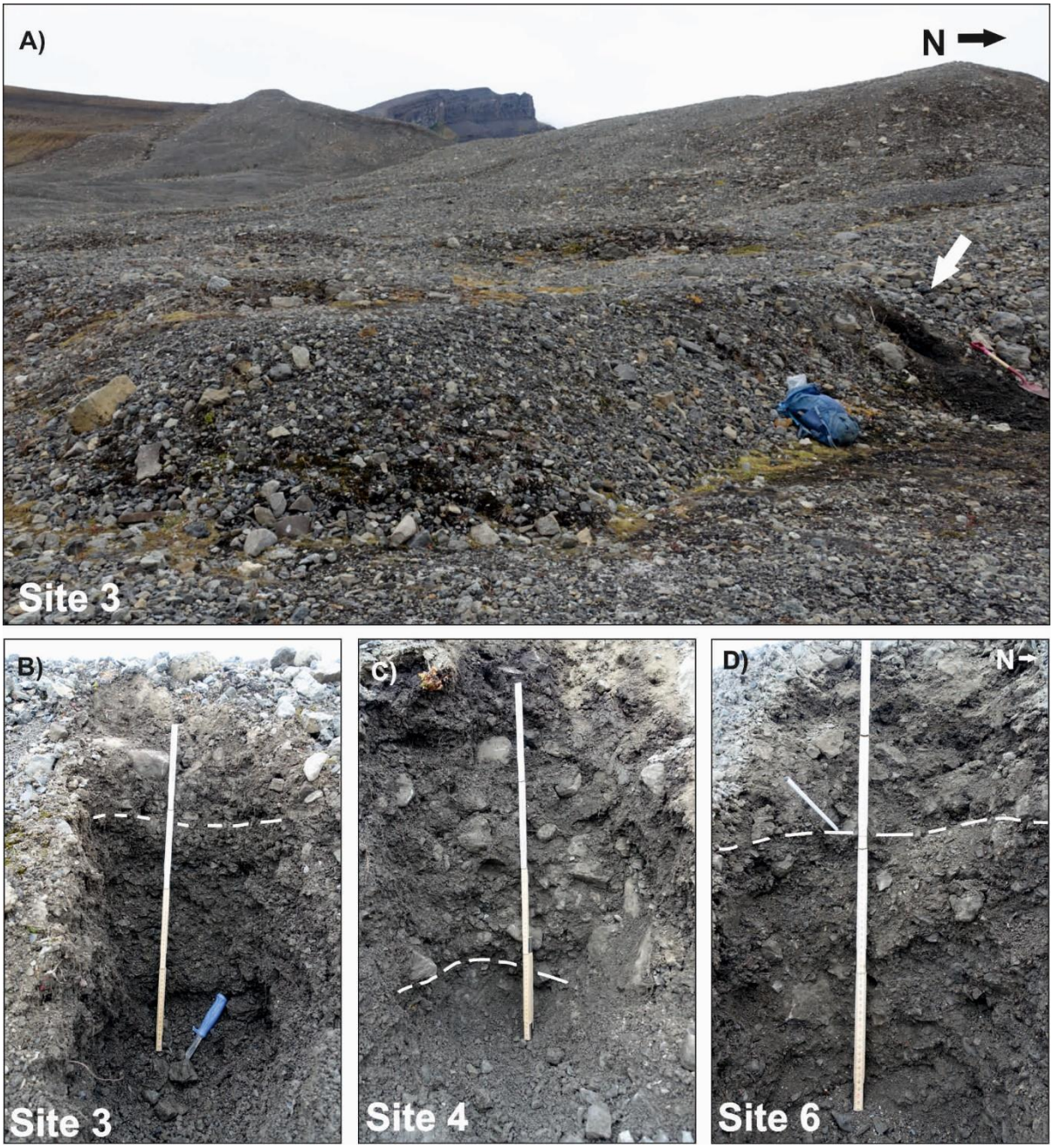

Figure 33. A) Overview of site 3 on the southern edge of the large sedimentary ridge. B) Boundaries between the upper part of section 3, a gravelly diamict and the lower part with stratified sandy gravel with some small shell fragments. C) The small exposure at site 4, gravelly diamict in the upper part and sandy gravel with small shell fragments in the lower part. D) The exposure at site 6. The upper part consists of gravelly diamict and the lower part is a silty-clayey gravel with white and orange coralline algae and small shell fragments.

Interpretation

Aerial photos from Aldegondabreen since 1911 reveal that the glacier did not cover this part of the forefield at that time (Fig. 9). However, the LIA maximum advance of the glacier might have occurred before 1911 and therefore it is hard to say if the uppermost diamict has been affected by the LIA advance of Aldegondabreen as unit 4 at site A, unit 3 at site D, unit 5 at site G and top part of sites H, I, J, 1, 2, 3 and 4. In a geomorphological map of the forefield from Kirkebøen (2018), the sediment cover on top of this section is interpreted to be a hummocky moraine due to mounds, depressions and slumping activity in the surrounding area. On aerial images of Aldegondabreen from 1990 and 2008 it is apparent which area of the forefield has been overridden and affected by the LIA advance, as the vegetation cover is much better developed outside of the LIA advance area. Site 6 is situated within the affected area of the forefield, indicating that the site was at some point partly covered or affected by the LIA advance of Aldegondabreen. Therefore, the hypothesis of Kirkebøen (2018) of a hummocky moraine will be applied here as well. Taken together, the upper part of the section at site 6 is interpreted to be a mixture of subglacial, englacial, and supraglacial debris which was deposited during melt-out of a debris covered glacier and has been affected by dead-ice melting and re-sedimentation due to slumping and ice melting from underneath the sediment cover (Kjær and Krüger, 2001; Benn and Evans, 2010). The lower part of the section is interpreted to be shallow marine sediments indicated by the number of white and orange coralline algae. It is hard to determine whether the sediments in the lower part have been affected by a glacier advance similarly to site F, 1 and 2. Site 6 is located further out in the fjord than sites F, 1 and 2 and data from this study do not provide evidence of the maximum extent of this pre-LIA glacier advance described at site F.

4.4 Sediment lithofacies associations

4.4.1 Lithofacies association 1 (LFA1)

Gravel units formed in a shallow glaciomarine environment, in a grounding-line fan or close to the grounding-line of a tidewater glacier

The units which fall under this lithofacies association are unit 1A, 1B, 2 and 3 at site A, unit 1 and 2 at site D, the lower part of the sections in sites I, J, 3, 4 and the sections at sites E, K and 5. These different units contain a variety of lithofacies. Some contain silty and sandy gravel while others are composed of cobbly-gravel or are pebble-rich. Small shell fragments are found in some of the units. This lithofacies association is interpreted to be the product of sedimentation in an ice-proximal, shallow glaciomarine environment, in a grounding-line fan in front of a tidewater glacier or close to the grounding-line.

Grounding-line fans can form at the mouth of subglacial and basal meltwater tunnels at the grounding zone of a marine-terminating glacier. These landforms may contain a variety of sediments, including sub-aquatic outwash, suspension settling of fine-grained material and gravity-flow sediments. Fluctuations in sediment transport and water discharge, movement of

the efflux location across the grounding line and glacier terminus stability can produce significant variety of sediment texture within grounding-line fans (Powell, 1990; Bennett et al., 1999; Koch and Isbell, 2013; Batchelor and Dowdeswell, 2015; Dowdeswell et al., 2015).

Grounding-line fans are usually formed when the grounding zone of the glacier is stable for some time. Fans produced in front of advancing glaciers will be modified and overridden with time and fans in front of glaciers with a rapid retreating ice margin will not have sufficient time to build up (Batchelor and Dowdeswell, 2015). It is therefore suggested that the sediments were deposited in front of a stable ice margin as there is no observed evidence of modification after deposition in the fan, aside from being overridden by the LIA advance and covered in subglacial till.

To summarize, these units are interpreted as the result of a glacier which advanced into shallow marine environment and remained stationary for some time. During the advance, the glacier overrode pre-existing marine sediments with shells. These marine sediments were reworked and transported downstream by subglacial and basal meltwater streams. Eventually the sediments were carried into the glaciomarine environment and re-deposited near the grounding-line of the tidewater glacier. The coarser-grained sediments were deposited in a grounding-line fan and finer particles were transported further away with a buoyant plume before settling out of suspension once the turbulence decreased.

Site A is suggested to have been located very close to the efflux of the meltwater channel where the discharge can be very high and fully turbulent. This is indicated by imbricated cobbles in unit 1B and by the coarse cobbles and gravel in unit 2. Mud coated clast surfaces, and gravel matrix in some units suggest fluctuation in discharge, permitting finer grained sediments to settle down in between larger clasts while the discharge was low. Subunit 3c at site A contains a high amount of silt and sand which forms a thick coating between and around larger clasts. This subunit was interpreted to represent a gravity-flow deposit. Unit 2 at site D and subunit 3e at site A contain coarse gravel and pebble lenses. They are suggested to imply deposition during pulses of increased discharge, sorting the sediments and moving finer particles away. The shell fragments found within some of these units represent reworking of pre-existing marine sediments, which the glacier overrode during the advance.

The fine grain size of unit 2 at site D, the lower part of sites I, K, 3 and 4, and site 5 indicate that these sediments were deposited along the runout distance of the jet in a grounding-line fan, rather than near the efflux of the meltwater channel, like site A. This proximal to distal fining reflects the drop of flow velocities with distance from the tunnel mouth. As sites I, K, 3, 4 and 5 are situated several dozen meters away from sites A and D, it is also possible that the sediment there might have formed in a different grounding-line fan than sites A and D. Location of an efflux across a grounding-line can change over a long distance from one melt season to the next and sometimes within one season. Fans may therefore build out in several places along the grounding-line and can overlap as younger fans prograde towards an older fan (Powell, 1990).

Unit 1A at site A, unit 1 at site D, and the sediments at sites E and in the lower part at site J are interpreted as wave or current influenced sediments indicated by their "washed" appearance where clasts within the units are clean, without any coating of fine-grained material. These units exhibit less cohesion compared to the units situated above and they fall down easily when excavated. This can be a result of the wave- or current washing, where finer grains are transported further away in suspension, sorting the sediment and decreasing the cohesion of the unit. The units containing these sediments are situated at the base of their sedimentary sections.

4.4.2 Lithofacies association 2 (LFA2)

Glaciotectonised gravel units formed in a subaerial glaciofluvial outwash plain

The units which represent lithofacies association 2 are units 1, 2, 3, 4 at site G and the lower part of the sections in site H. These units are generally described as stratified, pebble and cobble-rich sandy gravel with shell fragments. Some contain coarse gravel lenses while imbricated cobbles and boulder-sized clasts are found in others.

These units are interpreted as being deposited in a subaerial glaciofluvial outwash plain formed by meltwater from Aldegondabreen (Krigström, 1962; Maizels, 1993). The steep dip of unit 1, up glacier and the gentle dip of unit 2 - 4 in the opposite dip directions to unit 1, or down glacier, and the maximum age for these sediments derived from low-precision radiocarbon dating, indicate that these sediments have been glaciotectonised with a thrust block formation, by a glacier advance from Aldegondbreen which displaced and lifted these sediments to a higher elevation (Evans, 2000).

Glaciofluvial outwash is built up in large aggradational plains by meltwater streams which carry sediments across the forefield in the form of bedload and suspension. Different grain size of the sediments indicates fluctuations in the discharge of the meltwater streams (Krigström, 1962; Maizels, 1993).

It is worth noting the variance in the sediments from these units. Unit 2 at site G is coarse grained with boulders and imbricated cobbles. These sediments are interpreted to be transported as bedload under high water discharge, possibly during the peak of the meltwater season. However, unit 3 and 4 at site G are finer grained than unit 2. The sandy gravel in these units is suggested to be deposited with low energy streams which could have taken place during the initiation of the ablation season or towards the end of it.

Dates from units 3 and 4 yielded ages from both the Early and Middle Holocene. All of these ages were derived from shell fragments which indicates that they have been reworked. It is proposed that meltwater from Aldegondabreen cut into different kinds of sediments from the forefield, including marine sediments with shells from both the Early and Middle Holocene and re-deposited the mixture of sediments in the glaciofluvial outwash plain close to the coast.

To summarize, units 1, 2, 3 and 4 at site G and the lower part of the sections in site H are interpreted as glaciofluvial sediments, deposited in an outwash plain close to the coast by meltwater from Aldegondabreen. Later, the sediments were displaced and lifted to a higher elevation during a glacial advance from Aldegondabreen, which deformed the sediments and formed the ridge. This is proposed to have occurred after 4.72 cal. ka BP, assuming that the low-precision radiocarbon dates are reliable for interpretation of the maximum age for the ridge.

4.4.3 Lithofacies association 3 (LFA3)

Glaciogenic facies

The units which represent lithofacies association 3 are unit 4 at site A, unit 3 at site D, unit 5 at site G, site F, 1, and 2, top part of sites I, J, 3, 4 and 6, and the top part and surface of site H. These units are all interpreted to be glacial facies, including subglacial till facies with components of supra- and englacial debris and pre-existing gravel sediments from the units below, as well as glaciotectonised rafts and pods of displaced marine sediments with whole shells and numerous large shell fragments.

Units 4 at site A, unit 3 at site D, unit 5 at site G and top part of sites H, I, J, 1, 2, 3, 4 and 6 are described as matrix-supported, gravelly diamict. The diamict is clast-rich with clasts up to boulder size. The units are generally more compacted than the sediments situated in the below sections. At the main sites, A, D and G, lenses of coarse gravel were observed within the units, and they are more prominent towards the base. Striated clasts were found in unit 4 at site A and in unit 5 at site G. Unit 5 at site G contains generally fewer large clasts and is more stratified compared to other sites.

These units have been interpreted to be a combination of subglacial till with components of supra- and englacial debris, and pre-existing sediments from the units below which have been incorporated into the diamict and poorly modified. At sites A, D, I, J, 3, 4 and 6, the pre-existing sediments resting below, were deposited in a subaqueous grounding-line fan. However, at sites G and H the pre-existing gravel sediments are interpreted to have been deposited in a subaerial glaciofluvial outwash plain that was glaciotectonised and deformed with a fault block formation.

These units are therefore interpreted as a response to a glacier advance across a shallow glaciomarine grounding-line fan sediment or deformed glaciofluvial outwash plain, representing the LIA glacier advance of Aldegondabreen. Towards the end of the LIA, the glacier snout became thin and cold-based and underwent passive melting and degradation. Subsequently, sediment cover of supraglacial and englacial origin was left behind resting on top.

The nature of these units is dependent on the sediments which rest below at each site. At sites A, D and G, coarse gravel lenses are observed within the diamict. Very similar gravel lenses are presented in the units below which indicate that the lenses within the diamict originate from

the unit underneath and have been incorporated within the diamict and poorly modified when overridden by the glacier. The properties of these units are similarly reliant on the amount of supra- and englacial material that was incorporated in the glacier at each site before it melted away. At site G, the unit contains few large clasts and is more stratified compared to the other main sites. The reason for this could be due to the location of the site close to the shoreline and on the outer perimeter of the glacier where it was likely thin, limiting modification of the bed underneath and transportation of sediments.

The sediments at site F, on the surface of site H and in the lower part of sites 1 and 2 are generally described as sandy-, silty- and clayey gravel units with some larger cobbles, and whole shells and numerous large shell fragments. These sediments are interpreted as glaciotectonised rafts and pods of displaced shallow marine sediments.

The sediments therefore represent a glacier advance over marine sediments, which were lifted to a higher elevation. However, the sediments were only poorly modified during the advance indicated by whole shells and an abundance of large shell fragments. These sediments are therefore suggested to be close to their original depositional location. Considering the small size of the forefield, it is proposed that these sediments have only been transported for several hundreds of meters by the glacier.

These sediments are distinguished from lithofacies associations 1 and 2 as they are finer grained, contain whole shells and large shell fragments and do not have any evidence of being reworked by meltwater. However, the units within LFA 1 and 2 contain only very small shell fragments, have undergone some sorting, and imbrication and stratification are found within some of the units. Therefore, the sediments at site F, on the surface of site H and in the lower part of sites 1 and 2 are interpreted to be the old shallow marine sediments which were reworked with glacial meltwater and re-deposited to produce the sediments within LFA 1 and 2. This suggestion is supported by the high-precision radiocarbon dates from these LFAs. The age for a shell within LFA3, obtained from site F, yielded 10.79 cal. ka BP (sample F-01) which falls into the age range for shells dated from LFA 1 and 2, from sites A, D and G, 10.00 - 11.38 cal. ka BP. This indicates that the large shell fragments and the whole shells from LFA3 and the small shell fragments from LFA 1 and 2 originate from the same sediments.

The glaciotectonised shallow marine sediments at site F and H are situated at the surface in the forefield. Site F appears to be more diamicty than the other units and the sediments on the surface of site H contain striated clasts. These sites were overridden by the LIA glacier advance of Aldegondabreen and site F has also been affected by dead-ice melting following the retreat of the LIA glacial advance and permafrost processes, sorting the sediments in small polygons.

No natural sedimentary exposure exists in the forefield for these units and only small sections were excavated into these units at sites 1 and 2. Therefore, it is not known whether these sediments contain any deformation structure which would support the idea of these sediments being overridden by ice and glaciotectonised.

5 Discussion

In this chapter the results will be discussed and two conceptual models for the Holocene glacial history of Aldegondabreen will be presented. The first model is for the Deglaciation and the Early Holocene with an explanation for the formation of the large sedimentary ridge and the second model is for the period after 4.72 cal. ka BP, presenting the hypothesis for the formation of the small ridge (site G and H). The chapter will additionally focus on other discussion points such as grounding-line fan implications for past glacier dynamics and environmental settings, the Late Glacial and Early Holocene glacier readvance record from Svalbard, and different suggestions and ideas for the cause of these readvances. The final section in the chapter will focus on suggestions for further research.

5.1 Deglaciation of Grønfjorden and Early Holocene readvance of Aldegondabreen

During the Younger Dryas (12.9 - 11.7 ka BP) the Svalbard and Barents Sea Ice Sheet had retreated from the continental shelf and into fjords of Svalbard (Hormes et al., 2013; Reusche et al., 2014). Isfjorden is suggested to have been half-way deglaciated by 11.6 ka BP and as the ice retreated inside of the fjord, tributary fjords of Isfjorden began to deglaciate (Farnsworth et al., 2020). A new study from Heftyebreen moraine suggests ice-free marine conditions in the Heftyebreen catchment in Grønfjorden (Fig. 35) as early as 13.0 - 12.9 cal. ka BP (Farnsworth et al., 2022). In 1992, Mangerud et al., proposed that Grønfjorden was deglaciated by 11.5 cal. ka BP, based on a radiocarbon date from a bivalve shell in the forefield of Aldegondabreen. The oldest radiocarbon age from this study (11.38 cal. ka BP; Table 1) is in accordance with this previous suggestion from Mangerud et al., 1992. Therefore, it is suggested that the mouth of Grønfjorden, including the Heftyebreen catchment, may have deglaciated earlier then the Aldegondabreen forefield, around 13.0 - 12.9 cal. ka BP, while ice remained occupying most of the Aldegondabreen catchment until a minimum date of 11.38 cal. ka BP. By this time, the ice in Grønfjorden had retreated at least 14 km inward away from the mouth of the fjord to the location of Aldegondabreen. These new radiocarbon dates from Grønfjorden improve the current understanding of the ice retreat during deglaciation in the fjord.

The sea level in Grønfjorden had dropped from at least 52 m a.s.l. since the beginning of the Younger Dryas, to below 43 m a.s.l. at 12.2 ka BP (Farnsworth et al., 2022). Around 11.5 cal. ka BP, the sea level in the fjord is suggested to have been between 43 and 30 m a.s.l. (Forman, 1990; Salvigsen et al., 1990; Farnsworth et al., 2022). Based on sedimentological and chronological evidence from this study, it is suggested that in the part of Aldegondabreen's forefield below 30 m, marine sediments including bivalve shells were deposited and accumulated from at least 11.5 to 10.79 cal. ka BP (Fig. 34B), this includes all the study sites in this paper. These marine sediments are for instance present at sites F, H, 1 and 2 in the forefield of Aldegondabreen (Fig. 11).

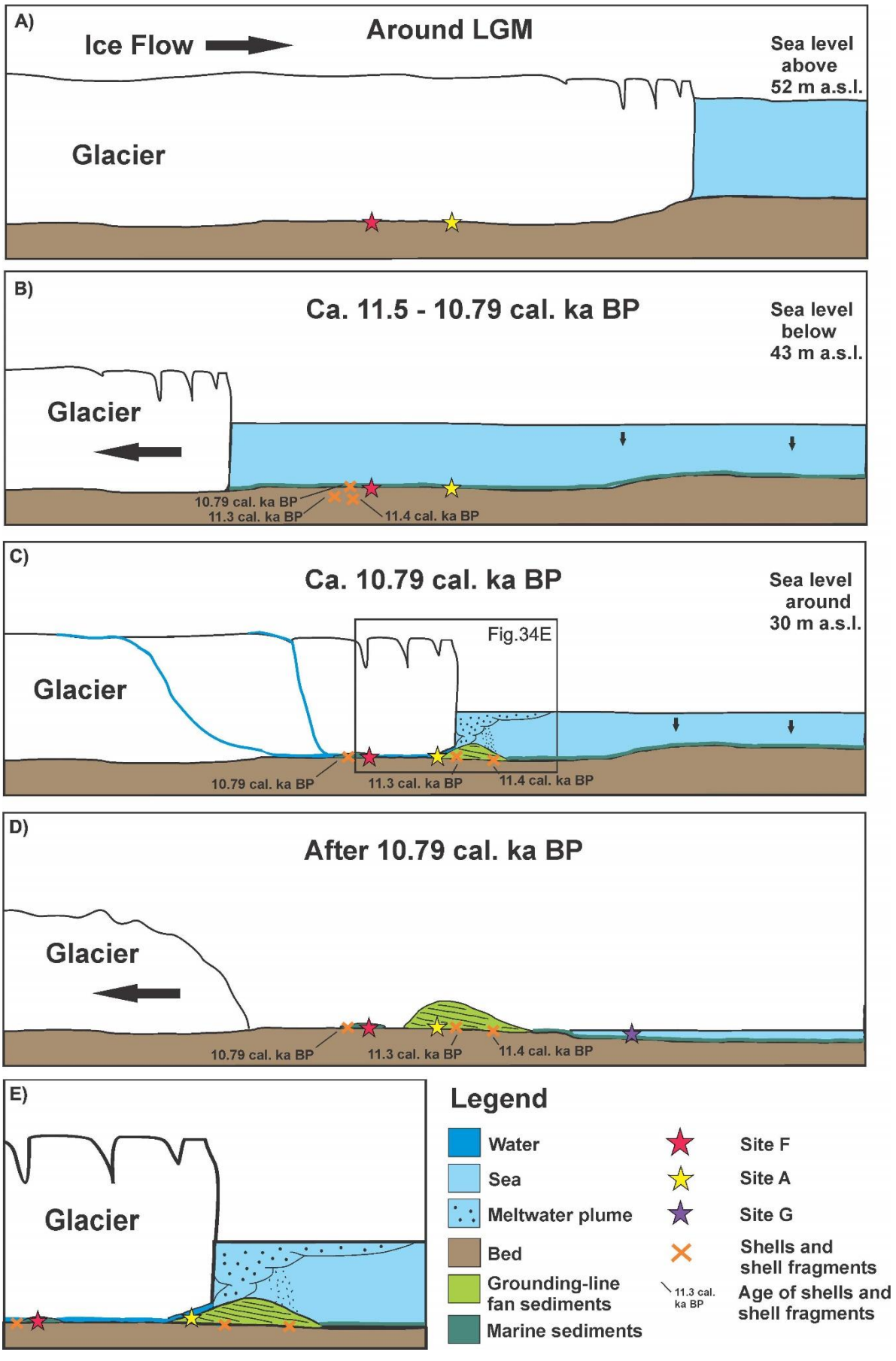
A)
Ice Flow
Around LGM
Sea level above 52 m a.s.l.
Glacier
B)
Ca. 11.5 - 10.79 cal. ka BP
Sea level below 43 m a.s.l.
Glacier
10.79 cal. ka BP
11.3 cal. ka BP
11.4 cal. ka BP
C)
Ca. 10.79 cal. ka BP
Sea level around 30 m a.s.l.
Fig.34E
Glacier
10.79 cal. ka BP
11.3 cal. ka BP
11.4 cal. ka BP
D)
After 10.79 cal. ka BP
Glacier
10.79 cal. ka BP
11.3 cal. ka BP
11.4 cal. ka BP
E)
Glacier
Legend
Water
Sea
Meltwater plume
Bed
Grounding-line fan sediments
Marine sediments
Site F
Site A
Site G
Shells and shell fragments
11.3 cal. ka BP
Age of shells and shell fragments

Figure 34. A conceptual model of Aldegondabreen from LGM to the Early Holocene demonstrating the formation of the grounding-line fan. A) Aldegondabreen during the LGM when the sea level was minimum 52 m a.s.l. B) From 11.5 - 10.79 cal. ka BP, the sea level in Grønfjorden is suggested to have been between 43 and 30 m a.s.l. The glacier was retreating at that time and marine sediments including bivalve shells were deposited and accumulated in the forefield of Aldegondabreen. C) Aldegondabreen readvances into the shallow fjord while the sea level was around 30 m a.s.l. The maximum age for this event is 10.79 cal. ka BP. Older marine sediments and bivalve shells and fragments were transported with subglacial meltwater into the shallow glaciomarine environment, forming a grounding-line fan at the grounding zone of the glacier. D) After the glacier readvance, Aldegondabreen retreated back while the sea level was lowering. The grounding-line fan emerged from the sea forming a ridge on dry land in the forefield. E) The figure demonstrates in detail the formation of the grounding-line fan in the Early Holocene. The meltwater reworked and transported older marine sediments and shells subglacially into the glaciomarine environment to the grounding-line. Coarse-grained sediments were deposited close to the meltwater efflux and accumulated to form a grounding-line fan. Finer particles were transported further away with a buoyant plume before settling out of suspension on the glacier distal site of the fan.

Analyses of the gravelly sediments from LFA1 at study sites A, D, E, I, J, K, 3, 4 and 5, indicate that these sediments were deposited in a grounding-line fan at the grounding zone of a tidewater glacier in a shallow glaciomarine environment. The formation of this grounding-line fan is suggested to represents a readvance of Aldegondabreen into the shallow sea of Grønfjorden (Fig. 34C). The earliest timing of this event is reconstructed with a radiocarbon age derived from a bivalve shell at site F, 10.79 cal. ka BP.

Studies focusing on the relative sea level during the Early Holocene in the regions around Grønfjorden, suggest a relative sea level of around 30 m higher then present around 10.79 cal. ka BP (Fig. 34C) (Salvigsen et al., 1990; Forman, 1990). Therefore, it is proposed that Aldegondabreen readvanced into the shallow fjord during a high relative sea level in the Early Holocene. The marine sediments at sites F (Fig. 34C), H, 1 and 2 in the forefield indicate that during this readvance the glacier overrode these older marine sediments which contained bivalve shells and fragments. These marine sediments and shells were reworked and transported with subglacial meltwater streams into the shallow glaciomarine environment. Once these sediments emerged from the tidewater glacier and into the shallow fjord, they were deposited with the reworked shell fragments in a grounding-line fan at the grounding zone of the glacier (Fig. 34C, E).

The sediments within the grounding-line fan contain bivalve shells spanning ages from 11.27 to 11.38 cal. ka BP. These dates are not suggested to represent the maximum age of the readvance because the interpretation from this study implies that the fan was formed with old reworked marine sediments similar to what is present at site F and dated 10.79 cal. ka BP. Therefore, the timing of the readvance and the formation of the fan cannot be older than the age from site F.

Figure 35. The figure demonstrates the ice margin of Aldegondabreen in 2020 and 1911. The minimum ice margin position of the glacier in the Early Holocene is also demonstrated, constructed with the location of the grounding-line fan deposit. It is suggested that in the Early Holocene, Aldegondabreen extended at least 2 km beyond the 2020 ice margin and ca. 230 m further up valley from the 1911 ice margin. Heftyevatnet and Heftyebreen moraine can be seen in the upper right corner which have recently been studied by Farnsworth et al. (2022). Base map provided by the Norwegian Polar Institute (2021b).

The total size and extent of this grounding-line fan is unknown, however based on examination of sediments in the forefield the minimum size of the fan can be reconstructed. The grounding-line fan is suggested to have extended for at least 620 m along the tidewater glacier ice margin (from site K, south to sites 4 and 5) with a minimum width of 170 m and height of at least 15 m above present sea level (Site K). The estimation for the minimum volume of the grounding-line fan is therefore 0.001581 km^3.

The maximum extent of Aldegondabreen during this Early Holocene cannot be reconstructed with data from this study. However, the minimum ice margin position of the glacier can be constructed with the location of the grounding-line fan deposit. These sediments were deposited at the tidewater ice margin. Because they are not considered to have been modified or reworked after deposition in the fan, aside from being overridden by the LIA advance and covered in subglacial till, they can provide the minimum extent of the glacier during the readvance in the Early Holocene. The palaeo-Aldegondabreen system is proposed to have extended at least 2 km beyond the modern ice margin (2020) in the Early Holocene and around 230 m further up

valley from the 1911 ice margin position at the end of the LIA (Fig. 35). The glacier may have advanced further out into the fjord prior to the deposition of the grounding-line fan in the Early Holocene and subsequently retreated back to the location of the fan where it stayed still while the fan was building up.

This Early Holocene readvance of Aldegondabreen provides further knowledge of glaciers and their behaviour in Svalbard at that time and is important additional data to the Late Glacial - Early Holocene glacier record in Svalbard.

5.2 Grounding-line fans and their implications for past glacier dynamics and environmental settings

Ancient grounding-line fans can provide indications of past glacier dynamics and the glaciomarine environment during the fan build up (Koch and Isbell, 2013; Dowdeswell et al., 2015). These landforms form at the grounding zone of a marine-terminating glacier at the mouth of subglacial meltwater channels (Batchelor and Dowdeswell, 2015). This implies that where these fans were formed, abundant meltwater was available which was able to form a network of subglacial drainage channels. The meltwater must have contained sediments that were delivered to the ice-margin of the tidewater glacier at point sources (Dowdeswell et al., 2015). It has further been described that grounding-line fans typically develop in glacial settings where meltwater is derived mainly from ice-surface melting during summer (Dowdeswell et al., 2015; Batchelor and Dowdeswell, 2015). Therefore, it has been suggested that where these ancient grounding-line fans were formed, the environment was relatively mild (Koch and Isbell, 2013; Dowdeswell et al., 2015). Similar conditions, which are favourable for a grounding-line formation, are found in the southeast Alaska, southern Chile and in Svalbard today (Trusel et al., 2010; Dowdeswell et al., 2015). Modern glaciers at these locations have been described to have a relatively high mass turnover, or renewal of the ice mass by mass balance processes. The snow precipitation at these glaciers is high to intermediate and surface melting is the main cause of mass loss. Offshore water temperatures are generally several degrees Celsius (Dowdeswell et al., 2015).

In contrast, high-polar environmental conditions have been described as unfavourable for a grounding-line fan development (Dowdeswell et al., 2015). This is because of low or absent glacier surface melting in the summer due to low air and water temperatures. The precipitation in these locations is also low, only few centimetres per year. Subsequently, offshore sedimentation rates are low and are mainly due to release of debris from melting icebergs. These conditions are present today in East Antarctica, in the Canadian high Arctic and in northern Greenland (Dowdeswell et al., 2015).

It is therefore proposed here that the climate and the environmental settings in Grønfjorden during the Early Holocene readvance of Aldegondabreen were mild with ocean water temperature of several degrees and high or intermediate snow precipitation. These climatic conditions permitted summer surface melting of Aldegondabreen, resulting in abundant glacial meltwater which formed a network of subglacial drainage channels. These suggestions are in

accordance with proposed climatic conditions from other studies and records in Svalbard during the Early Holocene (Mangerud and Svendsen, 2018).

A study from the Austfonna ice cap in Svalbard has demonstrated that the retreating ice margin has limited the formation of grounding-line fans over the past 40 years (Dowdeswell et al., 2015). This indicates that grounding-line fan formation requires a stable tidewater glacier terminus of over a year and up to several decades (Batchelor and Dowdeswell, 2015).

The meltwater discharge and sedimentation rate can vary significantly between glaciers, seasons, and locations. This can result in various sizes of grounding-line fans even from similarly long build up periods. A grounding-line fan formation in front of Muir Glacier in southeast Alaska was observed to occur over a 20-year period of glacier terminus stability. The size of the fan was estimated to be ca. 0.8 km^3 with a radius of ca. 4 km (Seramur et al., 1997). The discharge and the sedimentation rate for Muir Glacier is, however, two orders of magnitude greater than that observed in eastern Svalbard (Dowdeswell et al., 2015). Another study from Kongsfjorden in western Spitsbergen, demonstrates a grounding-line fan which formed over 22 years of ice margin stability with a volume of only 0.0196 km^3 and a building rate of 0.000891 km^3/year (Trusel et al., 2010). The estimate for the minimum volume of the grounding-line fan in the forefield of Aldegondabreen is 0.001581 km^3. By suggesting the same building rate for the grounding-line fan from Aldegondabreen in the Early Holocene to modern day Kongsfjorden, the minimum time for the formation of the grounding-line fan at Aldegondabreen is only 2 years. This means that the glacier terminus had to be stagnant for at least 2 years while the fan was building up. However, the sedimentation rate for Aldegondabreen in the Early Holocene and the building rate of the fan may have been higher or lower resulting in longer or shorter build up period.

The sediments within the grounding-line fan in front of Aldegondabreen appear to be unmodified since deposition, aside from being overridden by the LIA advance and covered in subglacial till. Therefore, it is suggested that the tidewater ice margin of Aldegondabreen was stable while the fan was building up.

5.3 Glacier readvances in Svalbard during the Late Glacial and Early Holocene

Due to lack of studies and low preservation potential of glacial landforms and sediments, the record of Late Glacial and Early Holocene glacial deposit in Svalbard is fragmented (Larsen et al., 2018). However, an increasing number of studies are focusing on glacial deposit from this period which have revealed that many glaciers in Svalbard experienced a readvance during overall warm climatic conditions in the Late Glacial and Early Holocene (Salvigsen et al., 1990; Lønne, 2005; Forwick et al., 2010; Farnsworth et al., 2017; Larsen et al., 2018; Farnsworth et al., 2018; Flink et al., 2018; Farnsworth et al., 2022). The data from this study further support these findings and adds to the Late Glacial - Early Holocene glacial record.

At least six glacier readvances have been reported from the west coast of Spitsbergen during the Late Glacial and Early Holocene. The time range for these events spans ca. 2.9 ka years, from about 10 to 12.9 cal. ka BP. The oldest glacial event is from the Younger Dryas, 12.9 to 12.2 cal. ka BP, and is reported from an abandoned moraine ridge in the Heftyebreen catchment (Fig. 35) in Grønfjorden, Isfjorden (Farnsworth et al., 2022). The well-defined timing of this glacial advance was constrained with radiocarbon dates and presence of the Vedde Ash in the lacustrine sediments of Heftyevatnet. This advance represents the first and the only glacier margin dated to the Younger Dryas in Svalbard. In the north-western part of Isfjorden, a study of a stratigraphic section from Ymerbukta outlined a glacier readvance shortly after 10.3 cal. ka BP from Esmarkbreen (Salvigsen et al., 1990). This glacial advance was proposed to be a brief and a local event with the maximum extent within the LIA moraines of Esmarkbreen. Lønne (2005) described another brief glacial event from Bolterdalen, in the inner part of Isfjorden, during the same period, 10.4 – 10.9 cal. ka BP. Geological sections indicate that an ice-contact delta was formed during a glacier readvance into shallow water, 58 m above the present sea level. The study proposed that the event was climatically driven and lasted for several decades with the maximum ice-front position around 7 km outside the present ice margin. Interestingly, a study from van Mijenfjorden (Larsen et al., 2018) south of Isfjorden, identifies glacial deposit linked to a glacier readvance that fits the time frame for the glacial events in Bolterdalen and in Ymerbukta. The glacier deposit from van Mijenfjorden is interpreted as a glacier-fed delta formed in a high relative sea level, during a glacier readvance after the regional deglaciation, ca. 10.4 cal. ka BP. The maximum extent of the ice margin during this event is well outside the LIA margins. Farnsworth et al. (2017) suggested that a glacier readvance occurred at Gunnarbreen in St. Jonsfjorden, north of Isfjorden, constrained between 10 and 12.8 cal. ka BP. The full glacier extent during this event is unknown, however they proposed that the snout extended at least 750 m further than it did in 1936. A thrust moraine, located in central Tempelfjorden in the innermost part of Isfjorden, has also been linked to a glacier readvance during the Late Glacial (Forwick et al., 2010).

At least two studies from north west Spitsbergen have identified glacial events in the Late Glacial and Early Holocene. Henriksen et al. (2014) suggested a valley glacier readvance in Kongsfjorden on the west coast of Spitsbergen, during the Younger Dryas or Early Holocene and van der Bilt et al. (2015), proposed a Holocene glacial maximum between 9.6 - 9.5 cal. ka BP on the Mitrahalvøya Peninsula, based on lake sediments from Hajeren.

Additionally, Late Glacial and Early Holocene glacial readvances have been outlined from the east coast of Spitsbergen and Edgeøya. An end moraine in de Geerbukta was proposed to have formed in a readvance of palaeo-Gullfaksebreen between 12.0 and 10.6 cal. ka BP (Farnsworth et al., 2018). The glacier extended further than the Late Holocene position of the glacier and over 5.5 km beyond the modern ice margin. Flink et al. (2018) suggested a glacier readvance during the Early Holocene in Mohnbukta, which was more extensive than the LIA advance and Ronnert and Landvik (1993) dated glacial sediments from Edgeøya, east of Svalbard to 9.8 cal. ka BP.

The age range for all the glacier readvances reported from Svalbard in the Late Glacial to Early Holocene is from 12.9 to 9 ka BP and more than half of these events occurred between 11 -10 ka BP (Farnsworth et al., 2020). The timing of the Aldegondabreen readvance (after 10.79 cal. ka BP) falls into this period of the highest frequency of glacier readvance during the Early Holocene.

The majority of the studies of these Late Glacial - Early Holocene glacial events suggest that the ice margin position during the readvance extended well beyond the maximum LIA extent in the Late Holocene. Farnsworth et al. (2018) suggested that at least five other locations in Svalbard, Tåbreen, Albertbreen, Lyckholmdalen, Flowerbreen and Richterbreen, demonstrated evidence of terrestrial, Late Glacial - Early Holocene end moraines which extend several kilometres further than the Late Holocene maximum ice extent. However, earlier studies from the west coast of Spitsbergen have indicated that cirque glaciers were less extensive during the Late Glacial than the Late Holocene (Mangerud and Svendsen, 1990; Svendsen and Mangerud, 1997). On the other hand, it has been noted that where these Late Glacial - Early Holocene readvances have been identified, the glaciers experienced minimal extension during the Late Holocene and some cirque and valley systems were almost ice free during this period (Farnsworth et al., 2022). If the glaciers which exhibited an Early Holocene readvance were more extensive during the Late Holocene, it is likely that the older glacial sediments from the Early Holocene may have been removed or eroded and not preserved in the landscape.

The position of the ice margin of Aldegondabreen in 1911 is 230 m beyond the minimum ice extent of Aldegondabreen during the Early Holocene readvance (Fig. 35). However, data from this study can only indicate the minimum advance of the glacier during the Early Holocene. Bathymetry studies of the sea-floor morphology in the fjord in front of Aldegondabreen may potentially indicate how far Aldegondabreen readvanced during the Early Holocene and reveal if the glacier extended beyond the 1911 ice position.

5.4 Suggestions and ideas for the cause of the Late Glacial - Early Holocene readvances in Svalbard

The question still remains as to why Aldegondabreen and other glaciers in Svalbard readvanced during the Late Glacial and Early Holocene. Different explanations and suggestions have been proposed. Warm and moist regional conditions with increased winter precipitation, and summer temperatures reaching 6°C warmer than today have been described for the period before and throughout the Early Holocene in Svalbard (Mangerud and Svendsen, 2018; Farnsworth et al., 2020; Kjellman et al., 2020). Ocean bottom water temperatures around Spitsbergen were approximately 6°C higher than at present, summer insolation was rising, and sea-ice extent declined (Beierlein et al., 2015; Larsen et al., 2018; Mangerud and Svendsen, 2018). These climatic conditions have been described as unfavourable for glacier growth in both marine and terrestrial environments, (Farnsworth et al., 2017) as demonstrated in earlier studies from west and north Spitsbergen, which suggests that some glaciers retreated to innermost fjord position

or even melted entirely away during the Early and Middle Holocene (Svendsen and Mangerud, 1997; Fjeldskaar et al., 2018; Allaart et al., 2020).

Despite this, Lønne (2005) described the readvance of the glacier in Bolterdalen as a climatically controlled event which was brief and lasted between 10.4 and 10.9 cal. ka BP. She pointed out that Esmarkbreen in Ymerbukta (Salvigsen et al., 1990) advanced in the same time period (10.3 cal. ka BP). Interestingly, the Early Holocene readvance of Aldegondabreen (10.79 cal. ka BP) and the readvance in van Mijenfjorden (10.4 cal. ka BP; (Larsen et al., 2018)) also fit this time frame. Larsen et al. (2018) stated that they were unable to confirm the main cause of the readvance in van Mijenfjorden but suggested that it might have been driven by an increase in moisture supply because of increased ocean temperature.

The majority of all the glacier readvances around Svalbard from the Late Glacial to Early Holocene occur between 11 and 10 ka BP (Farnsworth et al., 2020). However, with an increasing number of studies on glacial deposit from this time, it has been noted that there is no clear synchronicity of these readvance events (Farnsworth et al., 2018). Farnsworth et al. (2018) suggested that this indicated that these glacial fluctuations are less likely to be directly related to one specific climatic event. In a study from St. Jonsfjorden, Farnsworth et al. (2017) proposed that the ice-margin behaviour of some glaciers during the Late Glacial and Early Holocene was controlled by internal dynamics rather than by a regional mass balance trend caused by climatic forces.

As an explanation for glacier readvance during times of unfavourable climatic conditions, Farnsworth et al. (2017) developed a conceptual model on the basis of glacial advances from the inner part of St. Jonsfjorden, which excludes the sea-level component (Fig. 36). The idea of the model is that local glaciers experience small advances as a result of unbalanced glaciodynamic conditions, rather than a direct response to climate. When the dominant trunk glacier in the fjord is in balance, the surface profiles of the tributary glaciers in the fjord are in equilibrium with the back-stress of the trunk glacier (Fig. 36A). If the trunk glacier retreats an unbalanced system is created (Fig. 36B). The tributary glaciers must reorganize their over-steepened surface profiles in response to the release of back-stress. This can lead to advance of the ice fronts of tributary glaciers (Fig. 36C) until they retreat back to a new equilibrium state with a quasi-stable ice marginal position (Fig. 36D). Farnsworth et al. (2017), suggested that this model may represent the cause of Gunnarbreen's readvance in the Early Holocene, following the retreat of the dominant tidewater glacier in the fjord during the deglaciation. If this model can explain Late Glacial - Early Holocene glacial fluctuations, a readvance situated near the mouth of the fjord may be older than the age of a readvance located in an inner tributary fjord (Farnsworth et al., 2018). This has not yet been observed in the Late Glacial - Early Holocene glacial record from Svalbard and more studies are necessary to determine whether this may be the cause for these readvances.

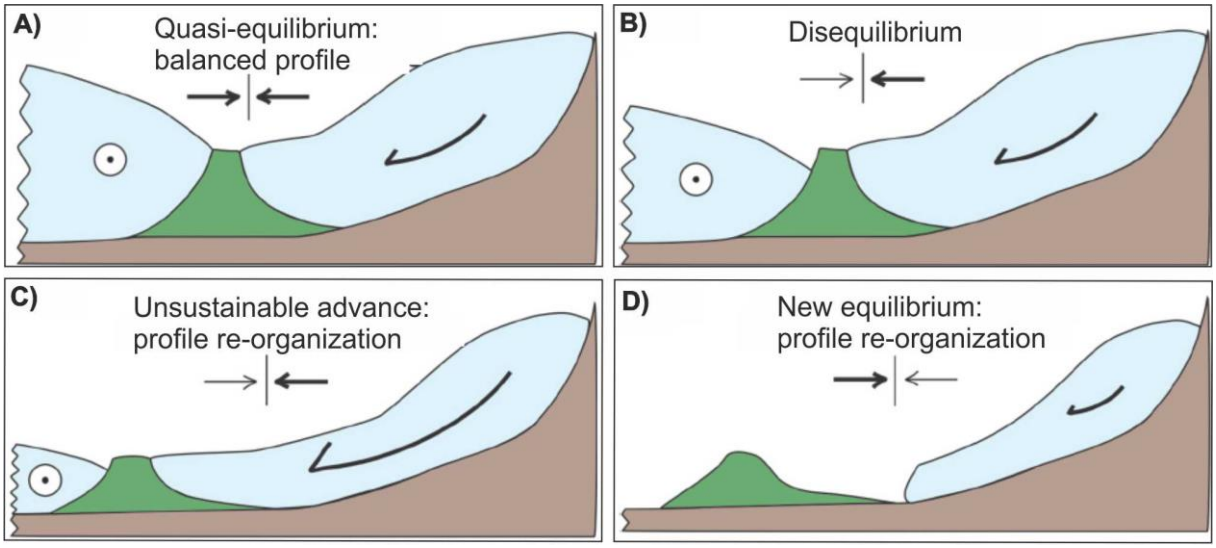

Figure 36. A conceptual model with a potential cause for a glacier readvance during times of unfavourable climatic conditions. The model excludes the sea-level component. A) The trunk glacier (marked with a circle) in the fjord is in balance and a tributary glacier in the fjord is in equilibrium with the back-stress of the trunk glacier. B) Once the trunk glacier retreats an unbalanced system is created. C) The unbalanced system leads to an advance of the tributary glacier which needs to reorganize its over-steepened surface profile in response to the release of back-stress. D) The tributary glacier retreats to a new equilibrium state with a quasi-stable ice margin. Figure modified from (Farnsworth et al., 2017).

Surges, as a result of internal glacial dynamics, are another explanation that has been proposed for these Late Glacial - Early Holocene readvances (Flink et al., 2018; Farnsworth et al., 2018). As many Svalbard glaciers are surge-type, the glaciers in the Late Glacial - Early Holocene may have undergone surge-type behaviour. Farnsworth et al. (2016) suggested that Aldegondabreen is a surging glacier based on surge-indicative landforms: crevasse squeeze ridges, observed from aerial images of the forefield of Aldegondabreen. Kirkebøen (2018), interpreted these ridges as crevasse infill ridges with material infill from supra and englacial environments and concluded that Aldegondabreen has not surged during the last glacial advance. Additionally, Holmlund (2021) stated in a study of a photogrammetric reconstruction of Aldegondabreen, that there is no clear indication since at least 1910, that the glacier is of surging-type. Regardless of this, palaeo-Aldegondabreen may have exhibited a different internal dynamic during the Early Holocene and therefore it is difficult to rule out the possibility of a surge event at Aldegondabreen in the Early Holocene.

However, it is unlikely that the readvance of Aldegondabreen during the Early Holocene, resulting in the formation of the grounding-line fan, was a surge event. As proposed above, the ice margin of Aldegondabreen is likely to have been stable for some time while the grounding-line fan built up. During the active phase of a surge event, the ice margin advance rate generally varies from 3 m/year up to 200 m/year (Burton et al., 2016). The ice margin retreat after the active phase can start very soon after the surge is over and it has been reported from some glaciers in Svalbard that the retreat started within a year from the end of the active phase (Lefauconnier and Hagen, 1991; Dowdeswell et al., 1991). Ice front retreat after the active phase of a surge event has been described as constant and continuous and a retreat of 400 - 500

m/year has been reported from some surge glaciers in Svalbard (Lefauconnier and Hagen, 1991). Thus, the Early Holocene readvance of Aldegondabreen was unlikely a surge event, based on the fact that there would have been insufficient time for the development of the grounding-line fan, both during the active phase and as the ice margin retreated after the surge. It should be noted, however, that meltwater floods with high water discharge can occur during the termination of a surge event and could represent a potential alternative way for a grounding-line fan to form at Aldegondabreen. These floods have been related to a shift in the basal drainage system of the glacier, back to a conduit system when the ice flow velocity is slowing down. However, this would require ice terminus stability during the flood event and a sediment resource with abundant material available for transport with the meltwater in order for the fan to build up.

As the maximum age for the Aldegondabreen readvance is 10.79 cal. ka PB and the adjacent Heftyebreen catchment was ice free as early as 13.0 cal. ka BP, 2.21 ka before, it is suggested that a climate response is more likely an appropriate cause for the Aldegondabreen readvance rather than a dynamic response to the removal of back-stress. However, to conclude whether this glacier advance and the other readvances in Svalbard during the Late Glacial - Early Holocene were climatically forced or a result of internal glacier dynamics, more investigations are needed focusing on Late Glacial - Early Holocene deposits, the climate at that time and precise dating of these events. Because of a lack of synchronicity and the fact that these Late Glacial - Early Holocene glacial deposits seem to correspond to glaciers of all sizes (Farnsworth et al., 2018) there might be various reasons behind each different readvance during this period.

5.5 Glacial history of Aldegondabreen after 4.72 cal. ka BP

The hypothesis (Fig. 37) proposed for the formation of the ridge at sites G and H suggests that the ridge was formed in a readvance of Aldegondabreen when the glacier overrode a glaciofluvial outwash plain (Fig. 37B). The glaciofluvial outwash sediment was glaciotectonised and deformed in a thrust block formation which pushed the sediment up to a higher elevation, forming the ridge (Fig. 37C). Shelly, silty, and clayey, marine sediments observed on the surface of the ridge at site H, are suggested to have been lifted up to the surface of the ridge in the same advance (Fig. 37C).

The youngest radiocarbon date from the ridge is 4.72 cal. ka BP which is suggested to be the maximum age for the formation of the ridge. The relative sea level for the area during that time was 3 m above present sea level (Salvigsen et al., 1990; Forman et al., 2004). Since then, relative sea level has lowered due to glacioisostatic rebound, until it reached the present-day level (Forman et al., 2004; Ingólfsson and Landvik, 2013).

The youngest age from the ridge (4.72 cal. ka BP) is derived from a *Mytilus edulis* shell fragment. *Mytilus edulis* is a shallow-water species living in the Arctic and has been considered an indicator of warmer sea conditions than those observed in Svalbard today (Blake, 2006; Mangerud and Svendsen, 2018). Following recent warming, *Mytilus edulis* re-appeared in Svalbard in 2004, after almost 4000 years of absence (Berge et al., 2005; Mangerud and

Svendsen, 2018). *Mytilus edulis* first arrived in Svalbard at 11.1 cal. ka BP. It was rare in the archipelago from ~9.0 to 8.2 cal. ka BP but became common once again after 8.2 cal. ka BP until 6.2 cal. ka BP when it decreased and was very rare until it became extinct on Svalbard around 3.7 cal. ka BP (Mangerud and Svendsen, 2018). The *Mytilus edulis* ages from this study correspond to the latest stage of the mollusc existence in Svalbard, from the Middle Holocene, before it became extinct around 3.7 cal. ka BP as ocean temperatures started to decrease during the Neoglacial.

During the LIA, Aldegondabreen advanced over the ridge at site G, as demonstrated from aerial images from 1911. It is suggested that unit 5 at site G, a mixture of glaciofluvial sediments from unit 4 and subglacial till with some englacial and supraglacial components, was formed when Aldegondabreen overrode the ridge during that advance (Fig. 37C, D). This LIA readvance of Aldegondabreen is also proposed to have formed unit 4 at site A, unit 3 at site D and the top part of sites H, I, J, 1, 2, 3, 4 and 6 (Fig. 37C, D).

However, the question remains of whether the ridge at site G and H was formed in a glacier advance of Aldegondabreen during the LIA or prior to the LIA, after 4.72 cal. ka BP. The only known advance of Aldegondabreen since 4.72 cal. ka BP was during the LIA and the glacier was already retreating in 1910 (Holmlund, 2021). The climate in Svalbard during the Middle Holocene has been described as warmer than present, although the climate had cooled since the Early Holocene (Farnsworth et al., 2020). In the end of the Middle Holocene, around 4.7 cal. ka BP, air temperatures had reached similar to modern levels (Mangerud and Svendsen, 2018).

Glaciers in Svalbard have been described at their Holocene minimum extent during the Middle Holocene and some even disappeared (Svendsen and Mangerud, 1997; Allaart et al., 2020). The climate cooled during the onset of the Neoglacial, providing more favourable climatic conditions for glacier growth demonstrated by glacial records from Svalbard during the Neoglacial (Werner, 1993; Svendsen and Mangerud, 1997; Reusche et al., 2014). The earliest Neoglacial readvance recorded from Svalbard is ca. 4 cal. ka BP (Miller et al., 2017). Hence, there is a possibility that Aldegondbreen readvanced somewhere in the Neoglacial and formed the ridge at sites G and H.

Another possibility is that the ridge at site G and H was formed at the onset of the LIA advance of Aldegondabreen. The glacier advanced across the glaciofluvial sediments, which were pushed up in thrust blocks in front of the glacier, forming the ridge. Later in the same advance the glacier could have overridden the deformed glaciofluvial sediments in the ridge and simultaneously formed unit 5 subglacially.

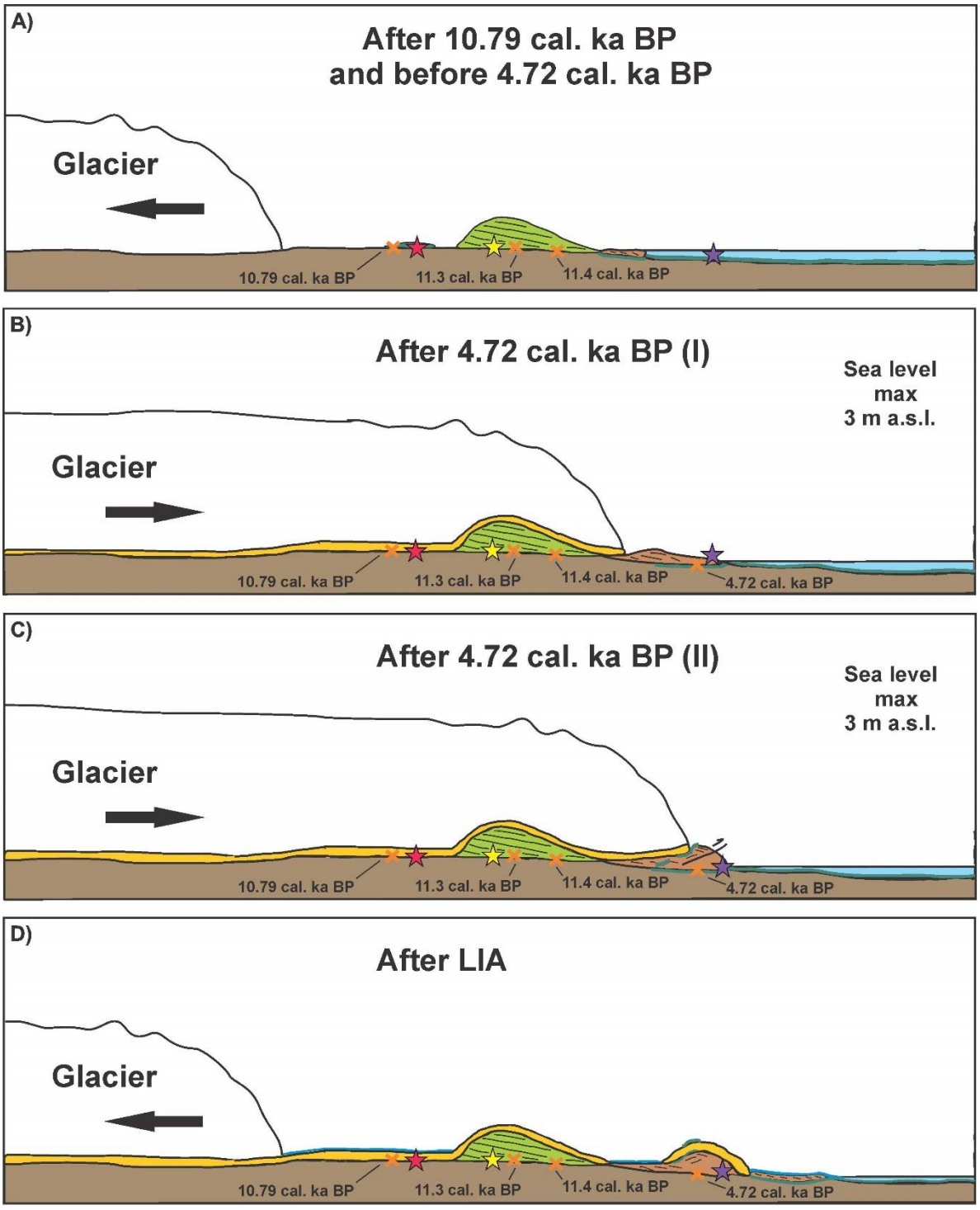
A)
After 10.79 cal. ka BP
and before 4.72 cal. ka BP
Glacier
10.79 cal. ka BP
11.3 cal. ka BP
11.4 cal. ka BP
B)
After 4.72 cal. ka BP (I)
Sea level
max
3 m a.s.l.
Glacier
10.79 cal. ka BP
11.3 cal. ka BP
11.4 cal. ka BP
4.72 cal. ka BP
C)
After 4.72 cal. ka BP (II)
Sea level
max
3 m a.s.l.
Glacier
10.79 cal. ka BP
11.3 cal. ka BP
11.4 cal. ka BP
4.72 cal. ka BP
D)
After LIA
Glacier
10.79 cal. ka BP
11.3 cal. ka BP
11.4 cal. ka BP
4.72 cal. ka BP
Legend
Water
Sea
Bed
Glaciofluvial outwash plain sediments
Grounding-line fan sediments
Subglacial sediments
Marine sediments
11.3 cal. ka BP
Age of shells and shell fragments
Shells and shell fragments
Site F
Site A
Site G

Figure 37. Conceptual model of Aldegondabreen from 4.72 cal. ka BP to the termination of the LIA demonstrating the hypothesis for the formation of the small sedimentary ridge at site G and H. A) Before 4.72 cal. ka BP a glaciofluvial outwash plain was forming in front of the grounding-line fan ridge while the sea level was lowering. The sediments within the glaciofluvial plain were reworked older marine sediments with bivalve shells both from Early and Middle Holocene. B) After 4.72 cal. ka BP while the sea level was maximum 3 m a.s.l. Aldegondabreen advanced over the glaciofluvial outwash plain which started to deform. C) As the glacier continued to advance into the glaciofluvial outwash plain the sediments within it were glaciotectonised with a thrust block formation, which lifted the sediments to a higher elevation and formed the ridge at site G and H. Older marine sediments were additionally pushed up to the surface of the ridge in the same advance. D) Aldegondabreen advanced over the small ridge at site G and H, and over the grounding-line fan ridge at site A and D during the LIA. During this advance the glacier formed subglacially unit 5 at site G, unit 4 at site A, unit 3 at site D and the top part of sites H, I, J, 1, 2, 3, 4 and 6. After the LIA when the glacier was retreating back, these subglacial sediments were left behind, draping the surface of the forefield.

Sediment composition and properties of unit 1 - 4 at site G indicate that the sediments were deposited in a subaerial glaciofluvial plain. Therefore, it is suggested that the ridge was formed when the sea level had lowered to modern day level, when a well-developed glaciofluvial plain had formed in the lower forefield. It is therefore more likely that the ridge was formed during the onset of the LIA, rather than in the Neoglacial. To further confirm the age of the ridge, it must be investigated in more detail and the *Mytilus edulis* shell fragments need to be dated with high-precision radiocarbon dating.

5.6 Further studies

The studied sediments and landforms from the forefield of Aldegondabreen provide new insights into the Holocene glacial history of Aldegondabreen prior to the LIA. However, the glacial history of Aldegondabreen is still fragmented and some uncertainties can be improved with further research of the glacier and its forefield.

Better age constraining evidence is needed for the timing and the length of the Early Holocene readvance of Aldegondabreen. Dateable organic material from sediments and landforms in the forefield could provide more precise timing for the readvance and the length of the event. This would also help to place the Early Holocene advance of Aldegondabreen into the larger context of other Early Holocene readvances in Svalbard. Since the maximum extent of Aldegondabreen during the Early Holocene readvance is unknown, studies of the sea-floor morphology and the bathymetry in the fjord in front of the forefield could indicate how far Aldegondabreen extended during the Early Holocene readvance. Bathymetry data may also reveal the maximum extent of the glacier in the LIA and therefore answer the question of whether the glacier extended further out in the Early Holocene or during the Late Holocene.

More detailed mapping of the grounding-line fan deposit in the lower forefield would improve estimates of the total size of the fan formed during the Early Holocene. Approximations can then be made for grounding-line fan accumulation time.

Further investigation is needed to determine the main cause for the Early Holocene readvance of Aldegondabreen and other glaciers on Spitsbergen. The current understanding of glacial fluctuations in Svalbard during the Late Glacial and Early Holocene is insufficient to validate whether these readvances were climatically driven or due to internal glacier dynamics. Future studies should focus on adding data to the Late Glacial and Early Holocene glacial record from Svalbard by studying glacial deposits from this period. There are several factors we need to understand better which might help to identify the main causes for these glacier fluctuations. This includes a better insight into past climate, including both winter precipitation and summer temperatures, and an improved understanding of glacioistostatic uplift of the land and its potential influence on glaciers mass balance (Farnsworth et al., 2018).

The hypothesis proposed for the formation of the small ridge at site G and H needs to be tested further as its formation is still unclear. Excavation of a larger section in the ridge, preferably a section which provides a profile view into the sediments, may reveal if there are any direct evidence for the ridge to be glaciotectonized, such as a fault plane structure or a fault block. A more precise age for the formation of the ridge is also needed. One approach could be to date the *Mytilus edulis* shell fragments from the ridge with high-precision radiocarbon dating. Old photos and aerial images of Aldegondabreen and from Grønfjorden, prior to 1910/1911 could potentially provide better information of whether the ridge was formed during the LIA advance or before.

6 Conclusions

- Sedimentary landforms in the lower forefield of Aldegondabreen were analysed with sedimentological and geomorphological methods and dated with radiocarbon dating in order to reconstruct the Holocene glacial history of Aldegondabreen, a small valley glacier on the west coast of Svalbard.

- Sediments and landforms in the forefield of Aldegondabreen indicate that the glacier readvanced during the Early Holocene into the shallow fjord during overall high relative sea level. The maximum age, 10.79 cal. ka BP, for this event is based on radiocarbon dating of bivalve shells and fragments from glacially overridden marine sediments.

- Sediments within a large sedimentary ridge in the lower forefield were deposited during an Early Holocene readvance of Aldegondabreen in a grounding-line fan, formed at the grounding zone of a tidewater glacier. The grounding-line fan consists of reworked marine sediments and shells, which accumulated in the forefield from ca. 11.5 to 10.79 cal. ka BP. They were transported during the readvance, with subglacial meltwater streams supplying sediments to the grounding-line and into the glaciomarine environment.

- The minimum extent of Aldegondabreen during the Early Holocene readvance, constrained by the location of grounding-line fan deposits, was at least 2 km beyond the modern ice margin (2020), being 230 m within the glacier's 1911 ice margin.

- The formation of the grounding-line fan during the Early Holocene readvance of Aldegondabreen suggests that the climate and the environmental settings in Grønfjorden were mild with ocean water temperature of several degrees and high or intermediate snow precipitation. These conditions permitted summer surface melting of Aldegondabreen and development of a network of subglacial drainage channels.

- Based on the structure and stratigraphy of a small ridge (Site G and H) in the lower forefield, Aldegondabreen appears to have advanced somewhere after 4.72 cal. ka BP into a glaciofluvial outwash plain. Consequently, the glaciofluvial outwash sediments were glaciotectonised in a thrust block formation that lifted the sediments up to a higher elevation, forming the ridge.

- The grounding-line fan sediments and the small ridge, containing sections G and H, were overridden during the LIA advance of Aldegondabreen which formed the uppermost unit of these landforms.

7 References

Aber, J.S., Ber, A., 2006. Glaciotectonism. Elsevier, Amsterdam.

Alexanderson, H., Backman, J., Cronin, T.M., Funder, S., Ingólfsson, Ó., Jakobsson, M., Landvik, J.Y., Löwemark, L., Mangerud, J., März, C., Möller, P., O'Regan, M., Spielhagen, R.F., 2014. An Arctic perspective on dating Mid-Late Pleistocene environmental history. Quaternary Science Reviews 92, 9-31.

Alexanderson, H., Henriksen, M., Ryen, H.T., Landvik, J.Y., Peterson, G., 2018. 200 ka of glacial events in NW Svalbard: an emergence cycle facies model and regional correlations. Arktos 4, 1-25.

Allaart, L., Müller, J., Schomacker, A., Rydningen, T.A., Håkansson, L., Kjellman, S.E., Mollenhauer, G., Forwick, M., 2020. Late Quaternary glacier and sea-ice history of northern Wijdefjorden, Svalbard. Boreas 49, 417-437.

Batchelor, C.L., Dowdeswell, J.A., 2015. Ice-sheet grounding-zone wedges (GZWs) on high-latitude continental margins. Marine Geology 363, 65-92.

Beierlein, L., Salvigsen, O., Schöne, B.R., Mackensen, A., Brey, T., 2015. The seasonal water temperature cycle in the Arctic Dicksonfjord (Svalbard) during the Holocene Climate Optimum derived from subfossil Arctica islandica shells. The Holocene 25, 1197-1207.

Benn, D.I., 2009. Glacial Sediments, in: Gornitz, V. (Ed.), Encyclopedia of Paleoclimatology and Ancient Environments. Springer, Dordrecht, pp. 382-384.

Benn, D.I., Ballantyne, C.K., 1993. The description and representation of particle shape. Earth Surface Processes and Landforms 18, 665-672.

Benn, D.I., Ballantyne, C.K., 1994. Reconstructing the transport history of glacigenic sediments: a new approach based on the co-variance of clast form indices. Sedimentary Geology 91, 215-227.

Benn, D.I., Evans, D.J.A., 2010. Glaciers and Glaciation, 2nd edition. Routledge, London.

Bennett, M.R., Hambrey, M.J., Huddart, D., Glasser, N.F., Crawford, K., 1999. The landform and sediment assemblage produced by a tidewater glacier surge in Kongsfjorden, Svalbard. Quaternary Science Reviews 18, 1213-1246.

Bennett, M.R., Huddart, D., Waller, R.I., 2000. Glaciofluvial crevasse and conduit fills as indicators of supraglacial dewatering during a surge, Skeiðarárjökull, Iceland. Journal of Glaciology 46, 25-34.

Berge, J., Johnsen, G., Nilsen, F., Gulliksen, B., Slagstad, D., 2005. Ocean temperature oscillations enable reappearance of blue mussels Mytilus edulis in Svalbard after a 1000 year absence. Marine Ecology Progress Series 303, 167-175.

Björnsson, H., 1998. Hydrological characteristics of the drainage system beneath a surging glacier. Nature 395, 771-774.

Blake, W., 2006. Occurrence of the Mytilus edulis complex on Nordaustlandet, Svalbard: radiocarbon ages and climatic implications. Polar Research 25, 123-137.

Boulton, G.S., 1978. Boulder shapes and grain-size distributions of debris as indicators of transport paths through a glacier and till genesis. Sedimentology 25, 773-799.

Brennand, T., Shaw, J., Sharpe, D., 1996. Regional-scale meltwater erosion and deposition patterns, northern Quebec, Canada. Annals of Glaciology 22, 85-92.

Burton, D.J., Dowdeswell, J.A., Hogan, K.A., Noormets, R., 2016. Marginal Fluctuations of a Svalbard Surge-Type Tidewater Glacier, Blomstrandbreen, Since the Little Ice Age: A Record of Three Surges. Arctic, Antarctic, and Alpine Research 48, 411-426.

Bush, S.L., Santos, G.M., Xu, X., Southon, J.R., Thiagarajan, N., Hines, S.K., Adkins, J.F., 2013. Simple, Rapid, and Cost Effective: A Screening Method for 14C Analysis of Small Carbonate Samples. Radiocarbon 55, 631-640.

Carrivick, J., Russell, A., 2007. Glacifluvial Landforms of Deposition, in: Scott, E. (Ed.), Encyclopedia of Quaternary Science. Elsevier, Amsterdam, pp. 909-919.

Chorley, R., Schumm, S., Sugden, D., 1984. Geomorphology. Methuen, London.

Coulson, S.J., Fjellberg, A., Gwiazdowicz, D.J., Lebedeva, N.V., Melekhina, E.N., Solhøy, T., Erséus, C., Maraldo, K., Miko, L., Schatz, H., Schmelz, R.M., Søli, G., Stur, E., 2013. The invertebrate fauna of anthropogenic soils in the High-Arctic settlement of Barentsburg, Svalbard. Polar Research 32, 19273.

Coulthard, R.D., Furze, M.F.A., Pieńkowski, A.J., Chantel Nixon, F., England, J.H., 2010. New marine ΔR values for Arctic Canada. Quaternary Geochronology 5, 419-434.

Cuffey, K.M., Paterson, W.S.B., 2010. The Physics of Glaciers. Elsevier, Burlington, Mass.

Dallmann, W.K., 2015. Geoscience atlas of Svalbard. Norwegian Polar Institute. Report Series No. 148, Oslo.

Dowdeswell, J.A., Hamilton, G.S., Hagen, J.O., 1991. The duration of the active phase on surge-type glaciers : contrasts between Svalbard and other regions. Journal of Glaciology 37, 388-400.

Dowdeswell, J.A., Hogan, K.A., Arnold, N.S., Mugford, R.I., Wells, M., Hirst, J.P.P., Decalf, C., 2015. Sediment-rich meltwater plumes and ice-proximal fans at the margins of modern and ancient tidewater glaciers: Observations and modelling. Sedimentology 62, 1665-1692.

Dunér, N., Malmgren, A.J., Nordenskiöld, A.E., Qvennerstedt, A., 1867. Svenska expeditioner till Spetsbergen och Jan Mayen utförda under åren 1863 och 1864. Nordstedt & Söner, Stockholm.

Evans, D., Benn, D.I., 2004. A Practical Guide to the Study of Glacial Sediments. Edward Arnold, London.

Evans, D.J.A., 2000. A gravel outwash/deformation till continuum, Skalafellsjokull, Iceland. Geografiska Annaler: Series A, Physical Geography 82, 499-512.

Evans, D.J.A., Phillips, E.R., Hiemstra, J.F., Auton, C.A., 2006. Subglacial till: Formation, sedimentary characteristics and classification. Earth-Science Reviews 78, 115-176.

Farnsworth, W.R., Allaart, L., Ingólfsson, Ó., Alexanderson, H., Forwick, M., Noormets, R., Retelle, M., Schomacker, A., 2020. Holocene glacial history of Svalbard: Status, perspectives and challenges. Earth-Science Reviews 208, 103249.

Farnsworth, W.R., Ingólfsson, Ó., Mannerfelt, E.S., Kalliokoski, M.H., Guðmundsdóttir, E.R., Retelle, M., Allaart, L., Brynjólfsson, S., Furze, M.F.A., Hancock, H.J., Kjær, K.H., Pieńkowski, A.J., Schomacker, A., 2022. Vedde Ash constrains Younger Dryas glacier re-advance and rapid glacio-isostatic rebound on Svalbard. Quaternary Science Advances 5, 100041.

Farnsworth, W.R., Ingólfsson, Ó., Noormets, R., Allaart, L., Alexanderson, H., Henriksen, M., Schomacker, A., 2017. Dynamic Holocene glacial history of St. Jonsfjorden, Svalbard. Boreas 46, 585-603.

Farnsworth, W.R., Ingólfsson, Ó., Retelle, M., Allaart, L., Håkansson, L.M., Schomacker, A., 2018. Svalbard glaciers re-advanced during the Pleistocene–Holocene transition. Boreas 47, 1022-1032.

Farnsworth, W.R., Ingólfsson, Ó., Retelle, M., Schomacker, A., 2016. Over 400 previously undocumented Svalbard surge-type glaciers identified. Geomorphology 264, 52-60.

Fjeldskaar, W., Bondevik, S., Amantov, A., 2018. Glaciers on Svalbard survived the Holocene thermal optimum. Quaternary Science Reviews 199, 18-29.

Flink, A.E., Hill, P., Noormets, R., Kirchner, N., 2018. Holocene glacial evolution of Mohnbukta in eastern Spitsbergen. Boreas 47, 390-409.

Forman, S.L., 1990. Post-glacial relative sea-level history of northwestern Spitsbergen, Svalbard. Geological Society of America Bulletin 102, 1580-1590.

Forman, S.L., Lubinski, D.J., Ingólfsson, Ó., Zeeberg, J.J., Snyder, J.A., Siegert, M.J., Matishov, G.G., 2004. A review of postglacial emergence on Svalbard, Franz Josef Land and Novaya Zemlya, northern Eurasia. Quaternary Science Reviews 23, 1391-1434.

Forman, S.L., Mann, D.H., Miller, G.H., 1987. Late Weichselian and Holocene Relative Sea-level History of Bröggerhalvöya, Spitsbergen. Quaternary Research 27, 41-50.

Forwick, M., Vorren, T.O., 2009. Late Weichselian and Holocene sedimentary environments and ice rafting in Isfjorden, Spitsbergen. Palaeogeography, palaeoclimatology, palaeoecology 280, 258-274.

Forwick, M., Vorren, T.O., 2010. Stratigraphy and deglaciation of the Isfjorden area, Spitsbergen. Norwegian Journal of Geology 90, 163-179.

Forwick, M., Vorren, T.O., Hald, M., Korsun, S., Roh, Y., Vogt, C., Yoo, K.-C., 2010. Spatial and temporal influence of glaciers and rivers on the sedimentary environment in Sassenfjorden and Tempelfjorden, Spitsbergen. Geological Society, London, Special Publications 344, 163-193.

Førland, E.J., Benestad, R., Hanssen-Bauer, I., Haugen, J.E., Skaugen, T.E., 2011. Temperature and Precipitation Development at Svalbard 1900-2100. Advances in Meteorology 2011, 1-14.

Førland, E.J., Hanssen-Bauer, I., Nordli, P.Ø., 1997. Climate statistics and longterm series of temperature and precipitation at Svalbard and Jan Mayen. Rapport Klima, 21/97. Norwegian Meteorological Institute.

Gilbert, G.L., O'Neill, H.B., Nemec, W., Thiel, C., Christiansen, H.H., Buylaert, J.P., Eyles, N., 2018. Late Quaternary sedimentation and permafrost development in a Svalbard fjord-valley, Norwegian high Arctic. Sedimentology 65, 2531-2558.

Glasser, N.F., Hambrey, M.J., 2003. Ice-Marginal terrestrial landsystem: Svalbard polythermal glaciers, in: Gooster, L. (Ed.), Glacial Landsystem. Taylor & Francis Group, London, pp. 65-88.

Goslar, T., Arnold, M., Bard, E., Kuc, T., Pazdur, M.F., Ralska-Jasiewiczowa, M., Rozanski, K., Tisnerat, N., Walanus, A., Wicik, B., Wieckowski, K., 1995. High concentration of atmospheric 14C during the Younger Dryas cold episode. Nature 377, 414-417.

Goslar, T., Arnold, M., Tisnerat-Laborde, N., Czernik, J., Więckowski, K., 2000. Variations of Younger Dryas atmospheric radiocarbon explicable without ocean circulation changes. Nature 403, 877-880.

Graham, D.J., Midgley, N.G., 2000. Graphical representation of particle shape using triangular diagrams: an Excel spreadsheet method. Earth Surface Processes Landforms 25, 1473-1477.

Gulliksen, S., Birks, H.H., Possnert, G., Mangerud, J., 1998. A calendar age estimate of the Younger Dryas-Holocene boundary at Kråkenes, western Norway. The Holocene 8, 249-259.

Hagen, J.O., Liestøl, O., Roland, E., Jørgensen, T., 1993. Glacier atlas of Svalbard and Jan Mayen. Meddelelser nr. 129. Norwegian Polar Institute, Oslo.

Hagen, J.O., Melvold, K., Pinglot, F., Dowdeswell, J.A., 2003. On the Net Mass Balance of the Glaciers and Ice Caps in Svalbard, Norwegian Arctic. Arctic, Antarctic, and Alpine Research 35, 264-270.

Hald, M., Korsun, S., 2008. The 8200 cal. yr BP event reflected in the Arctic fjord, Van Mijenfjorden, Svalbard. Holocene 18, 981-990.

Hallet, B., Prestrud, S., 1986. Dynamics of Periglacial Sorted Circles in Western Spitsbergen. Quaternary Research 26, 81-99.

Hambrey, M.J., Glasser, N.F., 2012. Discriminating glacier thermal and dynamic regimes in the sedimentary record. Sedimentary Geology 251-252, 1-33.

Hanáček, M., Nývlt, D., Jennings, S.J.A., 2021. Thermal basal regime of the Elsterian ice-sheet marginal zone in a hilly mountain foreland, Rychleby Mts., Eastern Sudetes. Boreas 50, 582-605.

Hanssen-Bauer, I., Førland, E.J., Hisdal, H., Mayer, S., Sandø, A.B., Sorteberg, A., 2019. Climate in Svalbard 2100 - a knowledge base for climate adaptation. Report no. 1/2019. Norwegian Centre for Climate Services.

Hanssen-Bauer, I., Kristensen Solås, M., Steffensen, E.L., 1990. The climate of Spitsbergen. Rapport Klima, 39/90. Norwegian Meteorological Institute.

Hart, J.K., Hindmarsh, R.C.A., Boulton, G.S., 1990. Styles of subglacial glaciotectonic deformation within the context of the anglian ice-sheet. Earth Surface Processes and Landforms 15, 227-241.

Heaton, T.J., Koehler, P., Butzin, M., Bard, E., Reimer, R.W., Austin, W.E.N., Ramsey, C.B., Grootes, P.M., Hughen, K.A., Kromer, B., Reimer, P.J., Adkins, J., Burke, A., Cook, M.S., Olsen, J., Skinner, L.C., 2020. Marine20-the marine radiocarbon age calibration curve (0-55,000 cal BP). Radiocarbon 62, 779-820.

Henriksen, M., Alexanderson, H., Landvik, J.Y., Linge, H., Peterson, G., 2014. Dynamics and retreat of the Late Weichselian Kongsfjorden ice stream, NW Svalbard. Quaternary Science Reviews 92, 235-245.

Hjelle, A., Brekke, A., Binns, R., 1993. Geology of Svalbard. The Norwegian Polar Institute, Oslo.

Hodgkins, R., 1997. Glacier hydrology in Svalbard, Norwegian High Arctic. Quaternary Science Reviews 16, 957-973.

Hodgkins, R., 2001. Seasonal evolution of meltwater generation, storage and discharge at a non-temperate glacier in Svalbard. Hydrological Processes 15, 441-460.

Hodson, A.J., Ferguson, R.I., 1999. Fluvial suspended sediment transport from cold and warm-based glaciers in Svalbard. Earth Surface Processes and Landforms 24, 957-974.

Hogg, A., Southon, J., Turney, C., Palmer, J., Ramsey, C.B., Fenwick, P., Boswijk, G., Buntgen, U., Friedrich, M., Helle, G., Hughen, K., Jones, R., Kromer, B., Noronha, A., Reinig, F., Reynard, L., Staff, R., Wacker, L., 2016. Decadally Resolved Lateglacial Radiocarbon Evidence from New Zealand Kauri. Radiocarbon 58, 947.

Holmlund, E.S., 2021. Aldegondabreen glacier change since 1910 from structure-from-motion photogrammetry of archived terrestrial and aerial photographs: utility of a historic archive to obtain century-scale Svalbard glacier mass losses. Journal of Glaciology 67, 107-116.

Hormes, A., Gjermundsen, E.F., Rasmussen, T.L., 2013. From mountain top to the deep sea - Deglaciation in 4D of the northwestern Barents Sea ice sheet. Quaternary Science Reviews 75, 78-99.

Humlum, O., 2002. Modelling late 20th-century precipitation in Nordenskiold Land, Svalbard, by geomorphic means. Norsk Geografisk Tidsskrift 56, 96-103.

Humlum, O., Elberling, B., Hormes, A., Fjordheim, K., Hansen, O.H., Heinemeier, J., 2005. Late-Holocene glacier growth in Svalbard, documented by subglacial relict vegetation and living soil microbes. The Holocene 15, 396-407.

Humlum, O., Instanes, A., Sollid, J.L., 2003. Permafrost in Svalbard: a review of research history, climatic background and engineering challenges. Polar Research 22, 191-215.

Ingólfsson, Ó., 2011. Fingerprints of Quaternary glaciations on Svalbard. Geological Society, London, Special Publication 354, 15-31.

Ingólfsson, Ó., Landvik, J.Y., 2013. The Svalbard-Barents Sea ice-sheet - Historical, current and future perspectives. Quaternary Science Reviews 64, 33-60.

IPCC, 2007. Climate Change 2007: Synthesis Report. Contribution of Working Groups I, II and III to the Fourth Assessment Report of the Intergovernmental Panel on Climate Change. Core Writing Team, Pachauri, R.K and Reisinger, A. (eds.). IPCC, Geneva, Switzerland, 104 pp.

IPCC, 2019. IPCC Special Report on the Ocean and Cryosphere in a Changing Climate. H.-O. Pörtner, D.C. Roberts, V. Masson-Delmotte, P. Zhai, M. Tignor, E. Poloczanska, K. Mintenbeck, A. Alegría, M. Nicolai, A. Okem, J. Petzold, B. Rama, N.M. Weyer (eds.). In press.

IPCC, 2021. Climate Change 2021: The Physical Science Basis. Contribution of Working Group I to the Sixth Assessment Report of the Intergovernmental Panel on Climate Change. Masson-Delmotte, V., P. Zhai, A. Pirani, S.L. Connors, C. Péan, S. Berger, N. Caud, Y. Chen, L. Goldfarb, M.I. Gomis, M. Huang, K. Leitzell, E. Lonnoy, J.B.R. Matthews, T.K. Maycock, T. Waterfield, O. Yelekçi, R. Yu, and B. Zhou (eds.). Cambridge University Press. In Press.

Jakobsson, M., Mayer, L., Coakley, B., Dowdeswell, J.A., Forbes, S., Fridman, B., Hodnesdal, H., Noormets, R., Pedersen, R., Rebesco, M., Schenke, H.W., Zarayskaya, Y., Accettella, D., Armstrong, A., Anderson, R.M., Bienhoff, P., Camerlenghi, A., Church, I., Edwards, M., Gardner, J.V., Hall, J.K., Hell, B., Hestvik, O., Kristoffersen, Y., Marcussen, C., Mohammad, R., Mosher, D., Nghiem, S.V., Pedrosa, M.T., Travaglini, P.G., Weatherall, P., 2012. The International Bathymetric Chart of the Arctic Ocean (IBCAO) Version 3.0. Geophysical Research Letters 39.

Kamb, B., Raymond, C.F., Harrison, W.D., Engelhardt, H., Echelmeyer, K.A., Humphrey, N., Brugman, M.M., Pfeffer, T., 1985. Glacier Surge Mechanism: 1982-1983 Surge of Variegated Glacier, Alaska. Science 227, 469-479.

Karandasheva, T.K., Demin, V.I., Ivanov, B., Revina, A.D., 2021. Air Temperature Changes In Barentsburg (Svalbard) In XX - XXI Centures. Justification For Introducing A New Climate Standard (In Russian). Russian Arctic 13, 26-39.

Kirkebøen, K.Ø., 2018. Glacial history and forefield development of Aldegondabreen since the Little Ice Age maximum extent. Unpublished Master's thesis, UiT The Arctic University of Norway, Tromsø.

Kjellman, S.E., Schomacker, A., Thomas, E.K., Håkansson, L., Duboscq, S., Cluett, A.A., Farnsworth, W.R., Allaart, L., Cowling, O.C., McKay, N.P., Brynjólfsson, S., Ingólfsson, Ó., 2020. Holocene precipitation seasonality in northern Svalbard: Influence of sea ice and regional ocean surface conditions. Quaternary Science Reviews 240, 106388.

Kjær, K.H., Krüger, J., 2001. The final phase of dead-ice moraine development: processes and sediment architecture, Kötlujökull, Iceland. Sedimentology 48, 935-952.

Knies, J., Matthiessen, J., Vogt, C., Laberg, J.S., Hjelstuen, B.O., Smelror, M., Larsen, E., Andreassen, K., Eidvin, T., Vorren, T.O., 2009. The Plio-Pleistocene glaciation of the Barents Sea-Svalbard region: a new model based on revised chronostratigraphy. Quaternary Science Reviews 28, 812-829.

Koch, Z.J., Isbell, J.L., 2013. Processes and products of grounding-line fans from the Permian Pagoda Formation, Antarctica: Insight into glacigenic conditions in polar Gondwana. Gondwana Research 24, 161-172.

Kokin, O., Mavlyudov, B., 2020. Geological and geomorphological indicators of the surge behavior of the aldegonda glacier (west spitsbergen) in the little ice age (in Russian). Geomorfologiya, 81-95.

Krigström, A., 1962. Geomorphological Studies of Sandur Plains and Their Braided Rivers in Iceland. Geografiska Annaler 44, 328-346.

Krüger, J., Kjær, K.H., 1999. A data chart for field description and genetic interpretation of glacial diamicts and associated sediment - with examples from Greenland, Iceland, and Denmark. Boreas 28, 386-402.

Larsen, E., Lysså, A., Rubensdotter, L., Farnsworth, W.R., Jensen, M., Nadeau, M.J., Ottesen, D., 2018. Lateglacial and Holocene glacier activity in the Van Mijenfjorden area, western Svalbard. Arktos 4, 1-21.

Lawson, D.E., 1981. Sedimentological characteristics and classification of depositional processes and deposits in the glacial environment. Cold Regions Research and Engineering Laboratory (CRREL), Report 81-27.

Lefauconnier, B., Hagen, J.O., 1991. Surging and calving glaciers in Eastern Svalbard. Meddelelser nr. 116. Norwegian Polar Institute.

Levine, A., Stanish, C., 2014. The Importance of Multiple ^{14}C Dates from Significant Archaeological Contexts. Journal of Archaeological Method and Theory 21, 824-836.

Lovell, H., Fleming, E.J., Benn, D.I., Hubbard, B., Lukas, S., Naegeli, K., 2015. Former dynamic behaviour of a cold-based valley glacier on Svalbard revealed by basal ice and structural glaciology investigations. Journal of Glaciology 61, 309-328.

Lowe, J.J., Walker, M., 2015. Reconstructing Quaternary Environments, 3 ed. Routledge, London.

Luckman, A., Benn, D.I., Cottier, F., Bevan, S., Nilsen, F., Inall, M., 2015. Calving rates at tidewater glaciers vary strongly with ocean temperature. Nature Communication 6, 8566.

Lukas, S., Benn, D.I., Boston, C.M., Brook, M., Coray, S., Evans, D.J.A., Graf, A., Kellerer-Pirklbauer, A., Kirkbride, M.P., Krabbendam, M., Lovell, H., Machiedo, M., Mills, S.C., Nye, K., Reinardy, B.T.I., Ross, F.H., Signer, M., 2013. Clast shape analysis and clast transport paths in glacial environments: A critical review of methods and the role of lithology. Earth-Science Reviews 121, 96-116.

Lundström, E., 2019. Development and analysis of digital elevation models created from photogrammetry. Unpublished course report for AG-210 at UNIS, Svalbard., pp. 1 - 26.

Lønne, I., 1993. Physical signatures of ice advance in a Younger Dryas ice-contact delta, Troms, northern Norway: implications for glacier-terminus history. Boreas 22, 59-70.

Lønne, I., 1997. Sedimentology and depositional history of an early Holocene ice-contact submarine fan: the Egge-Lyngås 'end-moraine', southern Norway. Norsk Geologisk Tidsskrift 77, 137-157.

Lønne, I., 2005. Faint traces of high Arctic glaciations: an early Holocene ice-front fluctuation in Bolterdalen, Svalbard. Boreas 34, 308-323.

Macheret, Y.Y., Zhuravlev, A.B., 1982. Radio Echo-Sounding of Svalbard Glaciers. Journal of Glaciology 28, 295-314.

Maizels, J., 1993. Lithofacies variations within sandur deposits: the role of runoff regime, flow dynamics and sediment supply characteristics. Sedimentary Geology 85, 299-325.

Maizels, J., 2002. Sediments and landforms of modern proglacial terrestrial environments, in: Menzies, J. (Ed.), Modern and Past Glacial Environments. Butterworth-Heinemann, Oxford, pp. 279-316.

Maizels, J.K., 1977. Experiments on the origin of kettle-holes. Journal of Glaciology 18, 291-303.

Mangerud, J., Bolstad, M., Elgersma, A., Helliksen, D., Landvik, J.Y., Lønne, I., Lycke, A.K., Salvigsen, O., Sandahl, T., Svendsen, J.I., 1992. The Last Glacial Maximum on Spitsbergen, Svalbard. Quaternary Research 38, 1-31.

Mangerud, J., Bondevik, S., Gulliksen, S., Karin Hufthammer, A., Høisæter, T., 2006. Marine 14C reservoir ages for 19th century whales and molluscs from the North Atlantic. Quaternary Science Reviews 25, 3228-3245.

Mangerud, J., Dokken, T., Hebbeln, D., Heggen, B., Ingólfsson, O., Landvik, J.Y., Mejdahl, Svendsen, J.I., Vorren, T.O., 1998. Fluctuations of the Svalbard-Barents Sea Ice Sheet during the last 150 000 years. Quaternary Science Reviews 17, 11-42.

Mangerud, J., Svendsen, J.I., 1990. Deglaciation chronology inferred from marine sediments in a proglacial lake basin, western Spitsbergen, Svalbard. Boreas 19, 249-272.

Mangerud, J., Svendsen, J.I., 2018. The Holocene Thermal Maximum around Svalbard, Arctic North Atlantic; molluscs show early and exceptional warmth. The Holocene 28, 65-83.

Mangerud, J.A.N., Landvik, J.Y., 2007. Younger Dryas cirque glaciers in western Spitsbergen: Smaller than during the Little Ice Age. Boreas 36, 278-285.

Marren, P.M., 2005. Magnitude and frequency in proglacial rivers: a geomorphological and sedimentological perspective. Earth-Science Reviews 70, 203-251.

Menzies, J., 2009. Glacial Geomorphology, in: Gornitz, V. (Ed.), Encyclopedia of Paleoclimatology and Ancient Environments. Springer, Dordrecht, pp. 361-374.

Miall, A.D., 1977. A Review of the Braided-River Depositional Environment. Earth-Science Reviews 13, 1-62.

Miller, G.H., Alley, R.B., Brigham-Grette, J., Fitzpatrick, J.J., Polyak, L., Serreze, M.C., White, J.W.C., 2010. Arctic amplification: Can the past constrain the future? Quaternary Science Reviews 29, 1779-1790.

Miller, G.H., Landvik, J.Y., Lehman, S.J., Southon, J.R., 2017. Episodic Neoglacial snowline descent and glacier expansion on Svalbard reconstructed from the 14C ages of ice-entombed plants. Quaternary Science Reviews 155, 67-78.

Navarro, F.J., Glazovsky, A.F., Macheret, Y.Y., Vasilenko, E.V., Corcuera, M.I., Cuadrado, M.L., 2005. Ice-volume changes (1936–1990) and structure of Aldegondabreen, Spitsbergen. Annals of Glaciology 42, 158-162.

Norwegian Meteorological Institute., 2021a. Annual mean temperature in Svalbard, filtered and unfiltered. Environmental monitoring of Svalbard and Jan Mayen, https://www.mosj.no/.

Norwegian Meteorological Institute., 2021b. Annual precipitation in Svalbard, Hopen and Jan Mayen, filtered. Environmental monitoring of Svalbard and Jan Mayen, http://www.mosj.no/.

Norwegian Polar Institute., 2014. Terrengmodell Svalbard (S0 Terrengmodell) [Data Set]. Norwegian Polar Institute.

Norwegian Polar Institute., 2021a. Svalbardkartet: https://svalbardkartet.npolar.no/.

Norwegian Polar Institute., 2021b. TopoSvalbard: https://toposvalbard.npolar.no/.

Nuth, C., Kohler, J., Aas, H.F., Brandt, O., Hagen, J.O., 2007. Glacier geometry and elevation changes on Svalbard (1936–90): a baseline dataset. Annals of Glaciology 46, 106-116.

Nuth, C., Kohler, J., Konig, M., von Deschwanden, A., Hagen, J.O., Kaab, A., Moholdt, G., Pettersson, R., 2013. Decadal changes from a multi-temporal glacier inventory of Svalbard. The Cryosphere 7, 1603-1621.

Oerlemans, J., 2005. Extracting a Climate Signal from 169 Glacier Records. Science 308, 675-677.

Ottesen, D., Dowdeswell, J.A., 2006. Assemblages of submarine landforms produced by tidewater glaciers in Svalbard. Journal of Geophysical Research 111, F01016.

Ó Cofaigh, C., Lemman, D.S., Evans, D.J.A., Bednarski, J., 1999. Glacial landform-sediment assemblages in the Canadian High Arctic and their implications for late Quaternary glaciations. Annals of Glaciology 28, 195-201.

Pieńkowski, A.J., Husum, K., Furze, M.F.A., Missana, A.F.J.M., Irvalı, N., Divine, D.V., Eilertsen, V.T., 2021. Revised ΔR values for the Barents Sea and its archipelagos as a pre-requisite for accurate and robust marine-based 14C chronologies. Quaternary Geochronology, 101244.

Postma, G., 1990. Depositional Architecture and Facies of River and Fan Deltas: A Synthesis, in: Colella, A., Prior, D.B. (Eds.), Coarse-Grained Deltas, Oxford, pp. 13-28.

Powell, R., Domack, G., 2002. Modern glaciomarine environments, in: Menzies, J. (Ed.), Modern and Past Glacial Environments. Butterworth-Heinemann, Oxford, pp. 361-389.

Powell, R.D., 1981. A Model for Sedimentation by Tidewater Glaciers. Annals of Glaciology 2, 129-134.

Powell, R.D., 1984. Glacimarine processes and inductive lithofacies modelling of ice shelf and tidewater glacier sediments based on Quaternary examples. Marine Geology 57, 1-52.

Powell, R.D., 1990. Glacimarine processes at grounding-line fans and their growth to ice-contact deltas, in: Dowdeswell, J.A., Scourse, J.D. (Eds.), Glacimarine environments: processes and sediments. Geological Society Special Publication, pp. 53-73.

Powers, M.C., 1953. A new roundness scale for sedimentary particles. Journal of Sedimentary Petrology 23, 117-119.

Reinig, F., Sookdeo, A., Esper, J., Friedrich, M., Guidobaldi, G., Helle, G., Kromer, B., Nievergelt, D., Pauly, M., Tegel, W., Treydte, K., Wacker, L., Buntgen, U., 2020. Illuminating IntCal during the Younger Dryas. Radiocarbon 62, 883-889.

Reusche, M., Winsor, K., Carlson, A.E., Marcott, S.A., Rood, D.H., Novak, A., Roof, S., Retelle, M., Werner, A., Caffee, M., Clark, P.U., 2014. 10Be surface exposure ages on the late-Pleistocene and Holocene history of Linnébreen on Svalbard. Quaternary Science Reviews 89, 5-12.

Rignot, E., Fenty, I., Xu, Y., Cai, C., Kemp, C., 2015. Undercutting of marine-terminating glaciers in West Greenland. Geophysical Research Letters 42, 5909-5917.

Roberts, M.L., Beaupré, S.R., Burton, J.R., 2013. A High-Throughput, Low-Cost Method for Analysis of Carbonate Samples for 14C. Radiocarbon 55, 585-592.

Robinson, P., Dowdeswell, J.A., 2011. Submarine landforms and the behavior of a surging ice cap since the last glacial maximum: The open-marine setting of eastern Austfonna, Svalbard. Marine Geology 286, 82-94.

Ronnert, L., Landvik, J.Y., 1993. Holocene glacial advances and moraine formation at Albrechtbreen, Edgeøya, Svalbard. Polar Research 12, 57-63.

Salvigsen, O., Elgersma, A., Hjort, C., Lagerlund, E., Liestøl, O., Svensson, N.O., 1990. Glacial history and shoreline displacement on Erdmannflya and Bohemanflya, Spitsbergen, Svalbard. Polar Research 8, 261-273.

Schomacker, A., 2008. What controls dead-ice melting under different climate conditions? A discussion. Earth-Science Reviews 90, 103-113.

Schomacker, A., Farnsworth, W.R., Ingolfsson, O., Allaart, L., Hakansson, L., Retelle, M., Siggaard-Andersen, M.-L., Korsgaard, N.J., Rouillard, A., Kjellman, S.E., 2019. Postglacial relative sea level change and glacier activity in the early and late Holocene: Wahlenbergfjorden, Nordaustlandet, Svalbard. Scientific Reports 9, 6799.

Seramur, K.C., Powell, R.D., Carlson, P.R., 1997. Evaluation of conditions along the grounding line of temperate marine glaciers: An example from Muir Inlet, Glacier Bay, Alaska. Marine Geology 140, 307-327.

Sessford, E.G., Strzelecki, M.C., Hormes, A., 2015. Reconstruction of Holocene patterns of change in a High Arctic coastal landscape, Southern Sassenfjorden, Svalbard. Geomorphology 234, 98-107.

Slater, D.A., Straneo, F., Felikson, D., Little, C.M., Goelzer, H., Fettweis, X., Holte, J., 2019. Estimating Greenland tidewater glacier retreat driven by submarine melting. The Cryosphere 13, 2489-2509.

Sneed, E.D., Folk, R.L., 1958. Pebbles in the Lower Colorado River, Texas a Study in Particle Morphogenesis. The Journal of Geology 66, 114-150.

Stuiver, M., Reimer, P.J., Reimer, R., 2021. CALIB 8.2 [WWW program]: http://calib.org.

Svendsen, J.I., Mangerud, J., 1997. Holocene glacial and climatic variations on Spitsbergen, Svalbard. The Holocene 7, 45-57.

Trusel, L.D., Powell, R.D., Cumpston, R.M., Brigham-Grette, J., 2010. Modern glacimarine processes and potential future behaviour of Kronebreen and Kongsvegen polythermal tidewater glaciers, Kongsfjorden, Svalbard. Geological Society, London, Special Publication 344, 89-102.

van der Bilt, W.G.M., Bakke, J., Vasskog, K., D'Andrea, W.J., Bradley, R.S., Ólafsdóttir, S., 2015. Reconstruction of glacier variability from lake sediments reveals dynamic Holocene climate in Svalbard. Quaternary Science Reviews 126, 201-218.

Walker, M., 2005. Quaternary dating methods. John Wiley and Sons, Chichester, England.

Werner, A., 1993. Holocene moraine chronology, Spitsbergen, Svalbard: lichenometric evidence for multiple Neoglacial advances in the Arctic. The Holocene 3, 128-137.

Wood, M., Rignot, E., Fenty, I., Menemenlis, D., Millan, R., Morlighem, M., Mouginot, J., Seroussi, H., 2018. Ocean-Induced Melt Triggers Glacier Retreat in Northwest Greenland. Geophysical Research Letters 45, 8334-8342.

Yde, J.C., Paasche, Ø., 2010. Reconstructing Climate Change: Not All Glaciers Suitable. Eos Transactions AGU 91, 189-190.

Zhuravskiy, D., Ivanov, B., Pavlov, A., 2012. Ice conditions at Gronfjorden Bay, Svalbard, from 1974 to 2008. Polar Geography 35, 169-176.